GABAERGIC SYNAPTIC TRANSMISSION, PLASTICITY AND INTEGRATION IN THE SUBTHALAMIC NUCLEUS

KAI YOON FAN

A thesis submitted for the degree of PhD

Department of Biomedical Science
University of Sheffield

August 2012

GABAERGIC SYNAPTIC TRANSMISSION, PLASTICITY AND INTEGRATION IN THE SUBTHALAMIC NUCLEUS

KAI YOON FAN
Department of Biomedical Science, University of Sheffield
Thesis submitted for the degree of PhD, August 2012

ABSTRACT

The reciprocally connected GABAergic external globus pallidus (GPe) and glutamatergic subthalamic nucleus (STN) occupy pivotal positions in cortico-basal ganglia-thalamo-cortical networks essential for normal voluntary movement. In both idiopathic and experimental PD characterized by degeneration of midbrain dopamine neurons, the GPe and STN exhibit hypo- and hyper-activity, respectively, and hypersynchronous rhythmic burst firing (<30 Hz). Deep brain stimulation (DBS) of STN (>60 Hz) suppresses the pathological oscillations and improves motor impairments, although the therapeutic mechanisms are unclear. Given the GPe potently patterns STN activity, the decorrelated nature of GPe–STN network is intriguing. Therefore, the main objective of this thesis is to study the regulation of GPe–STN input in health, PD and DBS, using complementary anatomical, molecular, electrophysiological and computational modelling approaches.

Studies comparing GPe–STN transmission in control and 6-OHDA-lesioned rodents revealed that following chronic dopamine depletion the GPe–STN projections strengthened remarkably through proliferation in the number of functional synaptic connections. The enhanced GPe–STN transmission is predicted to increase the capability of the GPe to generate synchronous rhythmic burst firing in the parkinsonian STN.

Recent optogenetic studies showed that high-frequency driving of afferents expressing channelrhodopsin-2 (ChR2) in the STN of *Thy1-ChR2* transgenic mice rescued parkinsonian symptoms. Characterization of the mouse line revealed ChR2 expression in not only glutamatergic but GABAergic afferents in the STN, implying DBS may exert its therapeutic effects through manipulation of GPe–STN transmission.

The work from this thesis also demonstrates that GABAergic inhibition in STN neurons activates HCN channel currents that limit synaptic hyperpolarisation and deinactivation of low-voltage-activated Ca^{2+} channels, hence reducing the propensity of rebound burst firing. Uniform HCN channel distribution across the somatodendritic axis most effectively counteracts the GABAergic inhibition. These results suggest that HCN channels in STN neurons may partly underlie the decorrelated nature of GPe–STN activity and prevent excessive burst firing observed in PD.

PREFACE

The work presented in this thesis is largely based on three manuscripts that have been published, accepted for publication, and are in preparation. The manuscripts and contributions from the authors to my thesis are detailed as below:

1) Chapter 2

Fan KY, Baufreton J, Surmeier DJ, Chan SC, Bevan MD (2012) Proliferation of globus pallidus-subthalamic nucleus synapses following degeneration of midbrain dopamine neurons (accepted for publication in the Journal of Neuroscience).

Author contributions. **KYF**, JB, DJS, CSC, and MDB designed the research; **KYF**, JB, and MDB performed and analysed the lesions; JB and MDB performed and analysed the electrophysiology; **KYF**, CSC and MDB performed the mRNA expression analyses; **KYF** and MDB performed the anatomical analyses; **KYF**, JB, and MDB wrote the manuscript.

2) Chapter 3

Fan KY, Atherton JF, Bevan MD (2012) Characterisation of channelrhodopsin-2 expression in the subthalamic nucleus of *Thy1-ChR2-EYFP* transgenic mouse line 18 (in preparation).

Author contributions. **KYF**, JFA and MDB designed the research; JFA and MDB performed and analysed the electrophysiology; **KYF** performed and analysed the immunocytochemistry; **KYF** wrote the manuscript.

3) Chapter 4

Atherton JF, Kitano K, Baufreton J, **Fan K**, Wokosin D, Tkatch T, Shigemoto R, Surmeier DJ, Bevan MD (2010) Selective participation of somatodendritic HCN channels in inhibitory but not excitatory synaptic integration in neurons of the subthalamic nucleus. J Neurosci 30: 16025-40.

Author contributions. JFA, KK, JB, **KF**, TT and MDB designed the research; TT and DJS performed and analysed the single-cell RTPCR; **KF**, SR and MDB carried out the immunohistochemical analysis of HCN2 expression; KK, JFA, JB and DW performed and analysed the electrophysiology; KK and MDB designed and analysed the computational models; JFA, KK, JB, **KF**, and MDB wrote the manuscript.

For My Parents

Koh Saw Choo & Fan Yuek Shen

ACKNOWLEDGEMENTS

This thesis is a presentation of my research work during which I turned from an old boy to an adult. First and foremost I would like to thank my supervisor Dr. Mark Bevan who had made this possible. He has shown me the vigorous process of solid scientific discovery and I have learned so much from working with him. I could not have had a better supervisor for my PhD, without a doubt. Lab members including Jonathan Chetrit, Jeremy Atherton, Kathleen Cosgrove, and Patrick Hackler as well as collaborator Dr. Savio Chan also helped me a lot along the way. I have certainly enjoyed being surrounded by these smart, hardworking and humourous colleagues in the laboratory environment.

Thanks to the former head of Biomedical Science department, Prof. Matthew Holley, who is also officially my secondary supervisor, I had the chance to continue my graduate studies in Northwestern University with Mark while maintaining my university studentship status. I deeply appreciate the assistance and advice from my advisor Prof. David Grundy and postgraduate tutor Dr. Andrew Furley, all the while I was away from Sheffield.

I would like to thank my parents who have never asked anything from me but give unconditional support for whatever I do. I am also grateful for Xin Zhou's always being supportive. As someone from a rural town of a developing country I did not think I could get this far. My hope is to continue doing great work that will one way or the other contribute to the society in the future.

CONTENTS

LIST OF TABLES

Chapter 2

Chapter 3

Chapter 4

LIST OF FIGURES

Chapter 1

Chapter 2

Chapter 3

Chapter 4

ABBREVIATIONS

6-OHDA	6-hydroxydopamine
ACSF	artificial cerebrospinal fluid
AMPA	amino-3-hydroxy-5-methyl-4-isoxazoleproprionic acid
AP	action potential
APV	d-(–)-2-amino-5-phosphonopentanoic acid
ChR2	channelrhodopsin-2
CAMKII	Ca^{2+}/calmodulin-dependent protein kinase
Ca_v	voltage-dependent Ca^{2+} (channel)
CGP 55845	(2S)-3-[[(1S)-1-(3,4-dichlorophenyl)ethyl]amino-2 hydroxypropyl](phenylmethyl)phosphinic acid
CREB	cAMP response element-binding
CT	cycle threshold
D1-MSN	striatal D1 dopamine receptor-expressing medium spiny neuron
D2-MSN	striatal D2 dopamine receptor-expressing medium spiny neuron
DAB	diaminobenzidine tetrahydrochloride
DBS	deep brain stimulation
DNQX	6,7-dinitroquinoxaline-2,3-dione
EcoG	electrocorticogram
EP	endopeduncular nucleus
EPSP	excitatory postsynaptic potential
GABA	gamma-aminobutyric acid
GABARAP	GABA receptor-associated protein
GABAzine	2-(3-Carboxypropyl)-3-amino-6-(4 methoxyphenyl)pyridazinium bromide
GP	globus pallidus
GPe	external segment of the globus pallidus
GPi	internal segment of the globus pallidus
HCN	hyperpolarisation-activated cyclic nucleotide-gated (channel)
HD	Huntington's disease
HFS	high-frequency stimulation
IC	internal capsule
I_h	inward, non-inactivating, non-selective cation current
IPSC	inhibitory postsynaptic current
IPSP	inhibitory postsynaptic potential
KATP	ATP-sensitive potassium (channel)
LFP	local field potential
LFS	low-frequency stimulation
LTDg	laterodorsal tegmental nucleus
MEA	midbrain extrapyramidal area
MFB	medial forebrain bundle
mIPSC	miniature inhibitory postsynaptic current
MPTP	1-methyl-4-phenyl-1,2,3,6-tetrahydropyridine

MSN	striatal medium spiny neuron
MTg	mesopontine tegmentum
NA	numerical aperture
Na_v	voltage-dependent Na^+ (channel)
NDS	normal donkey serum
NGS	normal goat serum
NMDA	N-methyl-D-aspartate
NSF	N-ethylmaleimide-sensitive factor
PB	phosphate buffer
PBS	phosphate buffered saline
PD	Parkinson's disease
PPN	pedunculopontine nucleus
scRTPCR	single cell reverse transcription polymerase chain reaction
SIF	simulated intestinal fluid
SK	small-conductance apamine-sensitive Ca^{2+}-dependent K^+ (channel)
SNc	substantia nigra *pars compacta*
SNr	substantia nigra *pars reticulate*
STN	subthalamic nucleus
SWA	slow-wave activity
TH	tyrosine hydroxylase
TTX	tetrodotoxin
VGAT	vesicular GABA transporter
VGLUT	vesicular glutamate transporter
VTA	ventral tegmental area
ZD7288	4-ethylphenylamino-1,2-dimethyl-6-methylaminopyrimidinium chloride

CHAPTER 1

GENERAL INTRODUCTION

1.1. Introduction to the basal ganglia

The basal ganglia are a group of interconnected subcortical nuclei crucial for the fundamental processes of action selection and reinforcement. Basal ganglia nuclei in primates include the striatum, external segment of the globus pallidus (GPe, homologous to globus pallidus or GP in rodents), internal segment of the globus pallidus (GPi, homologous to entopeduncular nucleus or EP in rodents), the subthalamic nucleus (STN) and the substantia nigra, consisting of the *pars compacta* (SNc) and the *pars reticulata* (SNr).

The basal ganglia receive external inputs primarily via the striatum (and to a lesser extent the STN and SNc). The striatum receives direct excitatory inputs from the cerebral cortex, limbic structures, and indirect inputs from the brainstem structures through the thalamus. It then relays signals, via direct and indirect routes, to the principal output nuclei, GPi and SNr. The output nuclei project directly to the thalamus, midbrain and brainstem structures, and indirectly, through the thalamus, to cortical and limbic regions from which the basal ganglia inputs originated (Redgrave et al., 1992; Smith et al., 2004; Takakusaki et al., 2004).

The arrangement of these connections can be viewed as a series of parallel projecting re-entrant circuits that are partially segregated (Redgrave et al., 2011). The spatial segregation between the loops is determined by the functional status of inputs: the ventral territories receive information from brain areas primarily involved in limbic functions, the dorsomedial territories from structures concerned with associative functions, and dorsolateral territories from brain regions involved in sensorimotor control of behaviour (Alexander et al., 1986). This unique architecture is maintained throughout the basal ganglia nuclei in a topographic manner. Although the internal microcircuits of the basal ganglia nuclei are of certain quantitative differences, each of the structure is qualitatively similar across the different functional zones. It is therefore proposed that similar input-output computations are applied to the vastly different functional signals (Redgrave et al., 1999; Redgrave et al., 2011).

Motor and non-motor regions of the basal ganglia differ mainly by their external connections, whereas the intrinsic connections within the basal ganglia are

the same for these circuits. In a simplistic view of the motor circuit, the basal ganglia receive information from the cerebral cortex and provide feedback input back to the cortex through the thalamus, forming a closed loop. The information flow through the basal ganglia is modulated by dopamine released from dopaminergic neurons in the SNc. Historically, the sensorimotor aspect of the basal ganglia has been receiving the most attention because its loss of function leads to debilitating movement disorders, including Parkinson's disease (PD), Huntington's disease (HD), hemiballismus and dystonia (Delong, 1990; Albin et al., 1995).

Because the architecture of the basal ganglia and their connections with the external structures have largely been conserved almost throughout the evolution of vertebrates (Stephenson-Jones et al., 2011; Stephenson-Jones et al., 2012), studies on rodent and primate models have provided important insights on the function and dysfunction of the basal ganglia in humans. To simplify the terminology used in this thesis, the term "GPe" will not only refer to that structure in primates but also include its homologous equivalent, GP in rodents. Likewise the term "GPi" will include reference to its rodent equivalent, EP.

1.2. Disease of the basal ganglia

Many movement disorders have origins in basal ganglia dysfunction. Three broad categories of these disorders are hyperkinetic (eg. HD), hypokinetic (eg. PD), and dystonia. The focus in this thesis is the pathophysiology of PD, which hence will be further described in this section.

1.2.1. Parkinson's disease

PD is the most common type of basal ganglia disorder, affecting 1-2% percent of people older than 65 years old. On a worldwide basis, approximately 10 million people are affected by PD. Because of the aging population, it is predicted that by the year 2020 over 40 million people in the world will have this debilitating neurodegenerative

condition (Morris, 2000). It is clinically characterised by motor disabilities including muscle stiffness (rigidity), poverty of movement (akinesia), slowness of movement (bradykinesia), tremor at rest, postural instability and gait disturbance (Samii et al., 2004). These symptoms manifest when more than 60% of dopaminergic neurons in the SNc degenerate (Dauer and Przedborski, 2003). The mechanisms of dopamine cell death are not exactly clear, but the main contributing molecular factors might be aberrant proteostasis (aggregation of α-synuclein), impaired mitochondrial function, oxidative stress, and/or perturbed Ca^{2+} homeostasis (Dawson and Dawson, 2003; Mattson, 2007; Henchcliffe and Beal, 2008; Surmeier et al., 2011).

Because of the obscurity of molecular events leading to neurodegeneration, a gold standard for treating PD patients has been dopamine replacement therapy using the prodrug levodopa. However, long-term drug use leads to the development of motor complications in up to 80% of patients (Thanvi and Lo, 2004). For patients who no longer respond to levodopa treatment, there have been efforts focused on fetal nerve cell transplantation into the SNc to replace the lost dopamine cells. Unfortunately the relief of motor symptoms often last only several years due to the spread of PD pathology to the grafted cells (Mendez et al., 2008; Kordower et al. 2008; Li et al., 2008).

For the last two decades, deep brain stimulation has emerged as an effective treatment for advanced PD patients. It is a technique used in functional neurosurgery, which involves delivery of high-frequency electrical stimulation through implanted electrodes into the STN (and less commonly the GPi). Acute and chronic DBS results in a dramatic and stable improvement of motor symptoms (Benabid, 2003). However, the therapeutic mechanisms of DBS are still not clearly defined. The understanding of basal ganglia functions in health and PD is therefore important to improve current treatment efficacy and/or to devise new mechanism-based functional therapies.

The progress in this field of research was hastened by the development of animal models carrying disease conditions. In particular, the use of dopamine-depleted models, including 6-hydroxydopamine (6-OHDA)-treated rodents, and the 1-methyl-4-phenyl-1,2,3,6-tetrahydropyridine (MPTP)-treated primates has remarkably improved our understanding of the underlying aberrations leading to motor symptoms of PD.

1.3. Information flow through the basal ganglia

The striatum is the main structure that receives glutamatergic cortical input in the basal ganglia. In the nucleus, this information is processed by a striatal network consisting of 90% gamma-aminobutyric acid-(GABA)ergic medium spiny neurons (MSNs) and 10% interneurons (Kreitzer, 2009). The output nuclei of the basal ganglia are the GPi and SNr, both of which express mainly GABAergic neurons and are often considered as one functional unit due to their anatomical and physiological similarities (Deniau et al., 2007; Nambu, 2007). Based on findings from post mortem human anatomical and neurochemical studies and experimental models of basal ganglia disease, a model of information flow through the basal ganglia that accounts for normal and abnormal motor function has been constructed (Albin et al., 1989; Delong, 1990).

1.3.1. Classical model of direct and indirect pathways

According to the direct/indirect model of the basal ganglia motor circuit, the intrinsic basal ganglia connections are divided into two pathways based on projections of the MSNs consisting of 2 subpopulations of similar size: neurons that express D1 dopamine receptors (D1-MSNs) and those that express D2 dopamine receptors (D2-MSNs). D1-MSNs that predominantly project to the GABAergic GPi/SNr neurons, which tonically inhibit the thalamus, constitute the direct pathway; D2-MSNs that preferentially project to the GABAergic GPe neurons, which innervate the glutamatergic STN neurons that project to the GPi/SNr, constitute the indirect pathway (Albin et al., 1989; Fig. 1). The striatum is heavily innervated by dopaminergic projections from the SNc. Dopamine release exerts an excitatory effect on the D1-MSNs through activation of D1 receptors, and an inhibitory effect on the D2-MSNs due to activation of D2 receptors. When D2-MSNs are activated, GPe neurons are inhibited, thereby disinhibiting the STN that excites the GPi/SNr. As a result motor signals are inhibited in the thalamus. When D1-MSNs are activated, GPi/SNr neurons are inhibited, hence disinhibiting thalamus that feeds back the motor signals to the cortex. Therefore, activation of the direct pathway

Figure 1. Schematic diagram of the direct/indirect pathway model of the cortico-basal ganglia thalamo-cortical motor circuitry and additional connections not considered by the model. Excitatory glutamatergic projections are shown as red arrows, while inhibitory GABAergic projections are indicated by blue arrows.

A. According to the direct/indirect pathway model, cortical signals sent to the striatum during movement is relayed to the basal ganglia output nuclei GPi and SNr via two pathways: direct and indirect. Striatal projection neurons that express D1 dopamine receptors (D1-MSNs) predominantly project to the GPi, which tonically inhibits the thalamus, constituting the direct pathway; MSNs that express D2 dopamine receptors (D2-MSNs) preferentially project to the GPe, which innervates the STN that projects to the GPi, constituting the indirect pathway. The dopamine projections (yellow arrows) from the substantia nigra pars compacta (SNc) regulate the corticostriatal information through dopamine opposing actions on D1- and D2-MSNs: dopamine activation of D1 receptors excites D1-MSNs, whereas D2 receptor activation inhibits D2-MSNs. When D1-MSNs are excited, GPi neurons are inhibited, hence disinhibiting thalamus that feeds back the motor signals to the cortex. When D2-MSNs are inhibited by dopamine, GPe neurons are disinhibited, thereby inhibiting STN that excites the GPi. As a result motor signals are also disinhibited in the thalamus. Therefore, dopamine signals promote movement by both upregulating and suppressing the direct and indirect pathway activities, respectively.

B. In Parkinson's disease, loss of dopaminergic neurons in the SNc causes imbalance of the direct and indirect pathway activities favouring the latter. Hence, the excitatory direct pathway becomes hypoactive, whereas the inhibitory indirect pathway is hyperactive, leading to the lack of motor movement generation. The relative increase and decreases in activity are represented by thickening or thinning of arrows, respectively, in comparison to A. Imbalanced direct/indirect pathways overall lead to the hyperactivity of GPi/SNr, which therefore excessively inhibits activity of thalamus. Excessive thalamic inhibition in turn suppresses the motor system in cortex, leading to motor impairment including akinesia and bradykinesia. Excessive inhibition of midbrain and/or brainstem locomotor regions by GPi/SNr may give rise to gait and posture abnormalities.

C. Recent studies have emphasised on the functional significance of several additional connections that challenge the role of direct/indirect pathway model in information flow through the cortico-basal ganglia thalamo-cortical network. Notably, direct projection from the cortex to the STN contradicts with the direct/indirect pathway model that is centered by striatal activity, hence acquired the term "hyperdirect" pathway. Additionally, the STN innervated by inhibitory GPe projects feedforward excitation back to the GPe, hence forming reciprocal connections between the nuclei. The existence of STN–GPe network contradicts the notion that STN is simply a relay station in the feedforward scheme of information flow explained by the classical model. STN, along with the GPe, also receives substantial dopaminergic innervations by SNc neurons, supporting the growing evidence that dopamine neuromodulation in the basal ganglia is far more complex than net activity influence on D1- and D2-MSNs. Note that this diagram is still a simplification as a number of other connections identified are not shown, some of which have also been implicated in PD pathophysiology.

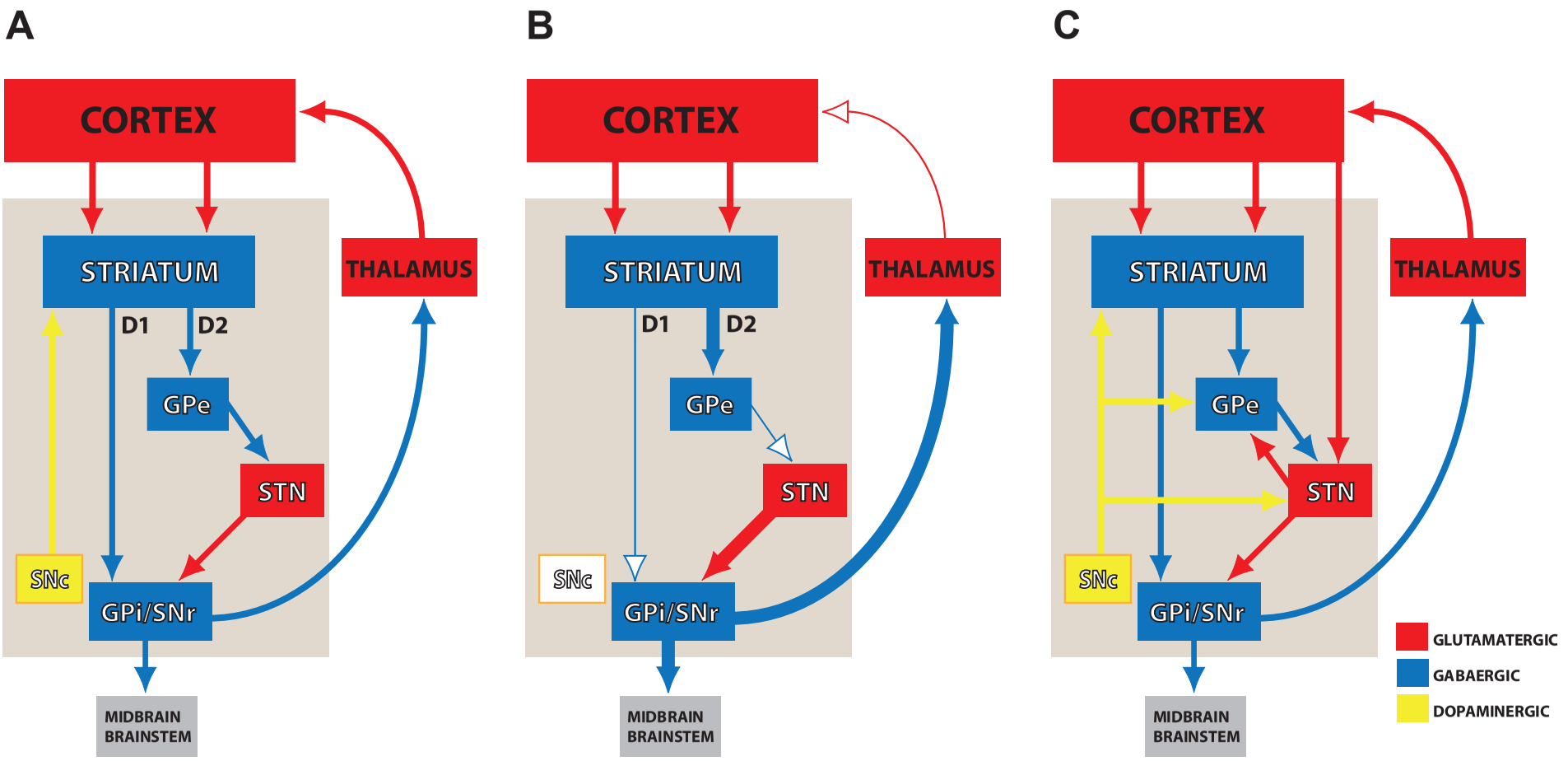
A
CORTEX
STRIATUM
D1
D2
GPe
STN
SNc
GPi/SNr
THALAMUS
MIDBRAIN
BRAINSTEM
B
CORTEX
STRIATUM
D1
D2
GPe
STN
SNc
GPi/SNr
THALAMUS
MIDBRAIN
BRAINSTEM
C
CORTEX
STRIATUM
GPe
STN
SNc
GPi/SNr
THALAMUS
MIDBRAIN
BRAINSTEM
GLUTAMATERGIC
GABAERGIC
DOPAMINERGIC

stimulates movement, whereas activation of the indirect pathway inhibits movement. SNc, another major input nucleus in the basal ganglia, integrates inputs from a diverse collection of areas including sensorimotor cortices and brainstem structures and conveys motivational signals through phasic dopaminergic neurotransmission (Matsumoto and Hikosaka, 2009; Watabe-Uchida et al., 2012). The general impact of dopamine action within the striatum might be to modulate cortical signals to balance the activity of the direct and indirect pathways for appropriate voluntary movement.

1.3.2. Dysfunction of direct/indirect pathways in PD

The excitatory balance between the two pathways in response to direct cortical inputs is modulated by dopamine, such that dopamine released from SNc afferents acting on D1- and D2-MSNs activates and inhibits the direct and indirect pathways respectively. According to this model, the loss of dopamine results in the imbalance of direct and indirect pathway favouring the latter (Fig. 1). Thus, the excitatory direct pathway becomes hypoactive, whereas the inhibitory indirect pathway is hyperactive, leading to the lack of motor movement. Imbalanced direct/indirect pathways lead to hyperactivity of GABAergic GPi/SNr neurons, which therefore excessively inhibit activity in the thalamus. Excessive thalamic inhibition in turn suppresses the motor system in the cortex, presumably leading to motor impairments including akinesia and bradykinesia (Drouot et al., 2004). On the other hand, excessive inhibition of midbrain and/or brainstem locomotor regions by GPi/SNr may instead give rise to gait and posture abnormalities (Takakusaki et al., 2008).

A considerable body of studies has shown that changes in the mean firing rates in GPe, STN, GPi and SNr in PD and PD models (predominantly MPTP-treated primates) are consistent with those predicted by the direct/indirect pathways (Filion and Tremblay, 1991; Boraud et al., 1998; Drouot et al., 2004). Thus, GPe activity may be reduced by 30% while STN and GPi activity may be increased by 40% and 25%, respectively (Galvan and Wichmann, 2008). D1 and D2 receptor antagonisms induce an imbalance of direct/indirect circuits in favour of the indirect pathway (Degos et al., 2005). An increase in neuronal firing rate in STN was reported to correlate with PD progression, implying its role in the manifestation of symptoms (Remple et al., 2011). The overactivation of the indirect pathway in PD is also consistent with improvement

of motor symptoms after lesioning of the STN or GPi, and exacerbation of symptoms after lesioning of GPe (Aziz et al., 1991; Baron et al., 1996; Patel et al., 2003; Zhang et al., 2006). Recent optogenetic studies in mice further demonstrated that specific photostimulation of the direct-pathway MSNs increased locomotion, whereas activation of the indirect-pathway MSNs suppressed movements (Kravitz et al., 2010).

These above-mentioned results, nonetheless, do not establish a causative relationship between aberrant firing rates in basal ganglia nuclei and motor impairments. Additionally, there have been other reports demonstrating a lack of firing rate changes after MPTP administration in primates (Bergman et al., 1994; Raz et al., 2000; Wichmann et al., 1999). The direct/indirect pathway model is inconsistent with the therapeutic effects of stimulating STN and GPi at high frequency. It is, likewise, paradoxical that GPi activity in PD and HD patients was found to be similar (Tang et al., 2005).

Therefore, changes in the mean firing rates in the direct and indirect pathways might not be necessary for parkinsonism, although they should not be overlooked as an important component of PD pathophysiology. The classical model has had substantial impact on our understanding of the way basal ganglia organise motor behaviour and provided a basic framework for our investigations into the basal ganglia dysfunctions in movement disorders.

However, the model is oversimplistic considering the intricacy of intrinsic basal ganglia connections. Many additional connections have not been considered by the model. First and foremost, dopaminergic modulation of the striatum is far more complex than postsynaptic influence on D1- and D2-MSNs. Striatal circuitry, a network of not just MSNs but various classes of interneurons, is dynamically regulated by dopamine *via* other types of dopamine receptors besides D1 and D2 expressed in MSNs, the expression of pre and postsynaptic dopamine receptors in striatal interneurons, and D2-class autoreceptors on dopamine terminals (Surmeier et al., 2011). Furthermore, dopamine modulation does not occur only at the level of striatum, but is found in the GPe (Fallon and Moore, 1978; Lindvall and Björklund 1979; Cossette et al., 1999) and STN (François et al., 2000; Cragg et al., 2004).

Notably, a second port of external input entry to the basal ganglia is overlooked: the direct projection from the cortex to the STN (Monakow et al., 1978; Kitai and Deniau, 1981; Bevan et al., 1995). Direct cortical-STN connection has been termed the "hyperdirect" pathway, reflecting its contradiction with the direct/indirect pathway model that is centered by striatal activity. Many of the STN neurons that receive GPe innervations also project back to the GPe, forming a unique reciprocal GPe–STN circuitry (Moriizumi et al., 1987; Groenewegen and Berendse et, 1990; Shink et al., 1996). The existence of STN–GPe network contradicts the notion that STN is simply a relay station in the feedforward scheme of information flow explained by the classical model.

Indeed, the activity of the cortico-basal ganglia thalamo-cortical network is more complicated than bidirectional changes in firing rates. A great amount of work has demonstrated that a range of oscillatory phenomena also exists in the network. Although the frequency of activity is likely crucial for basal ganglia function, activity pattern and synchronisation of neuronal discharge may be at least equally significant. The often dramatic effectiveness of DBS and the availability of data from PD patients during electrode implantation have turned our attention focus on the pathological role of oscillatory activity in the basal ganglia.

1.4. Oscillatory activity in the basal ganglia

The term "oscillation", in this thesis, refers to rhythmically recurring neuronal activities within and/or between neuronal structures, or rhythmic fluctuations of membrane potential recorded from single neurons. Various oscillatory phenomena occur in the basal ganglia and in related regions of the thalamus and cortex. Autonomous activity of GPe and STN neurons may also represent important sources of oscillatory activity in the cortico-basal ganglia-thalamocortical networks. The ionic mechanisms of intrinsic pacemaking in STN neurons, the main sources of oscillatory activity (except potential contributions from thalamic input which has not been explored in detail) in the basal ganglia and the role of abnormal oscillatory activity in PD pathophysiology will be discussed in this section.

1.4.1. Intrinsic pacemaking mechanisms of STN neurons

In slice recordings, most STN neurons tonically discharge at 5–15 Hz. AP initiation is driven autonomously by persistent and resurgent Na_v channels at the soma and axon initial segment (Atherton et al., 2008).The spontaneous firing is highly regular, due to the presence of small-conductance apamine-sensitive Ca^{2+}-dependent K (SK) channels that underlie the medium duration component of AP afterhyperpolarisation. SK current is activated by Ca^{2+} influx through $Ca_v2.2$ channels during depolarisation phase of action potential (AP) (Ramanathan et al., 2008). Besides $Ca_v2.2$ channels, $Ca_v1.2$–1.3 and Ca_v3 channels are also present in almost all STN neurons, but remain inactivated during autonomous firing (Bevan and Wilson, 1999; Song et al., 2000; Hallworth et al., 2003). Prolonged hyperpolarisation to – 80 mV leads to their deinactivation, leading to a rebound burst firing upon repolarization. During sustained hyperpolarisation, an inward, non-inactivating, non-selective cation current (I_h) mediated by HCN channels is activated (Bevan and Wilson, 1999; Beurrier et al., 2000), although they participate minimally in autonomous firing of STN neurons.

1.4.2. Oscillations in the GPe–STN network

Because of its reciprocal connectivity, the GPe–STN network has received a lot of attention as a potential pacemaker in the basal ganglia. The strongest supporting evidence comes from Plenz and Kitai (1999) who demonstrated that coculture of GPe and STN neurons *in vitro* spontaneously produces slow, synchronised bursting activity (<5 Hz). The generation of synchrony in the GPe–STN circuitry depends largely on the ability of STN neurons to generate rebound burst firing in response to strong hyperpolarised GABAergic input from the GPe neurons (Bevan et al., 2006). The rebound burst amplifies the feedback glutamatergic STN–GPe input and hence subsequent pallidal activity, thus generating and sustaining a sequence of inhibitory postsynaptic potential (IPSP) and rebound burst events in the STN. Similar IPSP-rebound sequence of feed-forward/feed-back interactions between the STN and GPe

have been observed in absence epileptic seizures (7–10 Hz). However, there is no evidence thus far of such oscillatory interactions *in vivo* or in native preparations with preserved GPe–STN connectivity under normal conditions.

1.4.3. Oscillatory interaction between cortex and STN

As the only extrastriatal basal ganglia structure receiving direct cortical input, STN in rodents and primates has been shown to be coherent with cortical activity (EcoG) under various brain states. This is true both when cortical synchronisation is widespread (eg. under slow-wave sleep and anaesthetised conditions), or reduced in awake state due to increased somatotopic activity within/between the structures and broader spectral power of activity (Magill et al., 2000; Urbain et al., 2000; Wichmann et al., 2002; Magill et al., 2004; Magill et al., 2005; Sharott et al., 2005a; Gatev et al., 2006). In urethane-anaesthetised rats exhibiting cortical SWA, simultaneous EcoG and STN single-unit or LFP recordings showed that coherence between the cortex and the STN is restricted to slow (~ 1 Hz) and spindle (7–12 Hz) frequency oscillations (Magill et al., 2005). The rhythm entirely relies on cortical input, because cortical ablation or depression leads to single spike firing in the STN and GPe (Magill et al., 2000), which is similar to that observed in slice preparations where cortical innervations of the STN are mostly severed.

1.4.4. Oscillatory interaction between cortex and striatum

The significant reentrant connectivity between the cortex and the basal ganglia has been shown to be a major contributor to the oscillatory activity observed in the basal ganglia. As mentioned previously, the striatum receives massive direct inputs from the cortex. Simultaneous electrocorticogram (ECoG) and *in vivo* intracellular, single unit or local field potential (LFP) recordings in the striatum demonstrated that striatal activity can be heavily influenced by cortical oscillatory inputs (Tseng et al., 2001a; Courtemanche et al., 2003; Berke et al., 2004). D1- and D2-MSN subtypes, which display nearly

identical intrinsic physiological properties, both exhibit “up” and “down” states. Up states are caused by synchronous upward membrane fluctuations of corticostriatal neurons. The depolarised membrane potential is important for AP discharge in the MSNs. Taking advantage of the cortical slow wave activity (SWA, similar to natural sleep waves) of urethane-anaesthetised rats, the up and down states of MSNs were shown to correlate tightly with the cortical oscillations (Tseng et al., 2001a). However, these neurons often do not fire APs even during up states owing to strong GABAergic inhibition from MSN collaterals and fast-spiking interneurons.

1.5. Excessive synchrony in PD

An increased tendency of basal ganglia neurons at multiple levels to fire in a synchronised oscillatory manner at low frequencies has been well documented in both PD patients and models. Currently, a leading view on the development of this disorder is that pathological oscillatory activity in the cortico-basal ganglia-thalamocortical networks interferes with the normal information coding in the basal ganglia, leading to the manifestation of motor symptoms in parkinsonism.

1.5.1. Observations in idiopathic and experimental PD

The excessive synchrony is largely observed in the extrastriatal basal ganglia structures. Under resting condition, STN, GPe, and GPi neurons fire at high frequency in distinct patterns, with minimal rhythm or correlations within or between the nuclei. During movement, the structures display complex somatotopically organised activity pattern with higher degree of synchronisation in functionally related territories. In PD, activity within and across the nuclei becomes correlated and rhythmic, with the loss of spatiotemporal patterns of somatotopical activity and increased bursting. LFP recordings from implanted DBS electrodes in STN or GPi of PD patients reveal coherent activity in the 8–12 Hz (delta), 13–30 Hz (beta) and 4–7 Hz (tremor) bands (Brown et al., 2007). These activity patterns are associated with different symptoms and may arise from distinct processes. While delta and beta band activity are highly correlated

with akinesia, bradykinesia and rigidity (Kühn et al., 2009), tremor band activity is associated with resting tremor. Additionally, tremor is not tightly correlated with the degree of dopamine loss like the other symptoms and is not developed in some PD patients (Hammond et al., 2007; Zaidel et al., 2009; Helmich et al., 2011).

Excessive widespread synchronisation is also observed in primates where parkinsonism is induced by neurotoxin MPTP treatment, although occurring at lower frequencies than in human patients. Coherent bursting of single cells in GPe, STN and GPi is typically around 3–8 Hz band and 8–15 Hz band (Gatev et al., 2006; Hammond et al., 2007). The lower frequencies could be attributed to more severe parkinsonian syndrome associated with MPTP treatment in primate models. However, in rodent PD models generated by unilateral midbrain lesioning with 6-OHDA, the enhanced oscillatory activity seen in the extrastriatal basal ganglia LFPs occurs at frequencies similar to those observed in PD patients (Sharott et al., 2005b; Mallet et al., 2008a).

1.5.2. Correlation with motor impairments

A substantial body of evidence indicates that the excessive beta band synchrony is particularly anti-kinetic. First, dopamine replacement therapy or high-frequency STN stimulation (>60 Hz in DBS) leads to the suppression of synchronised beta band activity, which correlates with the degree of motor symptom improvements (Benabid, 2003; Kühn et al., 2006; Kühn et al., 2008). Likewise, lesioning of the STN, a common PD treatment before being replaced by high-frequency stimulation (HFS), is shown to reduce synchronised burst firing (Ryan and Sanders, 1993; Burbaud et al., 1995; Ni et al. 2000; Tseng et al., 2001b). Moreover, the distribution of beta band activity in the STN is concentrated in the motor territories (Weinberger et al., 2006). The fact that low-frequency (<30 Hz) stimulation (LFS) of the STN in PD patients worsens the symptoms strongly suggests that the hypersynchronous activity is mechanistically crucial for causing motor impairments (Chen et al., 2007; Eusebio et al., 2008; Chen et al., 2011). The manifestation of parkinsonian symptoms due to excessive beta band activity is also consistent with its functional role in motor control. Under normal condition, beta band rhythm is particularly pronounced during steady contractions,

movement prevention in Go, NoGO tasks, and holding periods following movements, but is attenuated by movement preparation and execution (Engel and Fries, 2010). Therefore it has been suggested that the exaggerated beta-band synchronized bursting in PD restricts the ability of neurons to code information spatially and temporally, since both adjacent and spatially distributed neurons are preferentially locked to the same rhythm (Brown, 2007; Hammond et al., 2007).

1.5.3. Possible underlying pathophysiological mechanisms

How loss of dopamine in PD leads to excessive synchronised bursting in the STN and associated nuclei, and the anatomical origin(s) of its occurrence, is still unclear. The generation of pathological synchrony may have an intrinsic origin within the basal ganglia, and/or requires externally driven forces through the input nuclei.

Being potential pacemaker in the basal ganglia, the pathological rhythms could arise from the STN–GPe network under dopamine-depleted condition. As discussed previously, cocultured STN and GPe neurons in dopamine-free medium exhibit low-frequency (~ 1 Hz) rhythmic bursting activity (Plenz and Kitai, 1999). A critical component driving the rhythm is rebound burst firing in the STN neurons due to strong hyperpolarising input from GPe neurons. However, similar experimental observation of such oscillatory interaction in native preparations is lacking. Extracellular recordings of STN slices showed that the nucleus fails to exhibit synchrony even when the neurons are in burst firing mode (Wilson et al., 2004), or after chronic dopamine depletion with preserved GPe–STN connectivity (Wilson et al., 2006). Synchronised firing between neurons in the GPe and STN are also not observed either in resting state or when burst spiking in the STN and GPe is induced (Loucif et al., 2005).

These results suggest that external sources of input are required to entrain oscillatory activity in the STN–GPe network. This leads to another hypothesis, proposing that abnormal hypersensitivity of STN to idling cortical rhythms is required for pathological synchrony in STN–GPe–GPi network. In PD, low-frequency (<30 Hz) synchronisations within and across STN, GPe, and GPi are coherent with the cortical activity (Hutchison et al., 2004; Hammond et al., 2007; Dejean et al., 2008; Litvak

et al., 2011). PD patients and parkinsonian animals also exhibit cortical synchronized oscillations with overall phase that precedes those in the STN (Williams et al., 2002a; Magill et al., 2006), suggesting that cortical input is driving the widespread synchrony. In anaesthetised rats lesioned by 6-OHDA, coherence of oscillatory spiking activity in STN and GPe with the cortex is dependent on the cortical SWA (Magill et al., 2001). According to this hypothesis, STN relays the directly received cortical rhythmic activity to the GPe and GPi through feedforward excitation. Feedback inhibition from GPe may further enhance the coupling of excitatory input to intrinsic firing (Baufreton et al., 2005). In genetic absence epilepsy rats, cortical input is capable of driving ~ 7–10 Hz rhythmic activity within STN and GPe during cortical seizures, sustained through rebound burst excitation in the STN by feedback inhibition from GPe (Paz et al., 2005).

Another hypothesis puts forward striatum as the source of beta band frequency rhythms in PD. Acute dopamine depletion in dopamine transporter knockout mice is associated with a relative increase in beta (and delta) frequency band activities in the striatum (Costa et al., 2006). Enhanced levels of cholinergic drive, a condition found in 6-OHDA-lesioned rats (Ikarashi et al., 1997), lead to increased beta oscillations in the striatum of normal rats (McCarthy et al., 2011). Activity at beta band frequency can be readily detected in LFP recordings from distributed striatal regions of normal monkeys (Courtemanche et al., 2003). In 6-OHDA-lesioned rats, MSNs exhibit higher firing probability during the up states driven by cortical input (Tseng et al., 2001a). Although it has been proposed that the synchronised pauses and bursts in GPe neurons originate from the striatal–GPe input, there is little evidence from PD and classical PD models that beta band synchronisation is exacerbated in the MSNs. Instead, *in vivo* electrophysiological studies suggest that increased effective connectivity from the striatum to GPe in parkinsonism may profoundly contribute to beta band synchronisation in the extrastriatal basal ganglia (Cruz et al., 2011; Moran et al., 2011). Hyperactivity of the striatal–GPe input might alter the interaction mode between STN and GPe, thus contributing to the genesis of pathological activity pattern (Terman et al., 2002). Therefore, activity changes in the striatum are presumably more important for promoting the emergence of pathological synchronisations in the extrastriatal basal ganglia through altered connectivity in the indirect pathway.

1.6. Cellular principles underlying the regulation of GPe-STN inhibition

Growing evidence indicates strong correlation of activity patterns in STN with the symptoms of PD and has highlighted pivotal roles of GABAergic GPe–STN input in the emergence of synchronised, burst firing activity in the extrastriatal basal ganglia (as discussed in Section 1.5.3). Whether cortical–STN pathway, indirect pathway, and/or STN–GPe network itself are the primary generators of pathological activity patterns in PD, GABAergic transmission in the STN is likely to be crucial for their manifestation. The purpose of this section is to explore the cellular principles underlying the patterning of STN activity by GABAergic inhibition arising from the GPe in PD, the possible effect of DBS on GPe-STN transmission, and why GPe-STN activity is largely uncorrelated under normal conditions.

1.6.1. GABAergic inhibition in the STN

GABAergic input to the STN predominantly arises from the GPe. The GPe innervates widely distributed regions of STN through ipsilateral and topographically-organised projections (Smith et al., 1990; Shink et al., 1996; Bevan et al., 1997), and are largely reciprocated by an excitatory projection from the STN (Shink et al., 1996). The GPe–STN input is mainly mediated by phasic transmission at synaptic $GABA_A$ receptors (Hallworth et al., 2005), which are fast-acting, ligand-gated Cl^- channels (Goetz et al., 2007). Brief single electrical stimulation of GPe axons evokes a rapidly decaying inhibitory postsynaptic potential or current (IPSP or IPSC) that reverses at –83 mV and is blocked by $GABA_A$ receptors antagonists (Bevan et al., 2002, Hallworth et al., 2005, Loucif et al., 2005). Although perisynaptic $GABA_B$ receptors are also expressed on postsynaptic STN neurons, they are only activated by multiple synchronous GPe-STN inputs (Baufreton et al., 2005). Presynaptic $GABA_B$ receptors are only involved in tonic inhibition of synaptic inputs to the STN (Shen and Johnson, 2001; Chen and Yung, 2005). Therefore, GABAergic inhibition in the STN is predominantly defined by

GPe-STN input that is mediated through synaptic $GABA_A$ receptors.

1.6.2. The impact of GPe-STN inhibition on STN activity rate in PD

The loss of dopamine neuromodulation in PD lead to changes in the firing rate of elements within the indirect pathway of basal ganglia. Dopamine actions at the striatum are particularly crucial for the regulation of striatal–GPe transmission and thus the impact of GPe on STN activity. Specifically, dopamine acting at postsynaptic D2 receptors reduces the excitability of striatal–GPe neurons by reducing voltage-dependent Ca^{2+} (Ca_v) class 1.3 current (Hernandez-Lopez et al., 2000). Hypoactivation of postsynaptic D2 receptors due to dopamine depletion enhances $Ca_v1.3$ current (Day et al., 2006), thus increasing the firing activity of striatal–GPe projection neurons. This consequently leads to the enhancement of striatal–GPe transmission (Ingham et al., 1997).

SNc dopaminergic neurons also innervate the GPe (Rommelfanger and Wichmann, 2010). At striatal–GPe synapses, dopamine acting on presynaptic D2 receptors reduces release probability of GABA (Cooper and Stanford, 2001; Watanabe et al., 2009). Postsynaptic D4 receptors in GPe also mediate reduction of $GABA_A$ IPSCs (Shin et al., 2003). Intrapallidal injection of 6-OHDA caused moderate motor impairment, accompanied by reduction in spontaneous firing rate of GPe neurons (Bouali-Benazzouz et al., 2009), suggesting that local dopaminergic modulation overall exerts an excitatory effect on GPe neurons. Therefore, dopamine loss at both striatal and GPe level enhances the activity of indirect pathway, consistent with the prediction by classical Albin-Delong model (Albin et al.,1989; Delong, 1990).

The enhanced striatal–GPe pathway could be observed *in vivo* through the response of STN to cortical activation following loss of dopamine modulation. In response to a brief excitation of the cortex, STN exhibits a triphasic sequence of activity. First response is excitatory, mediated by cortical–STN pathway, followed by a brief period of strong feedback inhibition from the GPe. This is, in turn, followed by a second phase of excitation because of GPe inhibition by the striatal input, hence relieving inhibition on the STN. Application of dopamine receptor antagonists enhanced

the second phase of excitation, which could be explained by enhanced striatal–GPe transmission in the indirect pathway (Degos et al., 2005). Likewise, cortical activation in dopamine-depleted animals powerfully inhibits GPe neurons and disinhibits STN neurons (Magill et al., 2001).

Increased activity of the indirect pathway in PD following dopamine depletion leads to hyperactivity of the STN, which more powerfully excites the inhibitory basal ganglia output nuclei, GPi and SNr. Indeed, inactivation of the STN, either through chemical injections (lidocaine or GABA agonist muscimol) or ablative lesioning alleviates parkinsonian motor symptoms in MPTP-treated primates and humans with PD (Wichman et al., 1994; Levy et al., 2001; Patel et al., 2003). However, PD-related changes in activity rate are often accompanied by changes in abnormal pattern. The relationship between the two phenomena has yet to be defined due to the difficulty in studying these variables separately. Thus, besides reduced and increased GPe and STN mean firing rate respectively in experimental PD, firing activities of GPe and STN neurons are in synchronised bursting mode and more rhythmically entrained by the cortex (Mallet et al., 2008a,b). *In vivo* electrophysiological and computational modelling studies also suggested that increased activity of the striatal–GPe pathway in the dopamine-depleted and PD brain might promote rhythmic oscillatory activity in the STN–GPe network (Terman et al., 2002; Moran et al., 2011). Taken together, these results imply that the loss of dopamine actions alters firing rate and pattern of STN, both of which may be important for PD pathophysiology.

1.6.3. The impact of GPe-STN inhibition on STN activity pattern in PD

Synchronised, rhythmic low-frequency burst firing in the STN of idiopathic and experimental PD individuals is well documented, and is highly correlated to motor impairments, as described in previous section. Data from *in vivo* electrophysiological studies suggests that GPe–STN input plays a critical role in the manifestation of the abnormal activity pattern within the STN. Thus, GPe-STN neurons fire in antiphase synchrony with the STN neurons in experimental PD (Mallet et al., 2012). Inactivation of GPe with muscimol abolishes the synchronised burst firing in the STN and rescues

parkinsonian motor symptoms (Tachibana et al., 2011). *Ex vivo* studies, on the other hand, have provided us important observations for understanding the cellular mechanisms underlying the pathophysiological role of GPe–STN input in STN firing pattern.

Consistent with the anatomical studies, electrophysiological recordings from rodent brain slices found that STN neurons receive multiple synaptic connections from single GPe neurons because the unitary $GABA_A$ receptor-mediated conductance is about 10 times larger than the mean the miniature (univesicular) synaptic conductance (0.7 nS; Baufreton et al., 2009). Each STN neuron is estimated to receive ~ 880 GPe–STN synaptic inputs and each input contributes a conductance of ~ 0.7 nS. Therefore, the total conductance arising from GPe–STN transmission is potentially very potent (~ 600 nS). Although smaller single IPSPs tend to disrupt firing of STN in a more variable and partial fashion, large IPSPs, which may be provided by synchronous GPe input *in vivo*, reset the phase of oscillatory activity by complete deactivation of the voltage-dependent Na^+ (Na_v) channels that underlie autonomous activity (Bevan et al., 2002; Baufreton et al., 2005). Indeed, dynamic clamp approach (i.e. injecting various synthetic GPe–STN synaptic conductances into the STN neurons) suggests that only 4% synchronised GPe–STN inputs are sufficient to inhibit and synchronise autonomous firing of STN neurons (Baufreton et al., 2009).

Apart from direct patterning of GPe–STN input on STN firing activity, the GABAergic inhibition also plays a critical role in the synaptic integration of glutamatergic input. STN receives glutamatergic inputs mainly from the cortex and intralaminar thalamus (Bevan et al., 1995). Glutamatergic excitation of the STN neurons is mediated by rapidly deactivating, highly Ca^{2+}-permeable amino-3-hydroxy-5-methyl-4-isoxazoleproprionic acid (AMPA) receptors and slowly deactivating, relatively weakly voltage-dependent N-methyl-D-aspartate (NMDA) receptors (Gotz et al., 1997; Otsuka et al., 2001). Even though EPSPs alone are sufficient to advance spiking onset in STN neurons, EPSPs preceded by $GABA_A$ receptor-mediated IPSPs are coupled to the next APs more efficiently, i.e. increased rapidity and precision (Baufreton et al., 2005; Farries et al., 2010). This is because about 40% Na_v channels are in inactivated states during autonomous firing, but are deinactivated by IPSPs and hence become

available for depolarisation during the following AP (Do and Bean, 2003). Therefore, threshold of AP generation is lower after an IPSP-EPSP event.

The more effective EPSP-AP coupling in the presence of IPSPs may contribute to enhanced sensitivity of STN to cortical idling rhythms in PD. The rhythmic cortical input could more effectively entrain phase-locked firing in the STN neurons in the presence of feedback and feedforward inhibition from the reciprocally connected GPe. Therefore, synchronised GABAergic inhibition from the GPe might lead to excessive pathological synchrony with cortical beta band oscillations in the STN and subsequently in associated basal ganglia nuclei. Besides, enhanced excitation of GPe neurons due to feedforward hyperactive STN–GPe input in PD may be functionally important for sustaining recurrent inhibition and excitation of the STN–GPe network through stronger feedback GPe-STN inhibition. In addition, synchronised bursts of GPe–STN transmission can generate strong hyperpolarization required for rebound burst firing, mediated by the deinactivation of Ca^{2+} (Ca_v1 and Ca_v3) channels in STN neurons (Bevan et al., 2002; Hallworth and Bevan, 2005). Although inhibition through $GABA_A$ receptor alone is sufficient to hyperpolarize and generate rebound burst firing, synchronous phasic GPe–STN transmission leads to coincident recruitment of perisynaptic $GABA_B$ receptors that produces even longer and higher-frequency form of rebound activity (Hallworth and Bevan, 2005).

Indeed, *in vivo* electrophysiological studies and computational modelling suggest that enhanced functional connectivity between GPe and STN in PD will augment the capability of GPe input to synchronise STN neurons and generate rhythmic burst firing (Cruz et al., 2011; Moran et al., 2011). The strengthening of GPe–STN connectivity could be induced by long-term loss of dopamine neuromodulation in the basal ganglia. In experimental PD, $GABA_A$ receptor agonists generate larger whole cell currents in the postsynaptic STN neurons (Shen and Johnson, 2005). Autoradiography of $GABA_A$ receptor binding also revealed upregulation of its gene expression after chronic dopamine deletion (Yu et al., 2001). However, it is still not clear whether the receptor upregulation is due to changes in the receptor number at synaptic/extrasynaptic sites, receptor subunit composition, and/or the number of functional synapses.

1.6.4. DBS and its possible effects on GPe-STN input

The suppression of synchronised rhythmic bursting in the STN by local DBS is highly effective in improving motor symptoms in PD (Benabid, 2003). It is still not clear how DBS exerts its therapeutic effects, although several mechanisms have been proposed. One possibility is that HFS leads to inactivation of STN neurons (Beurrier et al., 2001; Deniau et al., 2010). Many STN neurons indeed display somatic inhibition during the stimulation (Beurrier et al., 2001; Deniau et al., 2010). However, their axons could be directly stimulated to transmit APs (Nowak and Bullier, 1998; Maurice et al., 2003; Miocinovic et al., 2006) and others may still be able to generate somatically-generated firing faithful to the stimulation frequencies (Garcia et al., 2003, 2005). In addition, afferent axons could be antidromically stimulated and therefore alter the firing activity of neurons projecting to the STN (Li et al., 2007; Santaniello et al., 2012; Walker et al., 2012). Through axon collaterals, antidromic activation of axon terminals can further lead to widespread activation or inhibition of targets remote from site of stimulation (Grill et al., 2008). Fibers of passage within the region of stimulation may also be activated (Miocinovic et al., 2006; Johnson and McIntyre, 2008). Therefore, the impact of DBS on the basal ganglia output nuclei is likely to be very complex.

Another theory proposes that DBS regularizes the firing of basal ganglia output nuclei neurons at high-frequency, increasing synchrony but abolishing pathological low-frequency oscillations (Rubin and Terman, 2004; Guo et al., 2008; Dorval et al., 2010). This is thought to regularize pallidothalamic inhibition and allow the passage of signals through the thalamus to the motor cortex. Contradictory to the belief that DBS entrains STN firing, optogenetic excitatory driving of the neurons at high frequency (and thus replaced the pathological low-frequency burst activity) did not improve motor symptoms in experimental PD (Gradinaru et al., 2009).

A relatively less emphasised feature of STN DBS is that it causes a diversification of basal ganglia output. The cellular and network effects of DBS are very heterogeneous depending on multiple factors, including the intensity and frequency of stimulation, the intrinsic neuronal excitability, the distance of neuronal structures from the stimulation electrodes, and the properties of synaptic transmission on target neurons (Deniau et al., 2010). STN DBS in PD patients and parkinsonian animals (rats and primates)

consistently lead a mixture of increased and decreased firing rates in the basal ganglia output nuclei, along with the suppression of synchronised burst firing (Hashimoto et al., 2003; Degos et al., 2005; Shi et al., 2006; Maltête et al., 2007; Dorval et al., 2008 Reese et al., 2011). Therefore, desynchronisation of firing in the STN (and hence the downstream output nuclei) by DBS could be a key therapeutic effect of the stimulation (Meissner et al., 2005; Wilson et al., 2011; Humphries and Gurney, 2012). The relief from widely synchronised activity may partially allow the coding and transmission of useful motor signals within the cortico-basal ganglia thalamo-cortical networks.

The mechanisms underlying the desynchronisation of neuronal activity in the STN remain unclear. Besides direct heterogenous effects of HFS on STN neuronal somata and their axonal processes, its synaptic effects on STN afferents may also critically underlie the desynchronising effect. Considering that GPe–STN synaptic transmission is heavily depressed even upon short bouts of stimulation (Baufreton et al., 2009), HFS of the afferents in DBS could effectively abolish GPe input to the STN, hence preventing the genesis and/or exacerbation of pathological oscillatory activity in STN. Indeed, optogenetic HFS driving of afferents within the STN of parkinsonian rodents rescued motor impairments (Gradinaru et al., 2009).

1.6.5. The decorrelated nature of GPe-STN network

Although unitary multisynaptic GPe–STN inputs powerfully pattern STN activity, correlated GPe–STN activity is rarely observed *ex vivo* or *in vivo* under normal conditions (Wichmann et al. 1994; Raz et al. 2000; Urbain et al. 2000; Hallworth and Bevan, 2005; Loucif et al., 2005; Mallet et al. 2008b). In slices where connections between the GPe and STN are retained, STN neurons fire less frequently and more irregularly compared to the absence of synaptic inputs due to the disruption by tonic but asynchronous autonomous firing of GPe neurons (Hallworth and Bevan, 2005). Given the potency of GPe input to pattern STN activity and high frequency tonic firing of GPe neurons *in vivo* (eg. ~ 33 Hz in rat; Urbain et al., 2000), it is surprising that the GPe–STN activity is uncorrelated in nature and that STN neurons are capable of maintaining their tonic discharge. The underlying cellular mechanisms could be

functionally important for the prevention of synchronised, rhythmic burst firing of STN neurons and hence dysfunctional motor coding in PD.

First, the decorrelated nature of the GPe and STN activity under normal conditions is in part attributed to the anatomical feature of GPe–STN network. In the rat, the GPe and STN consist of 46000 and 13600 neurons respectively (Oorschot, 1996). However, each GPe–STN neuron is estimated to maximally only innervate 2% of STN neurons (Baufreton et al., 2009). This is probably an overestimation because individual GPe–STN terminal fields are clustered, suggesting multiple terminations onto individual STN neurons. Each STN neuron is also thought to receive only input from less than 2% of GPe neurons. Simultaneous recordings from STN neurons confirm that neighbouring STN neurons share little inputs from common GPe neurons (Baufreton et al., 2009). Therefore, single GPe neurons innervate a tiny, sparsely distributed, fraction of STN neurons, and each STN neuron receives input from a similarly limited and distinct set of GPe neurons.

Another likely explanation is short-term plasticity of GABAergic synaptic transmission. Because synaptic depression occurs even during short period of intense stimulated transmission (Baufreton and Bevan, 2008), the strength of GPe–STN synaptic transmission may be heavily dependent on the recent firing history of GPe neurons. Indeed recent work from our research group showed that GPe–STN synaptic inputs exhibited a high probability and amplitude of transmission that declined dramatically within 2 s of stimulation at the mean rate of GPe activity *in vivo* (33 Hz), due to limited supply of release-ready vesicles (not published). Furthermore, synchronous inhibition of tonically active GPe–STN neurons or phasic activity of GPe–STN neurons was required to reliably pattern STN activity.

Third, local actions of dopamine in the STN at a variety of pre- and post-synaptic receptors are possibly a contributing factor. STN neurons express both D1-like (D5) and D2-like (D2 and D3) receptors (Flores et al., 1999; Baufreton et al., 2003; Ramanathan et al., 2008), whereas the axon terminals of STN afferents express D2-like receptors only (Shen and Johnson, 2000; Baufreton and Bevan, 2008). Dopamine acts on STN neurons directly through D1- and D2-like receptors, which overall depolarise the membrane potential and increase the frequency and irregularity of

their autonomous activity (Baufreton et al., 2003; Zhu et al., 2002a; Zhu et al., 2002b; Loucif et al., 2008; Ramanathan et al., 2008). This postsynaptic effect of dopamine could potentially reduce the impact of hyperpolarising GABAergic inhibition on STN firing. At inhibitory terminals, the synaptic GABA release is reduced by the activation of presynaptic D2 dopamine receptors (Shen and Johnson, 2000; Cragg et al., 2004; Baufreton and Bevan, 2008). Specifically, dopaminergic modulation suppresses the initial release probability of GABA but does not affect steady-state depression at GPe–STN synapses (Baufreton and Bevan, 2008). Therefore, phasic bursts of GPe–STN input are dampened in transmission strength by dopamine, making them less capable to reset, synchronise autonomous firing, and evoke rebound bursting in the STN.

Lastly, the complex interaction of inhibitory input with intrinsic properties of STN neurons could in part contribute to the decorrelation of GPe–STN network activity. In comparison to other major ion channels in STN neurons, the role of HCN channels is poorly understood, because they minimally contribute to autonomous firing and previously studied forms of synaptic integration (Bevan and Wilson, 1999; Beurrier et al., 2000; Do and Bean, 2003; Baufreton et al., 2005). Since they both require prolonged hyperpolarisation below voltages associated with spontaneous firing, the low-voltage-gated Ca^{2+} and I_h currents often occur together. This leads to the speculation that HCN channels are important to oppose GPe–STN inhibition that deinactivates Ca_v3 channels, thus reducing the propensity of rebound burst firing being generated in STN neurons.

1.7. Optogenetics

Optogenetics refers to the integration of optical and genetic methods to accomplish gain or loss of function of well-defined events within specific cell types of living tissue. It allows technologies for delivering light into tissues under investigation to control the activity of cells of interest and obtain readouts from the evoked activity (Deisseroth 2010, 2011). This section will briefly discuss the significance of optogenetics, the tools currently available, the methods of optogenetic targeting, and relevance of the technology to the pathophysiological study of basal ganglia network in PD.

1.7.1. Significance

The major challenge in the history of neuroscience research is the ability to control one cell type while leaving others unaltered as suggested by Francis Crick in 1979. Electrical stimulation has probably been the most common method to control neuronal activity, but is confounded by its non-specificity and heterogeneity of stimulation effects. Pharmacological manipulation resolves specificity issue, but is not temporally precise because drugs often act very slowly. Optogenetic control with spatial and temporal precision has been recently shown to be feasible in intact living mammalian tissue and even freely moving animals (Deisseroth et al., 2006; Adamanditis et al., 2007; Aravanis et al., 2007). This is achieved through the introduction of microbial opsin gene, which together with the expression of natural all-*trans* retinal – the cofactor necessary for photonic activation of microbial opsins, makes neurons precisely responsive to light (Deisseroth 2010, 2011). Optogenetics therefore enables us to causally dissect complex phenomena in the brain, from molecular, cellular, network to behavioural level.

1.7.2. Optogenetic tools

Three main classes of microbial opsin genes have been identified thus far (Yizhar et al., 2011). The first type is the haloarchaeal proton pump bacteriorhodopsins, which pumps protons from the cytoplasm into the extracellular medium as part of an alternative energy production system. The second class of microbial opsin genes encodes halorhodopsins. Instead of pumping protons, halorhodopsins pump chloride ions from the extracellular space into the cytoplasm. The third class identified is channelrhodopsins or ChRs. Unlike bacteriorhodopsins and halorhodopsins, ion-conducting activity of ChRs is largely uncoupled from photocycle - ion flux does not depend on retinal isomerisation but rather relies on the kinetics of channel closure (Feldbauer et al., 2009). ChRs, bacteriorhodopsins, halorhodopsins have all been demonstrated capable of activating or inhibiting neurons rapidly and safely in response to a diversity of light wavelengths. For fast optogenetic neuronal excitation, ChRs, particularly ChR2, is efficient in

depolarising and initiating action potentials with precise temporal control in response to time-locked light pulses (Zhang et al., 2006; Fenno et al., 2011).

1.7.3. Opsin targeting

Optogenetic tools are continuously being optimised for more efficient transcription, membrane expression and safety (Fenno et al., 2011). Additionally, specificity *in vivo* targeting of the optogenetic tools is also crucial for well-defined control of neuronal activity. Opsin targeting is generally performed through the use of viral expression system or generating genetically modified animal lines. Targeting with viruses (eg. lentiviral vector, adeno-associated viral vector) are advantageous in many aspects, including rapidity, flexibility, potency due to high expression levels, and genetic and anatomical specificity. It is still a challenge to design neuron-type-specific promoter fragments that are small enough to be carried by viral systems due to limited packaging capacity (Yizhar et al., 2011). This limitation can be overcome through the use of recombinase-dependent opsin-expressing viruses. Alternatively, cell-type specific opsin expression can also be achieved by generating mouse transgenic lines that express local promoter-driven opsin genes (Yizhar et al., 2011). Although producing and maintaining transgenic mouse lines require relatively more time, effort and cost, homogenous and consistent opsin expression between animals provides greater convenience and reliability.

1.7.4. Optogenetics and DBS

Thy1-ChR2-EYFP lines expressing ChR2 under control of the *Thy1* promoter are one of the early generated transgenic mouse strains that have been used in a variety of studies (Arenkiel et al., 2007). Many promoters including *Thy1* do not completely define cell types and therefore the expression pattern of opsins often requires detailed characterisation. Thy1-driven expression is mainly restricted to projection neurons (Arenkiel et al., 2007). Recent optogenetic study using one of the *Thy1-ChR2-EYFP* lines found that DBS in the STN is most effective in correcting parkinsonian symptoms

when the direct target is afferent axons within the structure (Gradinaru et al., 2009). It is however not clear which afferent axons are involved because the expression pattern of ChR2 in the STN of the mouse line has not been characterised. Cell-specific control of neuronal activity with optogenetics as demonstrated in this study should help us dissect PD circuitry and identify the most effective therapeutic manipulation in DBS.

1.8. Aims of the thesis

To conclude, the loss of midbrain dopamine in idiopathic and experimental PD results in not only changes in mean firing rates of the basal ganglia nuclei, but also changes in activity patterns that are critical for PD pathophysiology. Thus, GPe and STN exhibit hypo- and hyper-activity, respectively, and abnormal synchronous rhythmic burst firing at <30 Hz. Both acute and chronic loss of dopamine in the STN (in addition to striatum, GPe) may enhance the functional connectivity of GPe–STN input, hence strengthening its capability to synchronise firing in STN neurons and generate rhythmic burst firing.

Suppression of the pathological oscillations in the STN (and associated nuclei) by local DBS is highly correlated with the relief from motor impairments in PD. However, the mechanisms of DBS are still unclear. The emergence of optogenetics allows us to dissect the relevant neuronal circuits responsible for the manifestation of parkinsonian motor symptoms. Indeed, recent application of the technique suggests that HFS of STN exerts its therapeutic effects through manipulation of afferent activity in the nucleus, although the involvement of GPe-STN input is unknown.

Given the potency of GPe input to pattern and synchronise STN activity, the decorrelated nature of GPe–STN network under normal conditions is somewhat unexpected. The possible contributing factors include sparse and selective afferent connectivity, synaptic depression and dopaminergic modulation of the GPe–STN input. Intrinsic properties of STN neurons that affect inhibitory synaptic integration, such as HCN channels, might additionally be important, but yet to be characterised.

To further elucidate the mechanisms that regulate the GPe–STN input in health and disease, three studies were carried out in accordance to the following objectives:

1. To define alterations in GPe–STN connectivity following chronic depletion of dopamine in 6-OHDA-lesioned rodent models of PD.
2. To examine ChR2 expression in the STN of *Thy1-ChR2-EYFP* transgenic mice and hence elucidate the mechanisms underlying therapeutic effects of DBS.
3. To characterise the role of HCN channels in the STN neurons in integrating GABAergic synaptic input.

CHAPTER 2

PROLIFERATION OF GLOBUS PALLIDUS-SUBTHALAMIC NUCLEUS SYNAPSES FOLLOWING DEGENERATION OF MIDBRAIN DOPAMINE NEURONS

2.1. Introduction

The reciprocally connected GABAergic GPe and glutamatergic STN occupy pivotal positions in cortico-basal ganglia-thalamo-cortical networks necessary for action selection (Smith et al., 1998). In PD degeneration of SNc dopamine neurons leads to hyperactivity of D2-MSNs and hypo- and hyper-activity of GPe and STN neurons, respectively, which together contribute to the excessive inhibitory output of the parkinsonian basal ganglia (Gerfen and Surmeier, 2011; Wichmann et al., 2011). Abnormal hypersynchronous rhythmic (<30 Hz) burst firing may also contribute to motor symptoms because: 1) this activity pattern is prevalent in the parkinsonian basal ganglia; 2) reduction of hypersynchronous rhythmic activity through dopamine-based therapies or high frequency (>60 Hz) electrical stimulation is associated with the relief from motor symptoms; 3) electrical stimulation of the STN at <30 Hz exacerbates symptoms (Benabid et al., 2009; Zaidel et al., 2009; Jenkinson and Brown, 2011; Wichmann et al., 2011).

Although loss of dopaminergic neuromodulation directly contributes to abnormal STN activity in PD (e.g. Galati et al., 2009), alterations in cellular and network properties may also be significant because abnormal activity develops slowly over 2–3 weeks following lesion of midbrain dopamine neurons (Vila et al., 2000; Mallet et al., 2008a). During this period there are adaptive changes in elements of the "indirect" pathway. In D2-MSNs, corticostriatal axospinous synapses reduce and inhibitory inputs from fast spiking GABAergic interneurons remarkably increase in number, probably in response to reduced inhibition following loss of D2 receptor activation (Day et al., 2006; Gittis et al., 2011). In addition, autonomous firing activity of STN neurons is reduced (Zhu et al., 2002a; Wilson et al., 2006). These adaptations may reflect homeostatic compensatory processes triggered by hyperactivity of D2-MSNs and STN neurons but could also be maladaptive by contributing to the manifestation of abnormal firing patterns.

The GPe is the main source of GABAergic input to the STN (Smith et al., 1998) and patterns activity predominantly through $GABA_A$ receptors (Hallworth and Bevan, 2005). The hyperpolarised equilibrium potential of postsynaptic $GABA_A$ receptor current (Bevan et al., 2002) and the unitary and collective strength of GPe–STN inputs

(Baufreton et al., 2009) enable the GPe to: inhibit and synchronise STN activity through deactivation of pacemaker Na_v channels (Baufreton et al., 2005, 2009); promote synaptic excitation through deinactivation of Na_v channels (Baufreton et al., 2005); and generate rebound burst firing through deinactivation of Ca_v1 and Ca_v3 channels (Bevan et al., 2002; Hallworth and Bevan, 2005). Given the capability of GPe inputs to strongly pattern STN activity and evidence for enhanced functional connectivity between the parkinsonian GPe and STN *in vivo* (Mallet at al., 2008a, b; Cruz et al., 2011; Moran et al., 2011), this study therefore sought to determine whether the loss of midbrain dopamine neurons leads to adaptations in GPe–STN synaptic properties that may compensate for and/or contribute to abnormal STN activity.

2.2. Materials And Methods

Experiments were performed in accordance with institutional, NIH and Society for Neuroscience guidelines using male Sprague-Dawley rats (Charles River) except for quantitative PCR where male C57/B6 mice (Charles River) were used due to the availability of species specific primers.

2.2.1. Surgery and slice preparation

Under ketamine/xylazine anaesthesia unilateral, stereotaxic injections of 6-OHDA (mouse: 2.5 µl 3 mg/ml; rat: 4–5 µl 3–5 mg/ml at a rate of 0.5–1 µl/min) or vehicle were made in the substantia nigra or medial forebrain bundle (MFB). The animals were also treated with systemic injections of desipramine (25 mg/kg) and pargyline (50 mg/kg) to minimise the effect of 6-OHDA on noradrenergic fibres and to enhance the toxicity of the toxin, respectively. In order to assess the degree of associated motor impairment forelimb use asymmetry was assessed 1–2 weeks post-surgery, as described previously (Schallert et al., 2000). The number of spontaneous exploratory touches made by each forepaw on the wall of a clear plastic cylinder (18 cm wide for rats; 9 cm wide for mice) was recorded using a digital camcorder for 10–20 minutes over 2 sessions and scored using iMOVIE (Apple).

Approximately 2–3 weeks post-surgery 6-OHDA- and vehicle-injected animals were perfused transcardially under ketamine/xylazine anesthesia with ice-cold modified artificial cerebrospinal fluid (ACSF). 6-OHDA-injected animals (n = 44) were perfused 17.9 ± 4.2 days after surgery and vehicle-injected animals (n = 13) were perfused 19.4 ± 3.8 days after surgery. Age-matched control animals (n = 23) were also transcardially pefused with the same solution. At the time of perfusion 6-OHDA-injected, vehicle-injected and age-matched control animals were 55.3 ± 16.6, 67.3 ± 9.2 and 53.0 ± 15.1 days old, respectively. Modified ACSF was equilibrated with 95% O_2/5% CO_2, and contained (in mM): 230 sucrose, 26 $NaHCO_3$, 2.5 KCl, 1.25 NaH_2PO_4, 0.5 $CaCl_2$, 10 $MgSO_4$ and 10 glucose. Each brain was sliced at 250–300 μm (for *Electrophysiology/ quantitative PCR*) or at 125 μm (for *Immunocytochemistry for synaptic markers*) in the sagittal plane using a vibratome (Vibratome 3000; Leica Microsystems). Slices containing the STN were stored in ACSF, which was equilibrated with 95% O_2/5% CO_2 and contained (in mM): 126 NaCl, 26 $NaHCO_3$, 2.5 KCl, 1.25 NaH_2PO_4, 2 $CaCl_2$, 2 $MgSO_4$ and 10 glucose, prior to further processing.

2.2.2. Electrophysiology

Slices were perfused with ACSF, which was heated to ~ 35°C, equilibrated with 95% O_2/5% CO_2 and contained (in mM): 126 NaCl, 26 $NaHCO_3$, 3 KCl, 1.25 NaH_2PO_4, 1.6 $CaCl_2$, 1.5 $MgSO_4$, 10 glucose, 0.05 d-(–)-2-amino-5-phosphonopentanoic acid (APV), 0.02 6,7-dinitroquinoxaline-2,3-dione (DNQX) and 0.002 (2S)-3-[[(1S)-1-(3,4-dichlorophenyl)ethyl]amino-2 hydroxypropyl](phenylmethyl)phosphinic acid (CGP 55845). APV, DNQX and CGP55845 were used to block NMDA, AMPA/kainate and $GABA_B$ receptors, respectively, so that $GABA_A$ receptor-mediated currents could be studied in relative isolation (Bevan et al., 2002; Hallworth and Bevan, 2005). Miniature inhibitory postsynaptic currents (mIPSCs) were recorded in the additional presence of 0.5 μM tetrodotoxin (TTX). In some cases sulpiride (2 μM) was added to block D2 dopamine receptors. Drugs were purchased from Abcam except for sulpiride, which was obtained from Tocris.

Somatic patch clamp recordings were obtained under visual guidance

(Axioskop FS2, Zeiss) using computer-controlled manipulators (Luigs & Neumann) and a Multiclamp 700B amplifier and digidata 1440A digitizer controlled by PClamp 10 (Molecular Devices). Pipettes contained (in mM): 135 CsCl, 3.6 NaCl, 1 $MgCl_2$, 10 HEPES, 10 QX-314, 0.1 Na_4EGTA, 0.4 Na_3GTP and 2 $Mg_{1.5}ATP$ (pH 7.2, 290 mOsm) or 130 Kgluconate, 3.6 Nagluconate, 1 $MgCl_2$, 10 HEPES, 10 QX-314, TEA-Cl 5, 0.1 Na_4EGTA, 0.4 Na_3GTP and 2 $Mg_{1.5}ATP$ (pH 7.2, 290 mOsm) for the recording of $GABA_A$ receptor-mediated mIPSCs and evoked currents, respectively. mIPSCs were recorded at –60 mV. Evoked IPSCs and isoguvacine-evoked current were recorded at –50 mV. Weighted decay kinetics of mIPSCs were calculated from τ decay = $(A1*\tau1 + A2*\tau2)/(A1 + A2)$ where A and τ refer to the amplitude and decay constants, respectively, of biexponential fits of mIPSCs. Data were analysed with Clampfit 10 (Molecular Devices), Igor Pro 6 (Wavemetrics) and Origin 8 (OriginLab).

2.2.3. Quantitative PCR

The STN was microdissected from 250 μm sagittal slices prepared as described above. STN RNA was first isolated using RNeasy Plus Mini Kit (Qiagen). STN cDNA was then synthesised using qScript cDNA Supermix (Quanta Biosciences) under the following conditions: 5 min at 25°C, 30 min at 42°C, 5 min at 85°C, and then held at 4°C. Quantitative PCR was run in triplicate, including negative controls, using SYBR Green I on a StepOnePlus thermocycler (Applied Biosystems) under the following conditions: 95°C for 20 s, 40 cycles at 95°C for 3 s and 60°C for 30 s. The PCR cycle threshold (CT) values were set in StepOne Plus (Applied Biosystems) within the exponential phase of the PCR reaction. Custom synthesised primers (Invitrogen) were desalted and intron-spanning. Melting curves verified amplification of single PCR products. Primers were further validated with PCR and gel electrophoresis of whole brain tissue samples to confirm the amplification of PCR products with the predicted molecular weight. After performing quantitative PCR, outliers were removed from triplicates if the SD of the PCR cycle was >0.3. Samples that showed an SD >0.3 after outlier removal were excluded from further analysis.

A relative quantification approach, the ΔΔCT method, was used to compare

transcript levels. Expression levels were normalised to 5 housekeeping genes: gapdh, atp5b, sdha, uchl1 and cyc1. The contribution of each gene was weighted to its relative stability, based on the integration of four algorithms: geNorm (Vandesompele et al. 2002), Normfinder (Andersen et al. 2004), BestKeeper (Pfaffl et al. 2004) and the comparative ΔCt method (Silver et al. 2006; integration tool available at http://www.leonxie.com/referencegene.php). Expression data are presented as fold difference relative to control.

2.2.4. Immunocytochemistry of synaptic markers

125 µm thick sagittal slices, prepared as described above, were immersion-fixed in 4% paraformaldehyde in phosphate buffer (PB; 0.1 M, pH 7.4) at room temperature for 20 min. After washing in phosphate buffer saline (PBS; 0.01 M) slices were incubated in primary antibodies (Synaptic Systems), as indicated in Table 2.1, in PBS plus 0.3% Triton X-100 (Sigma-Aldrich) and 2% normal donkey serum (NDS) for 48 h at 4°C. After washing, slices were incubated in fluorescent secondary antibodies (Jackson Immunoresearch; Table 2.1) in the same diluent for 2 h at room temperature. Slices were then mounted in ProLong Gold (Invitrogen) on glass slides and coverslipped.

Immunofluorescent labelling was visualised using confocal laser scanning microscopy (Zeiss LSM 510). Image stacks (16 optical sections each) were acquired using a 63× oil immersion objective (NA 1.4) with a digital zoom of 1.5× (*x*, *y*: 1024 × 1024 pixels, 93 nm per pixel; *z*-step: 0.3–0.4 µm). For multichannel image acquisition fluorophores were excited alternately [excitation wavelengths and corresponding emission filters (in nm): 488, 503-530; 543, >560]. Pinholes were set to the same airy unit for each laser in order to obtain identical optical section thickness. Images were acquired using the same settings and analysed without post-processing. The density, fluorescent intensity and dimensions of immunoreactive structures were assessed with Image J (National Institutes of Health, Bethesda, USA).

The densities of gephyrin-, γ2-, vesicular GABA transporter(VGAT)- and bassoon-immunoreactive structures were quantified using the optical dissector method (West, 1999). Sample sites were chosen using a grid (frame size, 11.9 × 11.9 µm) that

was superimposed randomly on each image stack. Stereological counting commenced at an optical section ~ 4 μm below the slice surface. Immunoreactive structures were counted if they appeared within the sample frame and in the reference but not the adjacent look up section. For gephyrin and γ2 colocalisation, gephyrin-immunoreactive structures were selected stereologically and colocalisation of these structures with γ2-immunoreactive structures was then determined. For VGAT and bassoon colocalisation, VGAT -immunoreactive structures were first selected stereologically and colocalisation with bassoon-immunoreactive structures was subsequently determined. Removal or prior incubation of primary antibodies with their respective immunogenic synthetic peptides abolished specific labelling.

	Antibody	**Species**	**Primary Dilution**	**Secondary antibody**	**Secondary dilution**
double labelling	$GABA_A$ receptor γ2 subunit	Rabbit	1:1000	DyLight 594 donkey anti-rabbit IgG	1:250
	Gephyrin	Mouse	1:300	DyLight 488 donkey anti-mouse IgG	1:250
double labelling	VGAT	Mouse	1:250	Cyanine Cy3 donkey anti-mouse IgG	1:250
	Bassoon	Guinea pig	1:1000	Alexa 488 donkey anti-guinea pig IgG	1:250
single labelling	VGAT	Rabbit	1:1000	DyLight 594 donkey anti-rabbit IgG Or Biotinylated donkey anti-rabbit IgG	1:250

Table 2.1. Antibodies used for immunocytochemistry of GPe–STN synaptic markers

2.2.5. Electron microscopy

Under ketamine/xylazine anaesthesia animals were transcardially perfused with ~ 50 ml HEPES buffered ACSF, which was equilibrated with O_2 and contained (in mM): 140 NaCl, 3 KCl, 1.6 $CaCl_2$, 10 $MgCl_2$, 23 glucose, and 15 HEPES followed by 250 ml 0.1% glutaraldehyde and 4% paraformaldehyde in 0.1 M PB for 15 min, 4% paraformaldehyde in 0.1 M PB for 15 min, and finally 0.1 M PB for 15 min. 75 µm coronal sections were then prepared with a vibratome (VT1000s; Leica Microsystems). In order to permeabilise the tissue in a manner compatible with ultrastructural preservation, sections were equilibrated in cyroprotectant medium (25% sucrose, 15% glycerol in 0.05 M PB) rapidly frozen in cooled isopentane and liquid nitrogen and then thawed at room temperature. After washing in PBS, sections were incubated in rabbit anti-VGAT primary antibody (1:1,000) and 2% NDS in PBS for 48 h at 4°C. Sections were then washed and incubated in biotinylated donkey anti-rabbit IgG (1:500) in the same diluent for 2 h at room temperature. Sections were then washed and incubated in avidin–biotin–peroxidase complex (1:100 ABC-Elite; Vector Laboratories) in the same diluent for 2 h at room temperature before further washing in PBS. Finally, VGAT immunoreactivity was revealed by incubation in 0.025% DAB and 0.0025% hydrogen peroxide in Tris buffer (0.05 M, pH 7.4) for 5–10 min. Sections were then prepared for electron microscopy: sections were post-fixed with 1% osmium tetroxide in 0.1 M PB, dehydrated through a graded alcohol series, contrasted with 1% uranyl acetate and embedded in epoxy resin between coverslips and glass slides (Durcupan, Fluka). STN tissue was then re-sectioned at ~ 70 nm using an ultramicrotome (UCT, Leica Microsystems). Ultrathin sections were mounted on pioloform-coated slot grids, stained with lead citrate and examined using an electron microscope (Tecnai Spirit G2, FEI) equipped with a digital camera. Entire individual ultrathin sections were systematically scanned at ~ 10,000× for VGAT-immunoreactive structures. Each VGAT-immunoreactive structure was then imaged at higher magnification (20,000–25,000×) and measurements were taken using Image J (National Institutes of Health, Bethesda, USA). The dimensions of VGAT-immunoreactive structures, postsynaptic structures and synapses were measured. Synapses were defined according to classical

criteria, i.e. the presence of synaptic vesicles associated with the presynaptic active zone, the presence of a synaptic cleft with cleft material and the presence of pre- and post-synaptic membrane specializations.

2.2.6. Immunocytochemistry for tyrosine hydroxylase (TH)

Brain tissue was immersion-fixed in 4% paraformaldehyde in 0.1 M PB (see section 2.2.1. Surgery and slice preparation) or perfusion-fixed in 0.1% glutaraldehyde and 4% paraformaldehyde in 0.1 M PB (see section 2.2.5. Electron microscopy). Fixed tissue was then sectioned at 70 μm on a vibratome (VT1000s; Leica Microsystems) and processed for the detection of TH using immunofluorescent or immunoperoxidase techniques. For immunofluorescent detection, slices were incubated in 1:500 mouse anti-TH (Millipore) in PBS plus 0.3% Triton X-100 and 2% NDS for 48 h at 4°C. After washing, sections were incubated in 1:200 DyLight 488 donkey anti-mouse IgG in the same diluent for 2 h at room temperature. For immunoperoxidase detection, slices were treated as above except that 1:100 biotinylated donkey anti-mouse IgG (Jackson Immunoresearch) was used as the secondary antibody and sections were subsequently incubated in avidin–biotin peroxidase complex (1:100 ABC-Elite; Vector Laboratories) before peroxidase was revealed with diaminobenzidine tetrahydrochloride (DAB) and hydrogen peroxide, as described above. Sections were mounted on glass slides, coverslipped and then imaged under epifluorescent or brightfield illumination using a microscope (Axioskop, Zeiss) equipped with a software controlled CCD camera (Axiovision/Axiocam, Zeiss). Immunoreactivity was assessed from optical densities acquired with Image J (National Institutes of Health, Bethesda, USA). Specific immunoreactivity for TH was defined as immunoreactivity of the dorsal striatum minus immunoreactivity of the overlying motor cortex in the same section.

2.2.7. Statistics

Data are reported as mean ± SD. Cumulative and box (central line, median; dot, mean; box, 25–75%; whiskers, 10–90%) plots are used to illustrate sample distributions. The

Kolmogorov-Smirnov test was used to test for significant differences in cumulative distribution (Prism 5, GraphPad Software). Mann-Whitney and Wilcoxon signed rank tests were used to test for significant differences between unpaired and paired data, respectively (Prism 5, GraphPad Software). The level of significance was set at an α value of 0.05. Non significant differences are denoted as N.S..

2.3. Results

2.3.1. Impact of chronic dopamine depletion on miniature GABAergic events in STN neurons

In order to determine the impact of chronic dopamine depletion on GPe–STN transmission GABAergic transmission was compared in brain slices derived from animals that had received unilateral 6-OHDA injections in the substantia nigra or medial forebrain bundle ~ 2–3 weeks earlier (n = 44) and control animals that had received similarly timed vehicle injections (n = 13) or were age-matched (n = 23). Data derived from the control groups were similar and were therefore pooled. 6-OHDA-lesioned animals exhibited profound asymmetric forelimb use (forelimb ipsilateral to 6-OHDA injection normalised to total forelimb movement = 75.0 ± 15.7 %, n = 44), which is a faithful marker of substantial dopamine depletion ipsilateral to the preferred forelimb (Schallert et al., 2000). Indeed, TH immunoreactivity of the striatum ipsilateral to the injection of 6-OHDA and forelimb preference was found to be profoundly reduced compared to the contralateral striatum in each 6-OHDA-injected animal (ipsilateral = 1.7 ± 5.5% of contralateral immunoreactivity, n = 44).

Because the GPe is the principal source of GABAergic inputs to STN neurons (Smith et al., 1998) and these inputs are mediated largely through $GABA_A$ receptors (Baufreton et al., 2005, 2009; Hallworth and Bevan, 2005), $GABA_A$ receptor-mediated transmission and its associated molecular and anatomical markers in the STN were used as measures of GPe–STN transmission. The impact of chronic dopamine depletion

on GPe–STN transmission was first assessed by whole-cell patch clamp recording. The frequency of AP-independent transmission, measured in the presence of 0.5 μM TTX, was significantly increased by dopamine depletion (Fig. 2.1; control = 1.05 ± 0.36 Hz, n = 26; 6-OHDA = 1.80 ± 1.59 Hz, n = 35; $p < 0.05$). The decay time constant of mIPSCs was also increased by dopamine depletion (control = 6.48 ± 1.92 ms, n = 26; 6-OHDA = 7.78 ± 2.40 ms, n = 35; $p < 0.05$). However, the mean conductance underlying mIPSCs was unaltered (Fig. 2.1; control = 0.70 ± 0.24 nS, n = 26; 6-OHDA = 0.76 ± 0.23 nS, n = 35; N.S.). Application of the D2-like dopamine receptor antagonist sulpiride (2 μM) to control slices had no effect on the frequency, conductance or decay kinetics of mIPSCs (sulpiride data normalised to control: frequency = 0.95 ± 0.17, n = 7, NS; conductance = 0.86 ± 0.18, n = 7, NS; kinetics = 1.2 ± 0.12, n = 7; N.S.) confirming that basal activation of presynaptic D2-like dopamine receptors (Shen and Johnson, 2000; Baufreton and Bevan, 2008) does not underlie the relatively low frequency and rapid kinetics of mIPSCs in control slices compared to those derived from 6-OHDA-treated animals.

2.3.2. Chronic dopamine depletion augments GPe–STN transmission through postsynaptic mechanisms

In order to further address the contribution of pre- and/or post-synaptic mechanisms to the alteration in GPe–STN transmission, the effect of chronic dopamine depletion on IPSCs evoked by bipolar electrical stimulation of the internal capsule (IC) rostral to the STN at 10 or 50 Hz was studied. Electrical stimulation intensity was increased until the maximum IPSC was evoked. Although the intensity of stimulation required to generate the maximum IPSC was not significantly different in control and 6-OHDA lesion groups (control = 706 ± 78 μA, n = 20; 6-OHDA = 719 ± 69 μA, n = 15; N.S.), dopamine depletion significantly increased the conductance underlying evoked IPSCs (Fig. 2.2; Table 2.2). Dopamine depletion had no effect on the short-term synaptic plasticity of GPe–STN transmission (Fig. 2.2; Table 2.2). Application of the D2-like dopamine receptor antagonist sulpiride (2 μM) to control slices also had no effect on the conductance underlying evoked IPSCs (sulpiride data normalised to control:

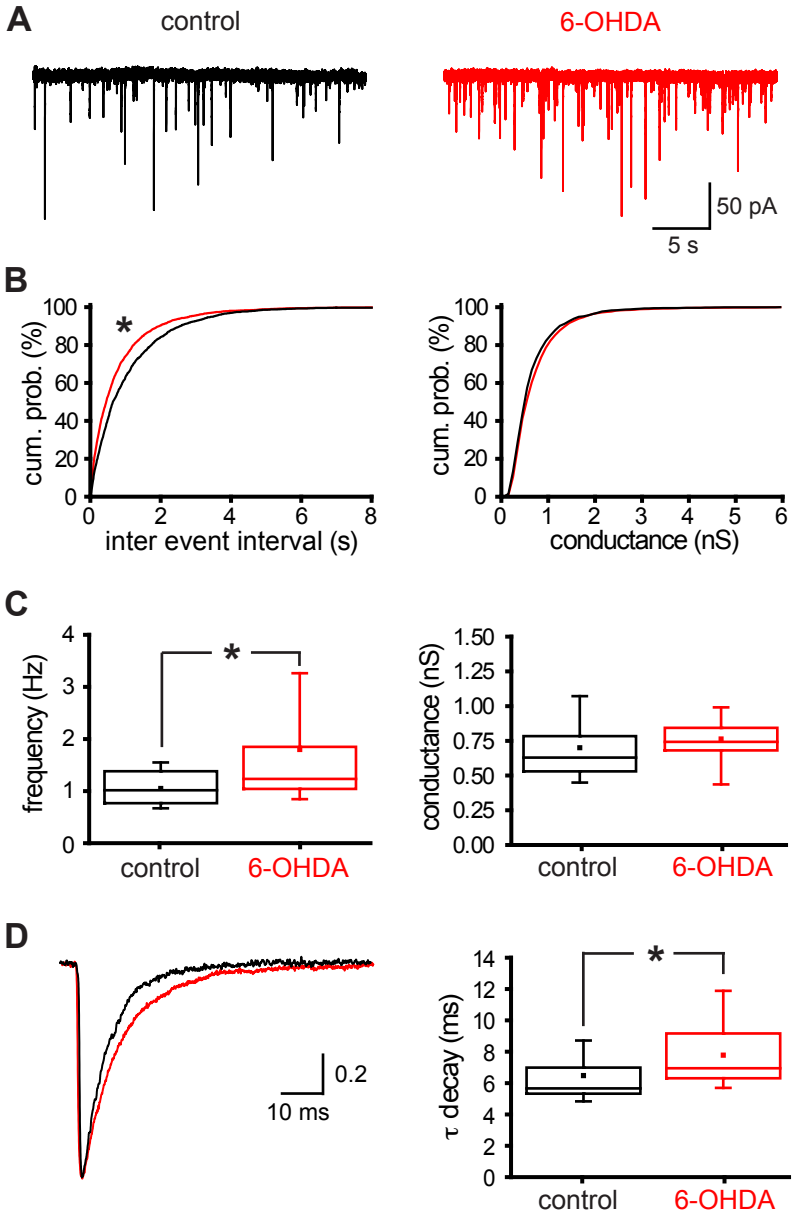

Figure 2.1. Chronic dopamine depletion increased the frequency and prolonged the decay kinetics of mIPSCs

A, representative recordings of mIPSCs in STN neurons derived from control and 6-OHDA-treated animals. The frequency but not the amplitude of mIPSCs was greater following dopamine depletion. B, Cumulative probability (cum. prob.) plots of the sample populations confirmed that dopamine depletion significantly reduced the intervals between mIPSCs but had no effect on the conductance underlying mIPSCs. C, The mean frequency of mIPSCs was significantly enhanced by dopamine depletion, whereas the mean conductance underlying mIPSCs was unaltered. D, The decay of mIPSCs was prolonged by chronic dopamine depletion, as evidenced by representative mean peak-scaled mIPSCs and box plots. * $p < 0.05$.

Figure 2.2. Chronic dopamine depletion increased the magnitude of evoked $GABA_A$ receptor-mediated synaptic transmission but had no effect on short-term synaptic plasticity

Following chronic dopamine depletion the magnitude of synaptic transmission evoked at 10 Hz (A–C) and 50 Hz (E–H) was enhanced with no alteration in short-term synaptic plasticity. A, E, representative recordings. B, F, Peak and normalised conductances plotted against IPSC number. Chronic dopamine depletion significantly increased the conductances underlying IPSC1 and 25 (C, G) but had no effect on the ratio of conductances underlying IPSC2 to IPSC1 nor IPSC25 to IPSC1 (D, H). *, $p < 0.05$.

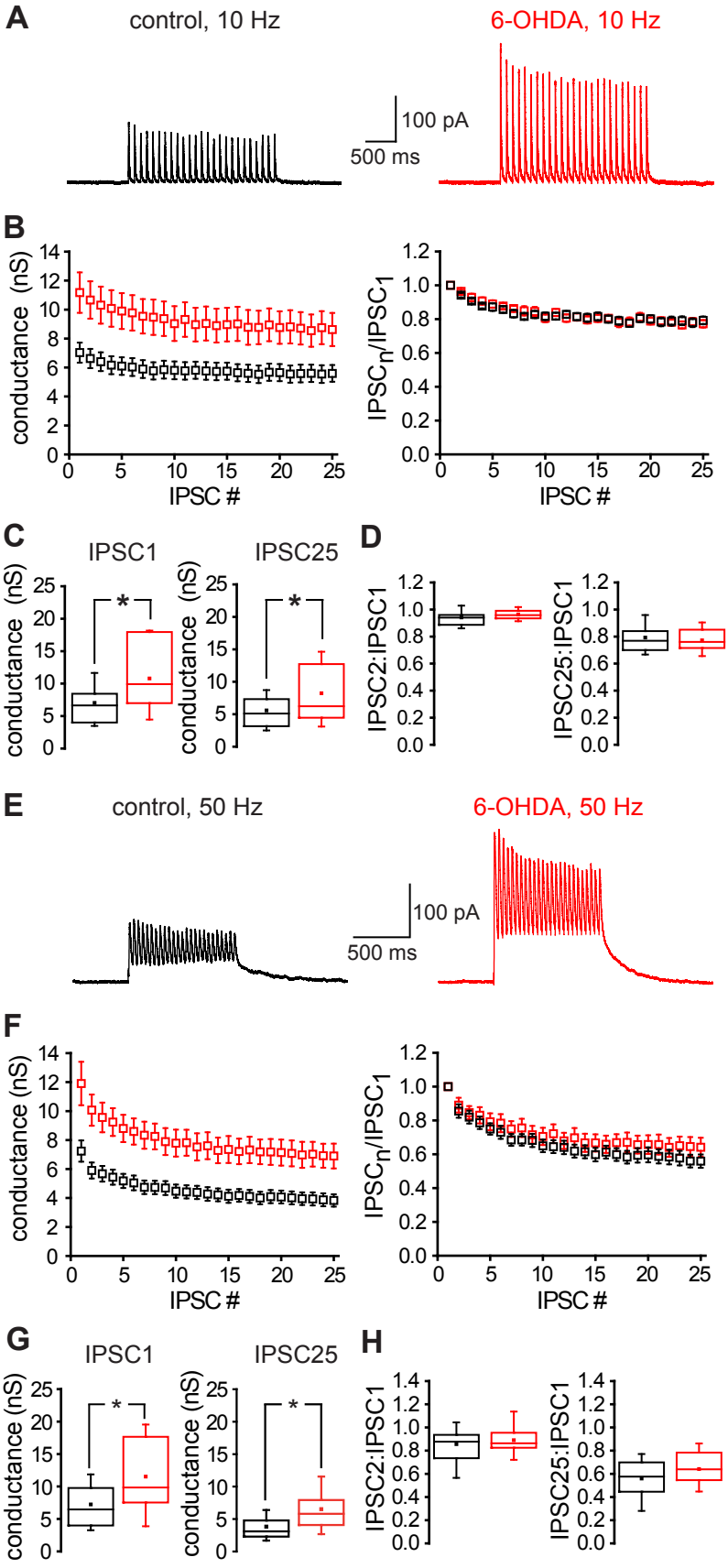
A
control, 10 Hz
6-OHDA, 10 Hz
100 pA
500 ms
B
conductance (nS)
IPSC #
IPSCn/IPSC1
C
IPSC1
IPSC25
D
IPSC2:IPSC1
IPSC25:IPSC1
E
control, 50 Hz
6-OHDA, 50 Hz
F
G
H

IPSC1 = 0.98 ± 0.21, n = 7, NS; IPSC 25 = 1.00 ± 0.37, n = 7, N.S.) nor the short-term plasticity of evoked IPSCs (sulpiride data normalised to control: 10 Hz IPSC2/IPSC1 = 1.03 ± 0.14, n = 4; 10 Hz IPSC25/IPSC1 = 0.98 ± 0.12, n = 4, NS; 50 Hz IPSC2/IPSC1 = 0.99 ± 0.09, n = 7; 50 Hz IPSC25/IPSC1 =1.01 ± 0.21 , n = 7, N.S.) confirming that basal activation of presynaptic D2-like dopamine receptors (Shen and Johnson, 2000; Baufreton and Bevan, 2008) does not underlie the relatively small amplitude of evoked IPSCs in control slices compared to those derived from 6-OHDA-treated animals. Together these data suggest that the augmentation of GPe–STN synaptic transmission following loss of dopamine is not mediated by an alteration in the probability of transmission.

	control	6-OHDA	significance
IPSC1	7.03 ± 3.10 nS (n = 20)	11.17 ± 5.41 nS (n = 15)	$p < 0.05$
IPSC25 (10 Hz)	5.59 ± 2.58 nS (n =20)	8.62 ± 4.42 nS (n = 15)	$p < 0.05$
IPSC2:IPSC1 (10 Hz)	0.94 ± 0.06 (n = 20)	0.96 ± 0.04 (n = 15)	NS
IPSC25:IPSC1 (10 Hz)	0.79 ± 0.10 (n = 20)	0.77 ± 0.09 (n = 15)	NS
IPSC2:IPSC1 (50 Hz)	0.86 ± 0.18 (n = 20)	0.89 ± 0.16 (n = 14)	NS
IPSC25:IPSC1 (50 Hz)	0.56 ± 0.18 (n = 20)	0.64 ± 0.21 (n = 14)	NS

Table 2.2. Chronic dopamine depletion increases the maximum evoked $GABA_A$-receptor-mediated synaptic conductance but has no effect on short-term synaptic plasticity. The frequency of electrical stimulation (10 Hz or 50 Hz) and number of the evoked IPSC (IPSC1, IPSC2 etc) are denoted.

In order to further address the contribution of postsynaptic mechanisms to the augmentation of GPe–STN transmission following depletion of dopamine, the magnitude of $GABA_A$ receptor conductance evoked by perfusion of 20 μM isoguvacine, a slowly desensitising $GABA_A$ receptor agonist, was examined. Chronic dopamine

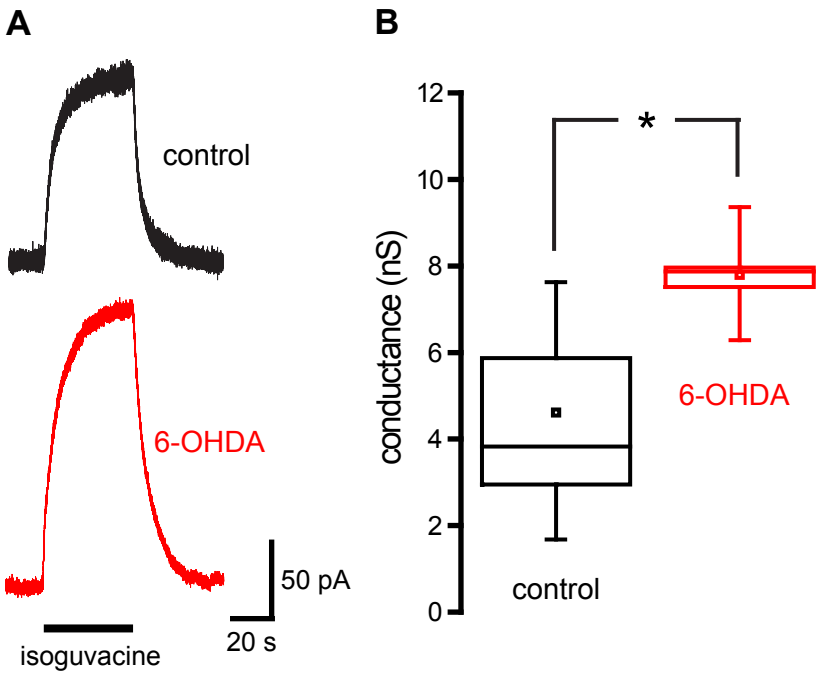

Figure 2.3. Chronic dopamine depletion increased the conductance evoked by the $GABA_A$ receptor agonist isoguvacine

A, Representative traces of isoguvacine-evoked currents in STN neurons derived from control and 6-OHDA treated animals. B, The conductance evoked by isoguvacine was significantly increased by chronic dopamine depletion. *, $p < 0.05$.

depletion significantly increased the peak amplitude of the isoguvacine-evoked conductance (Fig. 2.3; control = 4.61 ± 1.84 nS, n = 6; 6-OHDA = 7.80 ± 1.10 nS, n = 5; $p < 0.05$). This observation suggests that the expression of $GABA_A$ receptors by STN neurons is increased following the loss of dopamine. Together the electrophysiological data demonstrate that GPe–STN synaptic transmission is greatly enhanced by chronic dopamine depletion and that postsynaptic alterations contribute to this enhancement. Furthermore, the increased frequency of mIPSCs and amplitude of ensemble but not miniature $GABA_A$ receptor-mediated currents suggest that the collective rather than the individual strength of GPe–STN synapses is increased following the loss of dopamine.

2.3.3. Upregulation of gene transcriptions encoding $GABA_A$ receptor subunits in the STN following chronic dopamine depletion

In order to address molecular mechanisms underlying the enhancement of GPe–STN transmission by chronic dopamine depletion, the relative abundance of mRNA transcripts encoding the most commonly expressed $GABA_A$ receptor subunits in the STN (Wisden et al., 1992) were compared using quantitative PCR analysis. Data are expressed as fold change relative to median control values. Dopamine depletion significantly elevated the level of each transcript (Fig. 2.4; α1: control = 1.04 ± 0.21, n = 15; 6-OHDA = 1.20 ± 0.12, n = 12, $p < 0.05$; β2: control = 1.02 ± 0.21, n = 15; 6-OHDA = 1.34 ± 0.22, n = 12, $p < 0.05$; γ2: control = 1.05 ± 0.178, n = 15; 6-OHDA = 1.24 ± 0.15, n = 12, $p < 0.05$). In contrast the less abundantly expressed α3 subunit (Wisden et al., 1992), which is associated with relatively slow $GABA_A$ receptor-mediated IPSCs in neurons (Eyre et al., 2012), was unchanged following dopamine depletion (α3: control = 1.02 ± 0.18, n = 15; 6-OHDA = 1.14 ± 0.19, n = 12, N.S.). Together these data suggest that GPe–STN transmission is enhanced, at least in part, through persistent increases in the transcription of genes encoding the usually expressed $GABA_A$ receptor subunits.

2.3.4. Immunocytochemical analysis of markers for GABAergic synapses

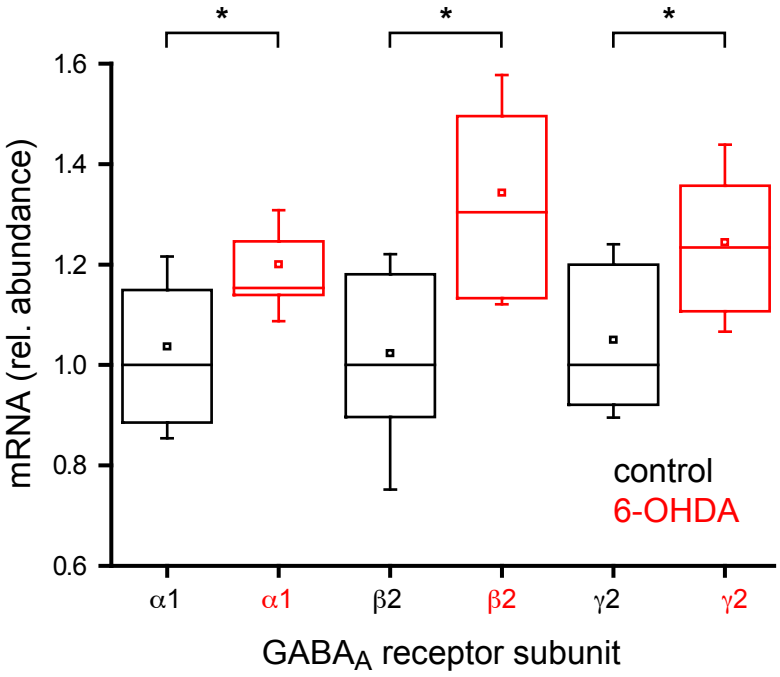

Figure 2.4. Chronic dopamine depletion increased the transcription of genes encoding commonly expressed $GABA_A$ receptor subunits

Quantitative PCR of the STN derived from control and 6-OHDA-lesioned animals revealed that the abundance of mRNA encoding $GABA_A$ α1, β2, and γ2 receptor subunits was significantly increased by chronic dopamine depletion. *, $p < 0.05$.

in the STN

In order to further address the molecular (and structural) mechanisms contributing to the enhancement of GPe–STN transmission by chronic dopamine depletion the density of postsynaptic structures expressing gephyrin and both gephyrin and γ2 $GABA_A$ receptor subunits and the density of presynaptic structures expressing VGAT and bassoon were estimated stereologically using immunofluorescent confocal microscopy. The inhibitory postsynaptic scaffold protein gephyrin and γ2 $GABA_A$ receptor subunits are critical for the clustering and retention of functional $GABA_A$ receptors at many GABAergic synapses (Smith and Kittler, 2010; Tyagarajan and Fritschy, 2010; Luscher et al., 2011), whereas VGAT is a transporter responsible for the concentration of GABA in synaptic vesicles (McIntire et al., 1997) and bassoon is an active zone protein at both inhibitory and excitatory synapses (tom Dieck et al., 1998; Micheva et al., 2010). Dopamine depletion significantly increased the density of immunoreactive structures expressing gephyrin and both gephyrin and γ2 $GABA_A$ receptor subunits (Fig. 2.5; gephyrin: control = 59.78 ± 22.40 million mm^{-3}, n = 14; 6-OHDA = 80.92 ± 24.65 million mm^{-3}, n = 15, $p < 0.05$; gephyrin plus γ2: control = 50.90 ± 22.80 million mm^{-3}, n = 14; 6-OHDA = 72.78 ± 22.58 million mm^{-3}, n = 15, $p < 0.05$) but had no effect on the absolute or relative densities of presynaptic structures expressing VGAT or both VGAT and bassoon (Fig. 2.6; VGAT: control = 65.46 ± 7.12 million mm^{-3}, n = 16; 6-OHDA = 68.47 ± 10.53 million mm^{-3}, n = 16, N.S.; VGAT plus bassoon: control = 44.53 ± 19.57 million mm^{-3}; 6-OHDA = 47.15 ± 17.8 million mm^{-3}, n = 16). The fluorescence intensity and dimensions of gephyrin-, γ2-, VGAT- and bassoon-immunoreactive structures were unaltered by dopamine depletion (data not shown). Together these data indicate that the density of postsynaptic markers is increased by chronic dopamine depletion but this is not matched by an increased density of axon terminals. Therefore one possibility is that the number of synapses per GPe-STN axon terminal increases following dopamine depletion. However the number of bassoon-immunoreactive structures per VGAT immunoreactive terminal was also apparently unaltered by dopamine depletion (control = 1.29 ± 0.56, n = 108; 6-OHDA = 1.39 ± 0.64, n = 105, N.S.). Given the resolution limit of standard confocal microscopy it is likely that distinct bassoon-immunoreactive structures were not fully resolved. In order to mitigate this confound further analysis was restricted to large VGAT-immunoreactive structures > 0.5 μm^2

Figure 2.5. Chronic dopamine depletion increased the densities of postsynaptic gephyrin- and γ2 $GABA_A$ receptor subunit-immunoreactive structures

Representative confocal micrographs of gephyrin (A1, B1: green), γ2 $GABA_A$ receptor subunit (A2, B2: red) and gephyrin plus γ2 $GABA_A$ receptor subunit immunoreactivity (A3, B3: yellow) in the STN of a control (A) and 6-OHDA-treated (B) animal. The densities of immunoreactive structures in the STN was increased by chronic dopamine depletion compared to control both in representative micrographs and across the sample population (C). The scale bar in A1 applies to each micrograph. *, $p < 0.05$.

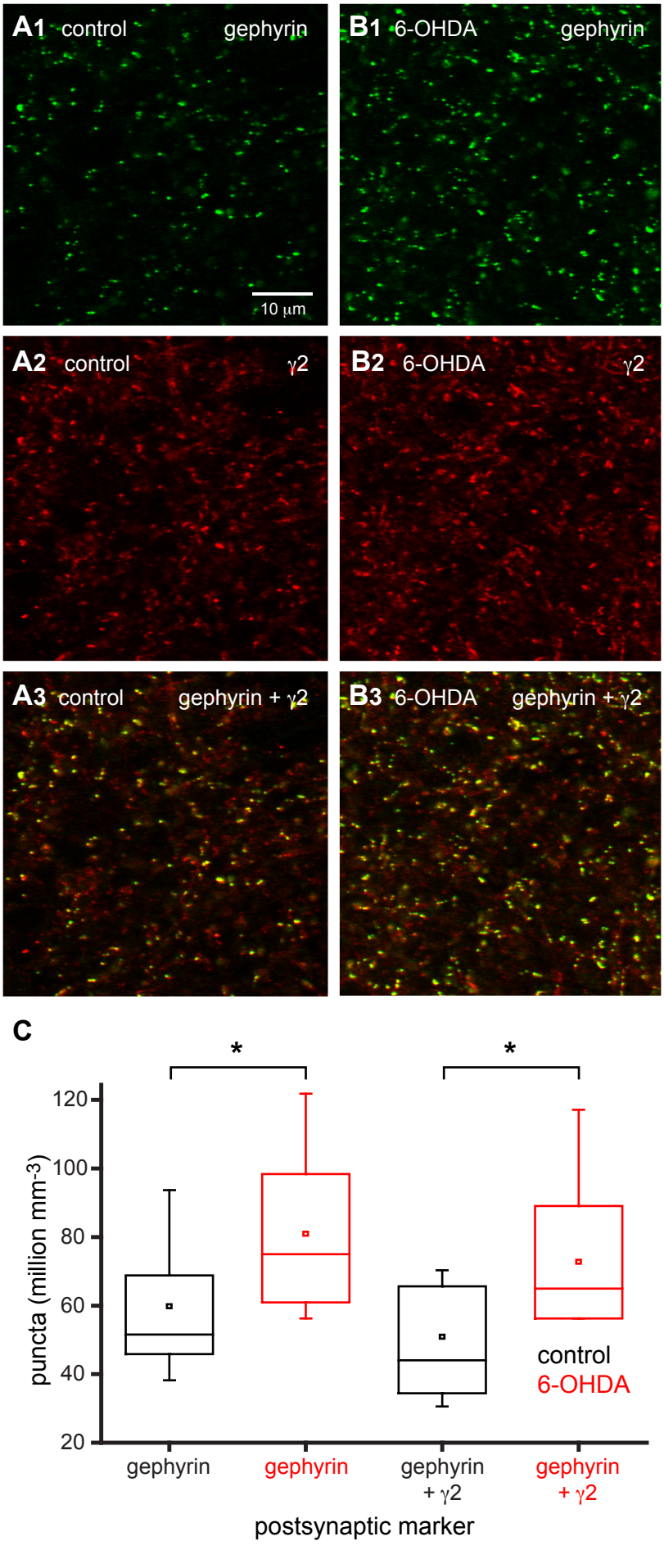
A1 control gephyrin
10 μm
B1 6-OHDA gephyrin
A2 control γ2
B2 6-OHDA γ2
A3 control gephyrin + γ2
B3 6-OHDA gephyrin + γ2
C
*
*
puncta (million mm-3)
120
100
80
60
40
20
control
6-OHDA
gephyrin
gephyrin
gephyrin + γ2
gephyrin + γ2
postsynaptic marker

Figure 2.6. Chronic dopamine depletion did not alter the densities of presynaptic VGAT- and bassoon-immunoreactive structures

Representative confocal micrographs of bassoon (A1, B1: green), VGAT (A2, B2: red) and bassoon plus VGAT immunoreactivity (A3, B3: yellow) in the STN of a control (A) and 6-OHDA-depleted (B) animal. The densities of immunoreactive structures in the STN were not altered by chronic dopamine depletion compared to control in the representative micrographs nor across the sample population (C). The scale bar in A1 applies to each micrograph. *, $p < 0.05$.

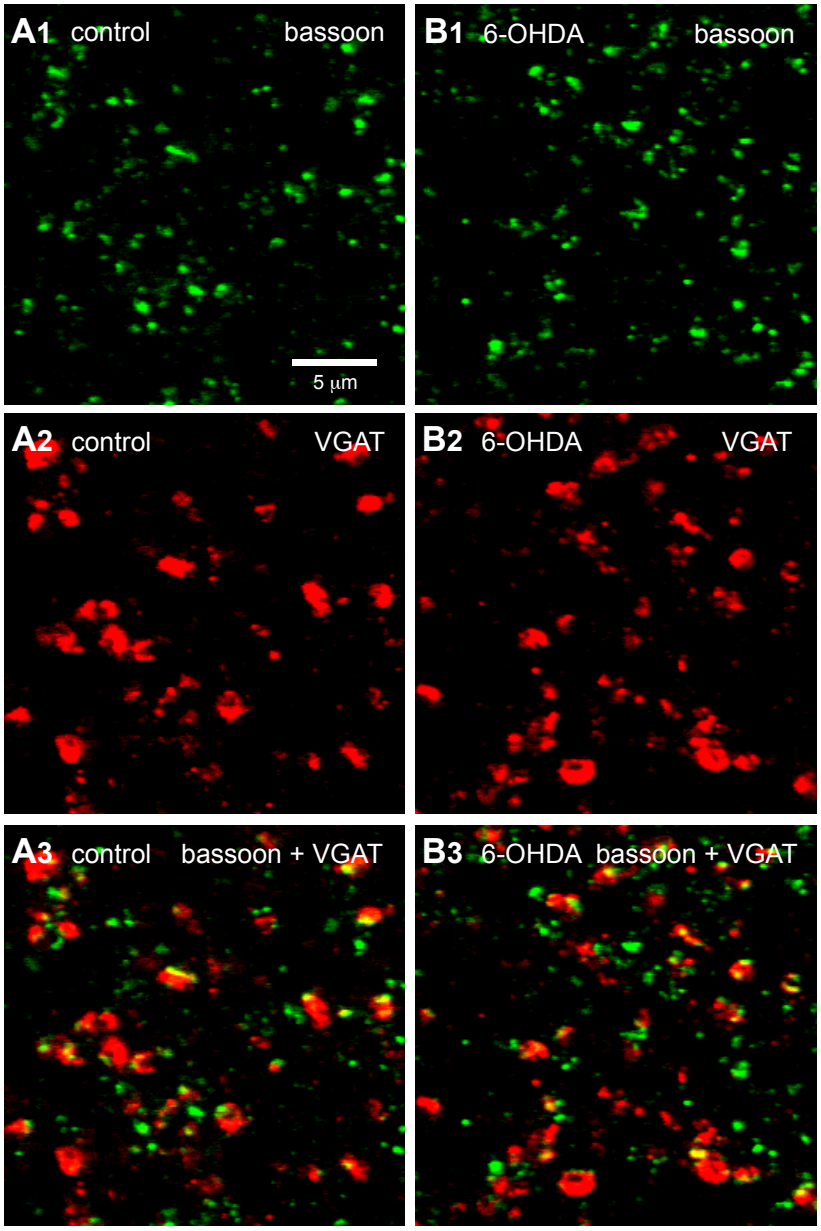
A1 control bassoon
B1 6-OHDA bassoon
5 µm
A2 control VGAT
B2 6-OHDA VGAT
A3 control bassoon + VGAT
B3 6-OHDA bassoon + VGAT

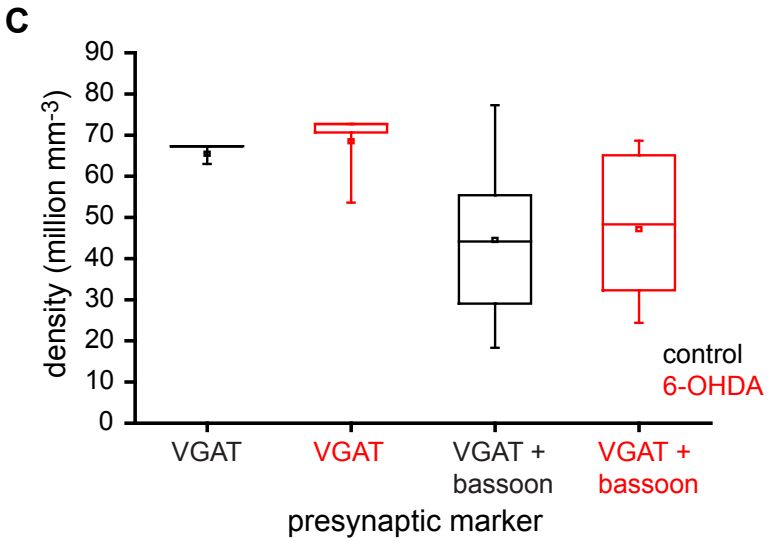
C
density (million mm-3)
90
80
70
60
50
40
30
20
10
0
VGAT
VGAT
VGAT + bassoon
VGAT + bassoon
control
6-OHDA
presynaptic marker

in their maximal cross-sectional area where bassoon-immunoreactive larger axon terminals the number of bassoon-immunoreactive structures per terminal was found to be significantly greater in dopamine-depleted tissue (Fig. 2.7; control = 1.56 ± 0.71, n = 48; 6-OHDA = 2.0 ± 0.70, n = 34, $p < 0.05$) suggesting that the number of active zones per GPe–STN axon terminal does indeed increase following loss of dopamine.

2.3.5. Ultrastructural analysis of GABAergic synapses in the STN

In order to investigate the structural basis for augmented GPe–STN synaptic transmission, the ultrastructural properties of VGAT-immunoreactive structures were analysed through electron microscopy. VGAT-immunoreactive structures were identified by the presence of an electron dense DAB reaction product, which adhered to the cytoplasmic face of the membrane of organelles including synaptic vesicles and mitochondria (Fig. 2.8). The cross-sectional area of VGAT-immunoreactive axon terminals in the STN of control and dopamine-depleted animals were similar (Fig. 2.8; control = 0.76 ± 0.54 μm^2, n = 63; 6-OHDA = 0.64 ± 0.34 μm^2, n = 61, N.S.) as were the diameter of postsynaptic dendrites (control = 0.83 ± 0.63 μm, n = 28; 6-OHDA = 0.81 ± 0.43 μm, n = 43, N.S.) and the proportion of STN somata postsynaptic to VGAT-immunoreactive axon terminals (control = 12.5 %, 4 of 32 postsynaptic structures; 6-OHDA = 14%, 7 of 50 postsynaptic structures). The synaptic contacts of VGAT-immunoreactive terminals were invariably symmetric and were therefore assumed to arise from the GPe (Smith et al., 1998; Baufreton et al., 2009). Although the dimensions of GPe–STN synapses were unaltered by dopamine depletion (length of synapses: control = 0.18 ± 0.06 μm, n = 41; 6-OHDA = 0.18 ± 0.67 μm, n = 78), the number of symmetric synapses per GPe–STN terminal was significantly greater in dopamine-depleted tissue (Fig. 2.8; number of synapses per terminal: control = 0.63 ± 0.75, n = 63; 6-OHDA = 1.26 ± 0.98, n = 61, $p < 0.05$). Taken together with electrophysiological and molecular data these findings suggest that chronic dopamine depletion enhances GPe–STN transmission through an increase in the number of GPe–STN synaptic connections. Furthermore, the enhancement in GPe–STN synaptic connectivity is mediated, at least in part, through an increase in the number of synapses per GPe–STN terminal.

Figure 2.7. Chronic dopamine depletion increased the number bassoon-immunoreactive structures associated with large VGAT-immunoreactive axon terminals

Representative through-focus confocal micrographs of bassoon (green) and VGAT (red) co-immunoreactive (yellow) axon terminals in the STN of control (A–C) and 6-OHDA-lesioned (D–E) animals. 3 examples (A–C and D–F) per condition are illustrated. The number of bassoon-immunoreactive structures per VGAT-immunoreactive axon terminal (arrows) was significantly increased by chronic dopamine depletion compared to control both in the representative examples and across the sample population (G). The scale bar in A applies to each micrograph. *, $p < 0.05$

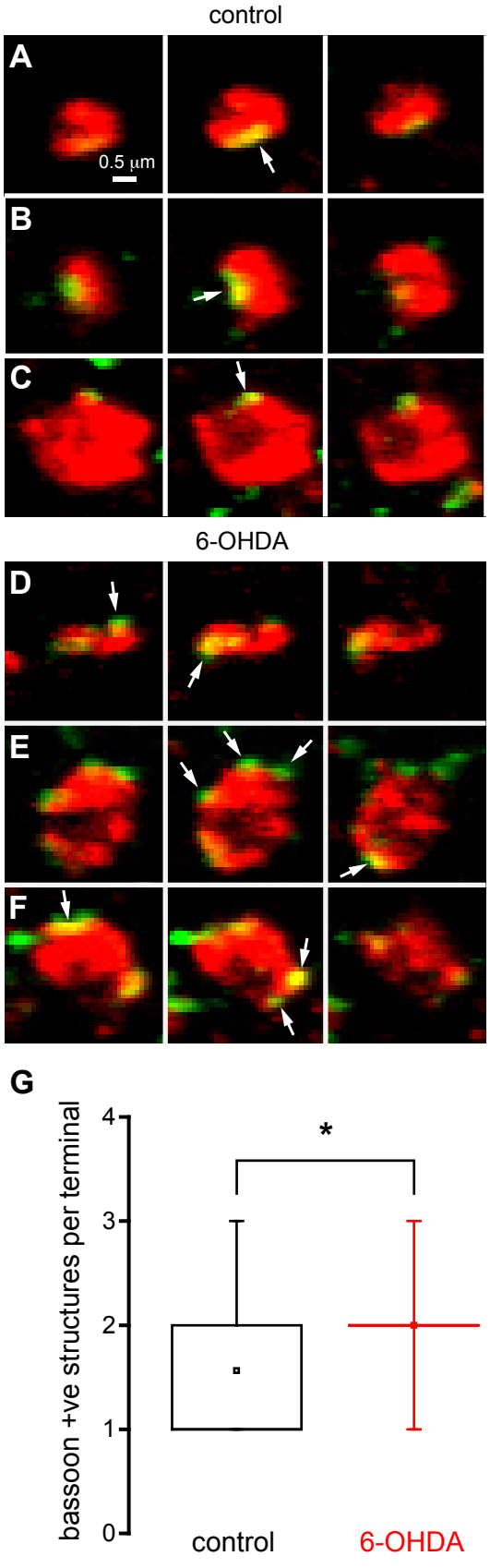
control
A
0.5 μm
B
C
6-OHDA
D
E
F
G
bassoon +ve structures per terminal
4
3
2
1
0
*
control
6-OHDA

Figure 2.8. Chronic dopamine depletion increased the number synapses per VGAT-immunoreactive axon terminal

Representative electron micrographs of VGAT-immunoreactive axon terminals in the STN of control (A–C) and 6-OHDA-lesioned (D–F) animals. VGAT-immunoreactive axon terminals were characterized by the presence of flocculent, electron dense DAB reaction product, which adhered to intracellular organelles, particularly synaptic vesicles. 3 examples per condition are illustrated (A–C and D–F). VGAT immunoreactive structures formed synapses (arrows) with the dendrites (d) and somata (s) of STN neurons. In some cases VGAT-immunoreactive structures did not form a synaptic connection in the ultrathin section that was examined (A). Although the dimensions of VGAT-immunoreactive structures, synapses and synaptic targets were similar in control and dopamine-depleted tissue, individual VGAT-immunoreactive axon terminals formed significantly more synapses (A–G). Scale bar in A applies to each micrograph. *, $p < 0.05$.

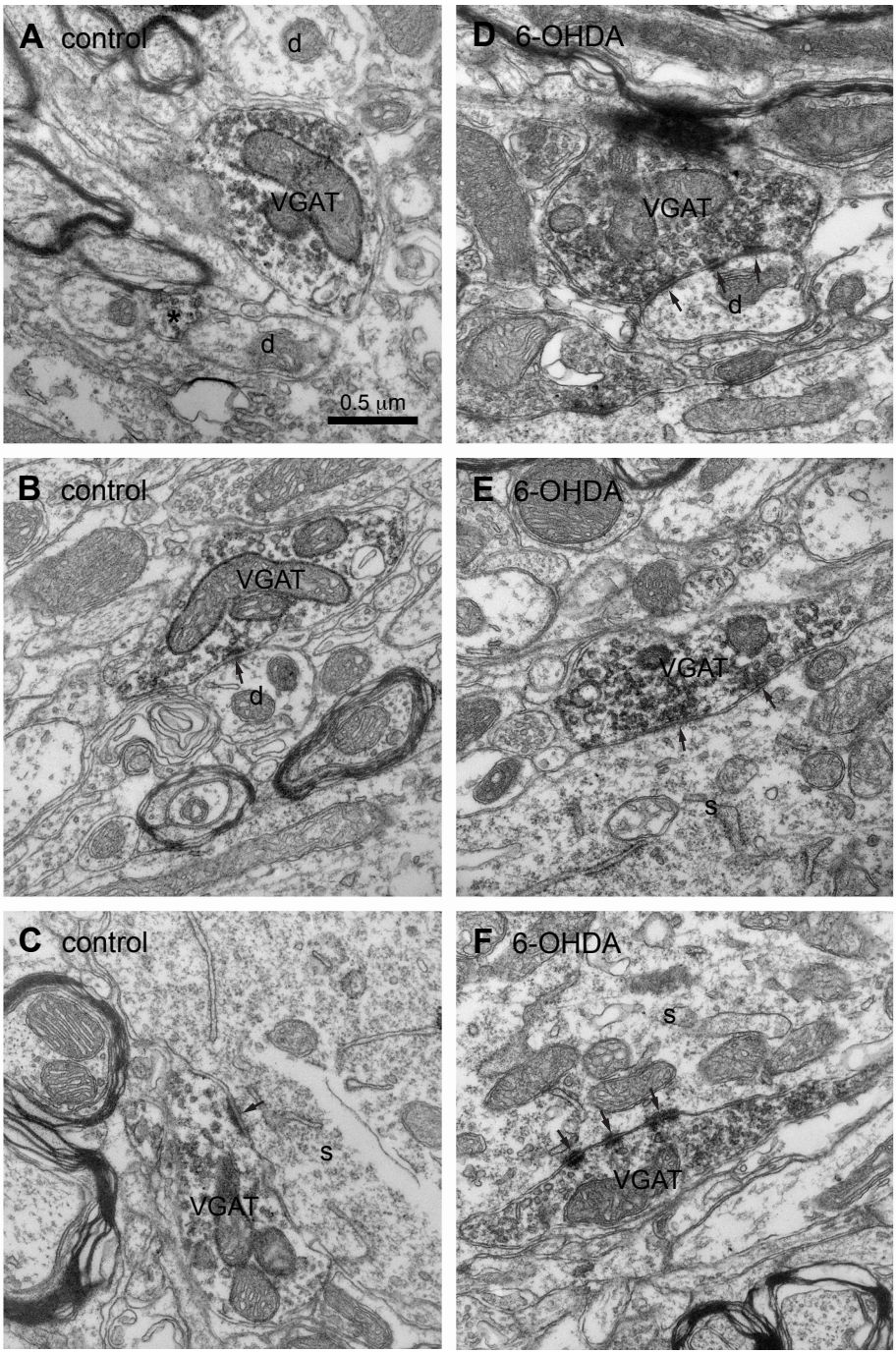
A control
d
VGAT
*
d
0.5 µm
D 6-OHDA
VGAT
d
B control
VGAT
d
E 6-OHDA
VGAT
s
C control
s
VGAT
F 6-OHDA
s
VGAT
G
control
6-OHDA
area (µm²)
2.0
1.5
1.0
0.5
0.0
dendritic diameter (µm)
2.0
1.5
1.0
0.5
0.0
*
length of active zone (nm)
300
250
200
150
100
50
number of active zones
3
2
1
0

2.4. Discussion

Following lesion of substantia nigra dopamine neurons hypersynchronous, <30 Hz rhythmic burst activity in the GPe, STN and associated brain nuclei gradually emerges and intensifies until it reaches a stable maximum after ~ 2–3 weeks. At this time point this study demonstrates through a variety of experimental approaches that loss of midbrain dopamine neurons leads to a substantial increase in the synaptic strength of the GPe–STN projection. The data are therefore concordant with studies, which reported increased $GABA_A$ receptor current and binding in the STN ipsilateral to dopamine depletion relative to the STN in the intact hemisphere (Yu et al., 2001; Shen and Johnson, 2005). However in these studies STN ipsilateral to dopamine lesions was compared to the STN from the intact hemisphere, which is a less satisfactory control than used here due to the existence of contralateral dopaminergic innervations (Fass and Butcher, 1981). Results from this study are also consistent with *in vivo* electrophysiological studies, which imply that the functional connectivity between the GPe and STN is strengthened by dopamine depletion (Mallet at al., 2008b; Cruz et al., 2011; Moran et al., 2011). Presented here are convergent but independent lines of evidence, which support the conclusion that following loss of dopamine the STN–GPe projection is strengthened through an increase in the number of GPe–STN synapses per axon terminal. The electrophysiological data demonstrated that 1) the frequency but not the amplitude of mIPSCs increased; 2) the amplitude of evoked IPSCs increased with no alteration in short-term plasticity; 3) current evoked by application of an exogenous $GABA_A$ receptor agonist increased. Thus, strengthening was mediated by an increase in GPe–STN synaptic connections with properties similar to those in control tissue. Quantitative PCR data demonstrated that transcription of usually expressed $GABA_A$ receptor subunits also increased, presumably to supply the newly formed synapses with receptors. Immunocytochemical data revealed that the density of pre- and postsynaptic synaptic markers was elevated but the density of GABAergic axon terminals was unaltered implying an increased number of synapses per GPe–STN terminal. Finally, electron microscopy confirmed that the number of synapses per GPe–STN axon terminal increased with no alteration in the dimensions of GPe–

STN terminals or their individual synapses or their postsynaptic target preference. The correspondence of the datasets both in terms of magnitude and mechanism is compelling, e.g. the frequency but not the amplitude of mIPSCs increased, which is concordant with both the increased density but not intensity of immunocytochemically visualised synaptic markers and the increase in the number but not the size of synapses per GPe-STN axon terminal at the electron microscopic level (cf. Nusser et al., 1997).

A homeostatic regulation of the excitatory and inhibitory balance has been proposed as preserving the structure and the function of neuronal networks (Turrigiano, 1999). Regulation of GPe–STN synaptic transmission through dynamic modification of GPe–STN connectivity may represent a homeostatic process for fine-tuning GPe–STN interactions. Specifically, the strengthening of the GPe–STN projection might occur in response to the hypoactivity of GPe neurons in PD. This process may be recruited excessively by profound alterations in pre- and postsynaptic activity, which follows the loss of dopamine. However strengthening the GPe–STN projection, aside from restricting hyperactivity of the parkinsonian STN, may also increase the capability of the GPe to generate synchronous, rhythmic burst firing in the STN and in that respect be maladaptive. Indeed, *ex vivo* and *in vivo* electrophysiological studies (Baufreton et al., 2005, 2009; Hallworth and Bevan, 2005; Mallet et al., 2008b; Tachibana et al., 2011) and computational modelling (Holgado et al., 2010; Moran et al., 2011) suggest that strengthening the GPe–STN projection will enhance the capability of the GPe (and cortical inputs) to synchronise STN neurons and generate rhythmic burst firing. Furthermore, in the non-human primate model of PD silencing the GPe with muscimol abolished hypersynchronous rhythmic burst firing in the STN (Tachibana et al., 2011), which implies a crucial role for GPe–STN synaptic transmission in the manifestation of parkinsonian STN activity.

Together with synaptic adaptations in D2-MSNs (Day et al., 2006; Gittis et al., 2011), reductions in the autonomous activity of STN neurons (Zhu et al., 2002a; Wilson et al., 2006) and downregulation of HCN channels in GPe neurons (Chan et al., 2011), this study suggests that loss of dopamine leads to adaptations in elements of the indirect pathway. In idiopathic PD it is possible that such adaptations are initially homeostatic and delay the symptomatic expression of the disease until the scale of

neurodegeneration and resulting adaptation is sufficiently severe that abnormal activity such as hypersynchronous firing is generated. Thus in the basal ganglia and other brain regions intrinsic cellular and synaptic plasticity mechanisms may ultimately contribute to rather than ameliorate brain dysfunction if the scale of neuronal degeneration or disruption is sufficiently extreme (Zhu et al., 2002a; Day et al., 2006; Wilson et al., 2006; Chan et al., 2011; Gittis et al., 2011; Lewis and Chetkovich, 2011).

The processes that regulate the strength of GPe–STN synaptic transmission both under normal conditions and following the loss of dopamine are unknown. Apart from dopamine's direct actions on the probability of GPe–STN transmission and the frequency and pattern of autonomous STN activity dopamine has also been shown to reduce the expression of synaptic $GABA_A$ receptors in the nucleus accumbens and MSNs through dephosphorylation of beta subunits leading to receptor endocytosis (Chen et al., 2006; Goffin et al., 2010). Although exogenous dopamine does not reduce whole-cell $GABA_A$ receptor current in STN neurons (Shen and Johnson, 2000) more prolonged receptor activation may be required to trigger/detect G protein-coupled receptor-dependent removal of receptors.

In addition, intracellular Ca^{2+} signalling is likely to be important due to its influence on protein kinases and phosphatases, which in turn regulate the translation, exocytosis, endocytosis, recycling, degradation and molecular interactions of synaptic receptors and associated molecules. In cortical pyramidal neurons the strength of GABAergic connections is regulated bidirectionally through postsynaptic activity pattern-dependent activation of $Ca_v2.3$ and Ca_v1 channels (Kurotani et al., 2008). Activation of Ca_v1 channels can also enhance the strength of GPe–STN synaptic transmission but this effect is mediated through increased extrusion of intracellular Cl^- (Wang et al., 2006) and cannot therefore account for (but could augment) the plasticity described here. Another potential source of postsynaptic Ca^{2+} is the NMDA receptor, which triggers an increase in the number and/or strength of some GABAergic synapses (Ouardouz and Sastry, 2000; Marsden et al., 2007). Hyperactivity of STN neurons and increased patterning by cortical inputs (Mallet et al., 2008b; Wichmann et al., 2011) suggest that activation of both STN Ca_v channels and NMDA receptors will be profoundly enhanced in the parkinsonian STN.

The plasticity described here is presumably mediated, in part, through activation of transcription factors e.g. cAMP response element-binding (CREB) and c-fos, which upregulate sufficient gene expression for the construction and maintenance of additional GPe–STN synapses. Indeed quantitative PCR confirmed that transcription of $GABA_A$ receptor subunits increased following loss of dopamine. Altered trafficking may also contribute to plasticity because NMDA receptor stimulation leads to activation of GABA receptor accessory protein (GABARAP) and N-ethylmaleimide-sensitive factor (NSF), which chaperone and position $GABA_A$ receptors in preparation for exocytosis (Marsden et al., 2007). Indeed, exocytosis of $GABA_A$ receptors rather than alterations in recycling is required for the potentiation of GABAergic synaptic transmission (Ouardouz and Sastry, 2000; Marsden et al., 2007; Kurotani et al., 2008).

Following export to the cell surface, the mechanisms responsible for the positioning of $GABA_A$ receptors and associated molecules at synapses are complex and connection specific. Tethering of $GABA_A$ receptors at synapses is often dependent on their interaction with the scaffolding protein gephyrin, whose positioning is in turn regulated by cell adhesion molecules such as neuroligin 2 and regulatory proteins like collybistin (Smith and Kittler, 2010; Tyagarajan and Fritschy, 2010; Luscher et al., 2011; Papadopoulos and Soykan, 2011). Indeed, the dynamic expression pattern of gephyrin and γ2 $GABA_A$ receptors in the STN argues that gephyrin is critical for both GPe–STN synaptic transmission and plasticity.

GPe–STN axon terminals are large (Smith et al., 1998; Baufreton et al., 2009) and thus provide readily available sites for the addition of synapses in the absence of axonal sprouting. Thus, the prolonged decay timecourse of mIPSCs following loss of dopamine may reflect cross-activation of receptors at neighbouring synapses rather than *de novo* expression of slowly gating $GABA_A$ receptor subunits. The processes that mediate coordinated remodelling of GABAergic pre- and postsynaptic machinery are poorly understood but presynaptic alterations accompany and often precede postsynaptic changes (Dobie and Craig, 2011). Therefore, retrograde messaging and cell-to-cell molecular interactions are likely to be critical for coordinated regulation of the pre- and post-synaptic elements of GPe–STN synapses both under normal conditions and in disease states.

CHAPTER 3

CHARACTERISATION OF CHANNELRHODOPSIN-2 EXPRESSION IN THE SUBTHALAMIC NUCLEUS OF *THY1-CHR2-EYFP* TRANSGENIC MOUSE LINE 18

3.1. Introduction

PD is a neurodegenerative disease clinically characterised by bradykinesia, akinesia, and resting tremor (Samii et al., 2004). The motor symptoms usually manifest when more than 60% of dopaminergic neurons in the SNc are degenerate (Dauer and Przedborski, 2003). Loss of dopaminergic neuromodulation in the striatum, GPe, and STN leads to changes in firing rate and activity pattern within the basal ganglia. The abnormal activity pattern appears to be crucial for the manifestation of the parkinsonian symptoms because HFS of the STN (DBS) at >100 Hz suppresses the pathological rhythmic burst firing and improves motor symptoms, whereas LFS makes the symptoms worse (Brown, 2007; Hammond et al., 2007).

However, the mechanism(s) of STN DBS is still not clear. A deep cellular and circuit-level understanding of PD circuitry and DBS mechanism has been challenging because of the limitations of traditional methods. Optogenetics is a recently pioneered approach involving the use of photosensitive microbial opsins that can be stimulated upon illumination to control neuronal activity with spatial and temporal precision (Deisseroth, 2010; Deisseroth, 2011). Therefore replacement of electrical stimulation with photostimulation allowing selective excitation or inhibition of specific cell types could facilitate precise interrogation and correction of abnormal neuronal microcircuits in PD. In spite of the ever-expanding optogenetic toolbox for more refined manipulations (Fenno et al., 2011), early optogenetic tools, particularly ChR2, are still useful for time-locked trigger of AP in response to light pulses.

For dissecting neural circuitries, it is important to target optogenetic constructs to specific neuronal subsets. A range of ChR2 gene delivery approaches have been in use, but they are often labour-intensive and technically challenging. Every experimental mouse requires stereotaxic surgery to deliver viral constructs encoding the ChR2 transgene. Not every injected mouse expresses the transgene, and those that do have variable spread of the viral infection, gradients of transgene expression in infected brain regions or potential tissue damage. These potential issues are eliminated in cell type-specific ChR2 transgenic mouse lines.

Thy1-ChR2-EYFP line 18 generated by Feng group (Arenkiel et al., 2007) is

one of the early transgenic mouse strains that has been used in a variety of studies. This mouse line has been proven to be useful for dissecting the PD circuitry and the therapeutic effects of DBS in STN. Using this mouse line, optogenetic driving of the cortical–STN connections at high frequency was shown to reverse motor impairments in parkinsonian animals (Gradinaru et al., 2009), suggesting that the therapeutic effects of DBS could at least in part be attributed to manipulation of this pathway.

Thy1-ChR2-EYFP line 18 is so far known to express high levels of ChR2 in multiple brain regions including the motor cortex, hippocampus, thalamus, midbrain and brainstem, cerebellum and the olfactory bulb under the *Thy1* promoter (Arenkiel et al., 2007). Because the STN receives both excitatory and inhibitory inputs from various brain regions, the sources of ChR2 expression in the STN is still undefined. Identifying and quantifying the sources of ChR2 expression will optimise the utility of this mouse strain to investigate and correct the PD circuitry. The objective of this study is therefore to characterise the expression of ChR2 from different input sources within the STN of *Thy1-ChR2-EYFP* line 18, using a combination of electrophysiological and immunocytochemical approaches.

3.2. Materials and Methods

Experiments were performed in accordance with institutional, NIH and Society for Neuroscience guidelines using (*Tg(Thy1-COP4/EYFP)18Gfng* (*Thy1-ChR2-EYFP*) mice (line 18) obtained from The Jackson Laboratory (Sacramento, USA). Embryo rederivation of the animals was performed by Charles River. *Thy1-ChR2* mice were genotyped following the protocol from The Jackson Laboratory to ensure that they were homozygotes. Mice used in this study were adult males aged 2 to 5 months old.

3.2.1. Immunocytochemistry

Animals were perfused transcardially under ketamine/xylazine anaesthesia with

room-temperature HEPES-buffered simulated intestinal fluid (SIF), equilibrated with O_2 and contained (in mM): 140 mM NaCl, 3 mM KCl, 1.6 mM CaCl2·2H2O, 1.5 mM MgCl2·6H2O, and 23 mM glucose, and 15 mM HEPES. Following blood clearance, animals were perfused with 4% paraformaldehyde in 0.1 M PB at pH 7.4 for 25 minutes, then with 0.1 M PB, pH 7.4, for 25 minutes. Each brain was sliced on a vibratome at 70 µm in the coronal plane in 0.01 M PBS. Slices were incubated with primary antibodies as shown in Table 3.1 in PBS, plus 0.3% Triton X-100 and 2% NDS for 48 h at 4°C. After washing, slices were incubated in fluorescent or biotinylated secondary antibodies (Jackson Immunoresearch; see Table 4.1) in the same diluent for 2 h at room temperature. Immunofluorescent slices were mounted in Prolong Gold or Prolong Gold with 4‘,6-diamidino-2-phenylindole (DAPI; Invitrogen) and coverslipped. Biotin-labelled slices were further reacted with avidin–biotin–peroxidase complex (1:100 ABC-Elite; Vector Laboratories) for 2 h at room temperature. Peroxidase linked to the EGFP-tagged ChR2 channels by the avidin-biotin bridge was revealed by placing the sections in Tris buffer (0.05 M, pH 7.4) containing 0.025% DAB and 0.0025% hydrogen peroxide for 5 min. The reaction was terminated by rinsing several times in Tris buffer. 0.5% Cresyl Violet Acetate was used as a counterstain to reveal neuronal structures. The slices were then mounted on Vectabond-treated (Vector Laboratories) slides and dehydrated with alcohol and xylene before being coverslipped in Entellan New (Electron Microscopy Sciences, Hatfield, USA).

Immunofluorescent labelling was visualised using confocal laser scanning microscopy (Zeiss LSM 510 or Nikon A1R). Image stacks of immuno (16 optical sections each) were acquired using a 63× oil immersion objective (NA 1.4) with a digital zoom of 1.5× (*x*, *y*: 892 × 892 pixels, 93 nm per pixel; *z*-step: 0.4 µm) and analysed with Image J (National Institutes of Health, Bethesda, USA) or Nikon Elements (Nikon, Tokyo, Japan). Sample sites were randomly determined from a grid (frame size 11.9 × 11.9 µm) superimposed on each image stack captured from STN slices. Vesicular glutamate transporter(VGLUT)1, VGLUT2 and VGAT-immunoreactive puncta were stereologically selected ~ 4 µm below the slice surface, using the optical dissector method (West, 1999). Colocalisation of the counted puncta with EGFP-positive terminals was then determined.

	Antibody	Source	Species	Primary dilution	Secondary antibody	Secondary dilution
double labelling	EGFP	Clontech	Mouse	1:2500	DyLight 488 donkey anti-mouse IgG	1:250
	VGLUT1 or	Synaptic Systems	Guinea pig	1:1500	DyLight 594 donkey anti-guinea pig IgG	1:250
	VGLUT2 or	Synaptic Systems	Guinea pig	1:1500	Dylight 594 donkey anti-guinea pig IgG	1:250
	VGAT	Synaptic Systems	Rabbit	1:1000	Dylight 594 donkey anti-rabbit IgG	1:250
single labelling	EGFP	Clontech	Mouse	1:2500	Biotin-SP donkey anti-mouse	1:500
					or	
					DyLight 488 donkey anti-mouse IgG	1:250

Table 3.1. Antibodies used for immunocytochemical analysis of ChR2 expression in the STN

3.2.2. Electrophysiology

Slice preparation. Animals were deeply anaesthetised by intraperitoneal injection of a mixture of ketamine (87 mg kg^{-1}) and xylazine (13 mg kg^{-1}) and perfused transcardially with ice-cold modified ACSF equilibrated with 95% O_2 and 5% CO_2 and contained: 230 mM sucrose, 26 mM $NaHCO_3$, 2.5 mM KCl, 1.25 mM Na_2HPO_4, 0.5 mM $CaCl_2$, 10 mM $MgSO_4$ and 10 mM glucose. The brain was then removed, blocked in the sagittal plane, glued to the stage of a vibrating microtome (Vibratome 3000; Leica Microsystems), and submerged in ice-cold modified ACSF. Slices of 300 μm thick through STN were

cut and transferred to a holding chamber at room temperature containing 'traditional' ACSF that was equilibrated with 95% O_2 and 5% CO_2 and contained: 126 mM NaCl, 26 mM $NaHCO_3$, 2.5 mM KCl, 1.25 mM Na_2HPO_4, 2 mM $CaCl_2$, 2 mM $MgSO_4$ and 10 mM glucose.

Recording. Brain slices were transferred to a recording chamber that was perfused at a rate of 3–5 $mlmin^{-1}$ with ACSF that was modified to more closely match rodent brain interstitial fluid. ACSF contained 126 mM NaCl, 3 mM KCl, 1.25 mM NaH_2PO_4. H_2O, 1.6 mM $CaCl_2.2H_2O$, 1.5 mM $MgSO_4.7H_2O$, 10 mM glucose, and 26 mM $NaHCO_3$ (equilibrated with 95 % O_2 and 5 % CO_2) and was heated to ~ 35˚C. Somatic recordings were made using borosilicate glass micropipettes containing (in mM): 135 CsCl, 3.6 NaCl, 1 $MgCl_2$, 10 HEPES, 10 QX-314, 0.1 Na_4EGTA, 0.4 Na_3GTP, and 2 $Mg_{1.5}$ATP (pH 7.2, 290 mOsm). For the recording of evoked glutamatergic currents, 2-(3-Carboxypropyl)-3-amino-6-(4 methoxyphenyl)pyridazinium bromide (GABAzine; 20 μM) and CGP 55845 (2 μM) were used to block $GABA_A$ and $GABA_B$ receptors respectively. To isolate NMDA current, DNQX (20 μM) was also applied to block AMPA/Kainate receptors. AMPA current trace was relatively isolated by recording in the absence of DNQX and substracting it from the NMDA current trace. For the recording of evoked GABAergic currents, APV (50 μM) and DNQX (20 μM) were used to block NMDA and AMPA/ Kainate receptors. Photostimulation was generated from 470 nm laser wavelength (Polychrome V monochromator; TILL Photonics), by gradually increasing the laser output power until a physiological response was elicited (~ < 10 mW),

3.2.3. Statistics

Data are reported as mean ± SD. Cumulative and box (central line, median; dot, mean; box, 25–75%; whiskers, 10–90%) plots are used to illustrate sample distributions. Mann-Whitney and Kruskal-Wallis tests were used to test for significant differences between two and more than two independent samples respectively. The level of significance was set at an α value of 0.05. Non significant differences are denoted as N.S..

3.3. Results

3.3.1. ChR2 expression in glutamatergic and GABAergic afferents in the STN

STN receives substantial glutamatergic projections from multiple cortical and subcortical regions (Bevan et al., 1995). In order to determine the expression of ChR2 in glutamatergic afferents in the STN immunocytochemistry was performed on fixed brain sections of adult *Thy1-ChR2-EYFP* line 18 mice, using VGLUT1 and VGLUT2 antibodies as cortical and subcortical terminal markers respectively (Fujiyama et al., 2004, 2006; Hur and Zaborszky, 2005; Kubota et al., 2007). Strong immunofluorescence of EGFP-tagged ChR2-EYFP (EYFP is recognized by EGFP antibody) can be observed along afferents and within terminal structures, with more intense labelling along the membrane structures. Both VGLUT1 (Fig. 3.1 A1) and VGLUT2 (Fig. 3.1 A2) immunoreactive structures in the STN showed colocalisation with ChR2. Many of the VGLUT2-immunoreactive structures, however, were not seen ChR2-positive in comparison with VGLUT1 terminals. Because STN also receives GABAergic projections, VGAT antibody was used as a GABAergic terminal marker (McIntire et al., 1997) to determine the expression of ChR2 in these inhibitory afferents. A large proportion of VGAT puncta colocalised with ChR2-EYFP immunofluorescence (Fig. 3.1 A3). Putative somata of STN neurons were devoid of ChR2-EYFP (Fig. 3.1), consistent with observations from single EGFP-labelled STN sections counterstained with nuclear marker DAPI (data not shown).

To quantify the proportion of glutamatergic and GABAergic afferents expressing ChR2, VGLUT1, VGLUT2 and VGAT immunoreactive structures were first selected using stereological method, and their colocalisations with ChR2 were then determined. The percentage of VGLUT1 (76.7 % ± 22.37, n = 16) that colocalised with ChR2-EYFP was significantly higher than that of VGLUT2 (19.8% ± 21.3, n = 16; $p < 0.05$), but not VGAT (70.6% ± 21.27, n = 16; N.S.; Fig. 3.1 B). The absolute densities of the three immunoreactive structures were not significantly different from each other (VGLUT1 = 44.6 ± 20.4 million mm^{-3}; VGLUT2 = 43.8 ± 21.1 million mm^{-3}

Figure 3.1. Anatomical and functional characterisation of ChR2 expression in the STN

A1–3, colocalisation of ChR2-EYFP (green) with terminal markers (red) for cortical (VGLUT1) and subcortical (VGLUT2) glutamatergic afferents and GABAergic (VGAT) afferents. ChR2-EYFP immunofluorescence colocalised mostly with VGLUT1 (A1) and VGAT (A3), and to a much less extent VGLUT2 (A2) immunoreactive-puncta (indicated by yellow arrows). Putative neuronal somata (denoted by the white symbol *) were largely devoid of ChR2-EYFP fluorescence. B, quantification of colocalisation percentage of VGLUT1, VGLUT2 and VGAT immunoreactive structures with ChR2-EYFP immunofluorescence. The percentage of VGLUT1 puncta (n = 16) positive for ChR2-EYFP was similar was significantly higher than that of VGLUT2 puncta (n = 16) (but not VGAT puncta; n = 16). C1–2, Brief single photostimulation (denoted by arrow) of an STN neuron evoked AMPA, NMDA (C1) and GABA (C2) currents at different holding potentials. *, $p < 0.05$.

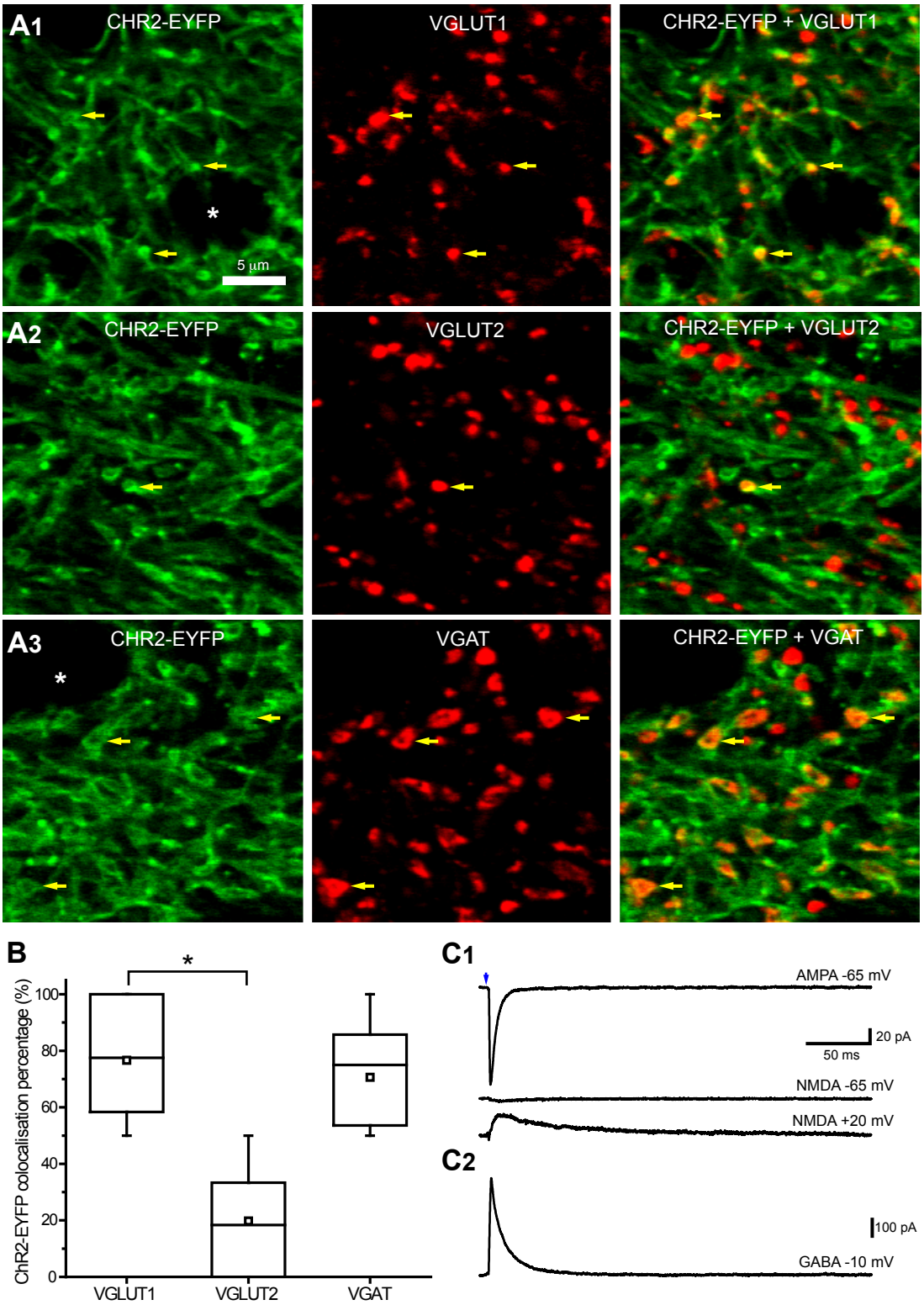
A1
CHR2-EYFP
VGLUT1
CHR2-EYFP + VGLUT1
5 µm
A2
CHR2-EYFP
VGLUT2
CHR2-EYFP + VGLUT2
A3
CHR2-EYFP
VGAT
CHR2-EYFP + VGAT
B
ChR2-EYFP colocalisation percentage (%)
100
80
60
40
20
0
VGLUT1
VGLUT2
VGAT
C1
AMPA -65 mV
20 pA
50 ms
NMDA -65 mV
NMDA +20 mV
C2
100 pA
GABA -10 mV

; VGAT = 46.5 ± 17.2 million mm^{-3}; N.S.).

To confirm that ChR2 expressed in the glutamatergic and GABAergic afferents was functional, whole-cell patch clamp recordings of evoked synaptic currents were performed in acute brain slices from young adult mice. In the presence of GABAzine ($GABA_A$ receptor antagonist) and CGP 55845 ($GABA_B$ receptor antagonist), single photostimulation (1 ms) over an STN neuron triggered excitatory AMPA but not NMDA current respectively at –65 mV holding potential (Fig. 3.1 C1; for methods see section 4.2.2. Electrophysiology). NMDA current was revealed when the cell was held at +20 mV (Fig. 3.1 C1), consistent with its known voltage-dependent activation due to ion channel block by Mg^{2+} (Mayer et al., 1984). In the presence of APV (NMDA receptor antagonist) and DNQX (non-NMDA receptor antagonist), inhibitory GABA current was evoked at –10 mV holding potential (Fig. 3.1 C2). These results suggest that the both glutamatergic and GABAergic afferents STN express functional ChR2 channels sufficient to elicit postsynaptic response upon photoactivation.

3.3.2. Sources of ChR2-expressing projections to the STN

The possible sources of ChR2-expressing afferents in the STN were examined using enzyme immunohistochemistry through DAB staining of ChR2-EYFP. The STN is known to receive substantial projections from several regions of the cerebral cortex, including prefrontal regions, primary motor cortex and primary somatosensory cortex (Canteras et al., 1990; Feger et al., 1994). Intense and widespread cellular labelling of layer V cortical neurons was seen throughout the cerebral cortex of the *Thy1-ChR2* transgenic mice, including the primary M1 motor regions (Fig. 3.2 A). GABAergic projection to the STN predominantly arises from the GPe (Smith et al., 1998). Indeed, intense staining of many neuronal somata and their processes was observed throughout the GPe (Fig. 3.2 B).

In contrast to the cortex, no cellular staining was detected in parafascicular thalamic nucleus (PF; Fig. 3.3 A), which is the main subcortical glutamatergic input to the STN (Feger et al., 1994; Bevan et al., 1995). Other known subcortical input sources (Bevan and Bolam, 1995; Coizet et al., 2009) were also examined, including the

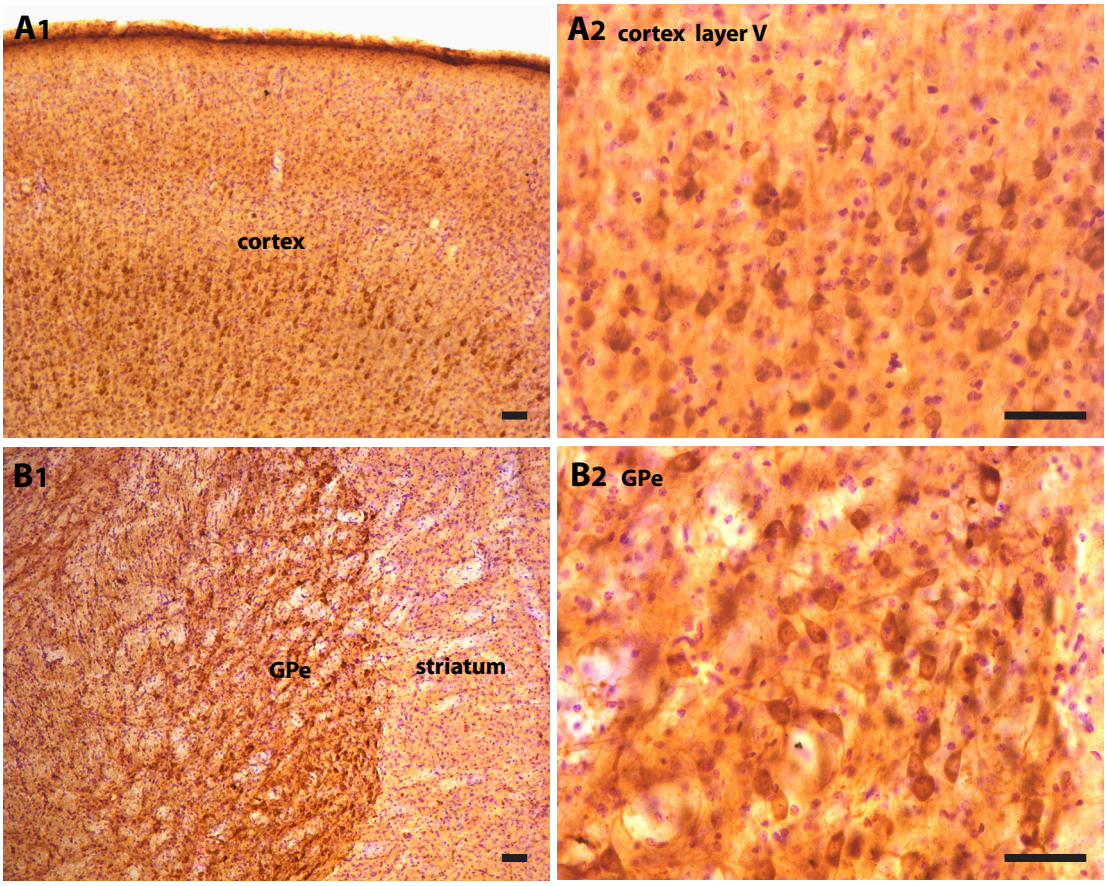

Figure 3.2. Neuronal expression of ChR2 in the cerebral cortex and GPe

A–B, DAB staining of ChR2-EYFP revealed cell body and dendritic expression of ChR2 in the cerebral cortex and GPe, the main glutamatergic and GABAergic inputs respectively to the STN. A1, Cerebral cortex (shown here primary motor area), displayed abundant ChR2-EYFP staining in Layer V cortical neurons. High power image from the Layer V is shown in A2. B1, GPe, was also labelled strongly in many neurons over distributed regions of the nucleus. High power image from the dorsolateral area of the GPe is shown in B2. All scale bars represent 50 μm in length.

Figure 3.3. Subcortical sources of ChR2-expressing glutamatergic and GABAergic projections to the STN

A–D, ChR2-EYFP DAB staining in subcortical regions that project to the STN. No cellular labelling of ChR2-EYFP was observed in parafascicular thalamic nucleus or PF (A1, A2). Labelled cell bodies was detected in the superior colliculus or SC (B1, B2). Laterodorsal tegmental nucleus or LTDg did not display any cellular labelling (C). A very small number of cells was faintly labelled in the pedunculopontine nucleus or PPN (D1, D2). In contrast, midbrain extrapyramidal area or MEA (D1, D3) showed strong labelling within both cell bodies and neuronal processes. All scale bars represent 50 μm in length.

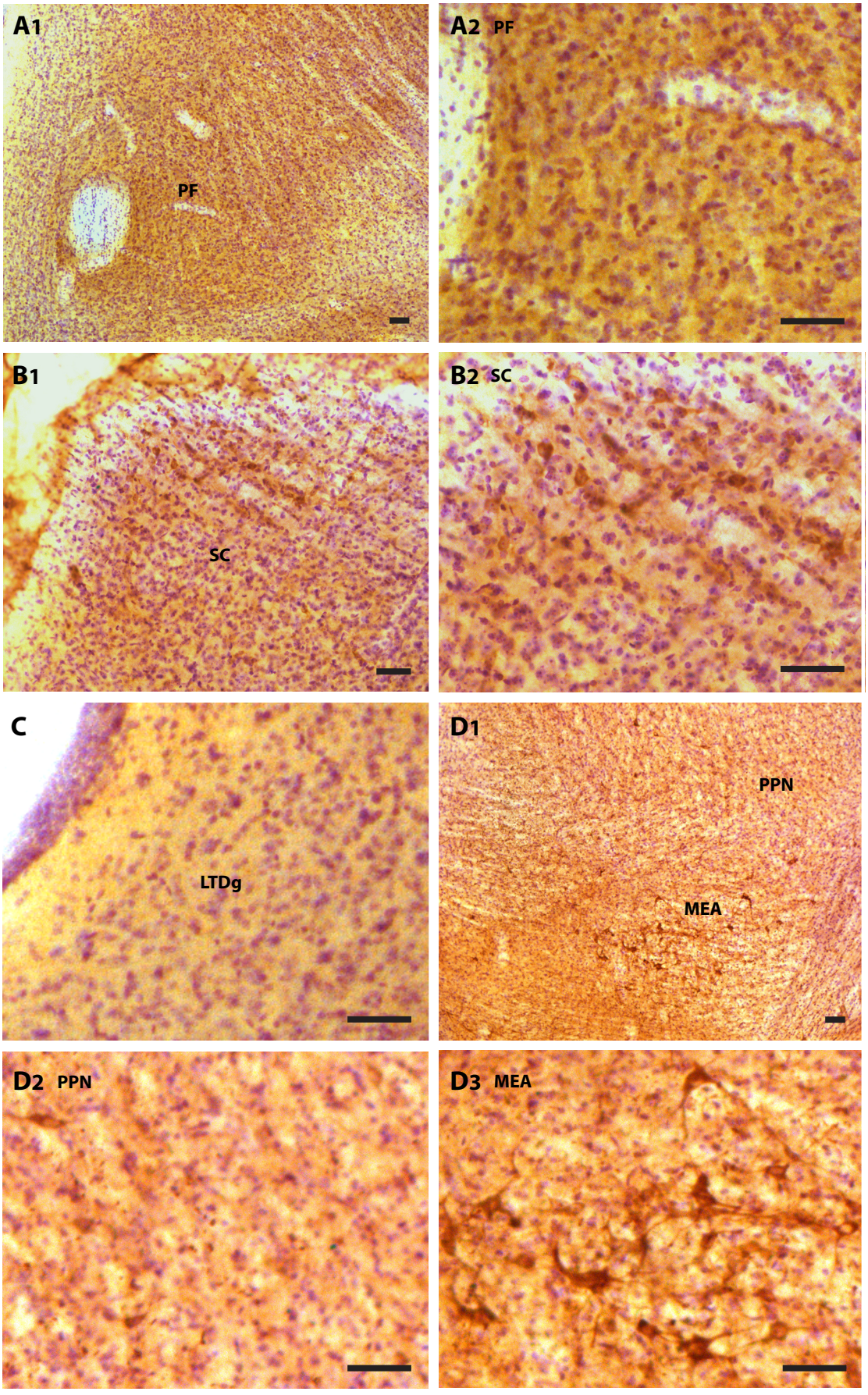
A1
PF
A2 PF
B1
SC
B2 SC
C
LTDg
D1
PPN
MEA
D2 PPN
D3 MEA

superior colliculus (SC; Fig. 3.3 B) and three divisions of the mesopontine tegmentum (MTg): the laterodorsal tegmental nucleus (LDTg; Fig. 3.3 C) the cholinergic neurons from pedunculopontine nucleus (PPN; Fig. 3.2 D), the noncholinergic midbrain extrapyramidal area (MEA; Fig. 3.3 D) and. Cell body immunostaining of ChR2-EYFP in these midbrain structures was not observed, except for minor labelling in the SC and MEA (Fig. 3.3 D). Faint DAB staining in the PPN was also observed in a very small number of cell bodies (Fig. 3.3. D).

Animals of *Thy1-ChR2-EYFP* line 18 used in this study were embryo-rederived due to pathogen contamination of the original mutant strain. To eliminate the possibility of spontaneous genetic or epigenetic changes of the embryonic stem cell genome (Nagy et al., 1993; Fedorov et al., 1997) causing alterations in ChR2 expression pattern, animals of the original line were also subject to anatomical characterisation of ChR2 expression in the STN. The percentages of VGLUT1, VGLUT2, and VGAT puncta colocalising with ChR2 were not significantly different from the values obtained from embryo-derived individuals (VGLUT1 = 81.5% ± 16.6, n = 16; VGLUT2 = 22.2% ± 17.2, n = 16; VGAT = 70.6% ± 17). The densities of these immunoreactive structures were also similar to those obtained from embryo-derived individuals (VGLUT1 = 41.5 ± 14.6 million mm^{-3}; VGLUT2 = 43 ± 21.9 million mm^{-3}; VGAT = 45.1 ± 15.5 million mm^{-3}). In addition, ChR2 expression patterns in various brain regions (i.e. motor cortex, GPe, PF, SC, PPN, MEA, and LTD) projecting to the STN were also qualitatively similar (not shown). These results suggest that the embryo-derived animals are a reliable substitute to the original *Thy1-ChR2-EYFP* line with quantitatively similar ChR2 expression pattern in the VGLUT1, VGLUT2 and VGAT terminals within the STN.

3.4. Discussion

Immunocytochemical data in this study revealed that EYFP-tagged ChR2 is expressed in both glutamatergic and GABAergic afferents within the STN of the embryo-derived animals from *Thy1-ChR2-EYFP* line 18, with similar expression pattern to that observed in the original line. Using VGLUT1 and VGLUT2 as cortical and subcortical glutamatergic terminal markers respectively, analysis of ChR2-EYFP colocalisation

suggested that most of the cortical afferents (~ 4 out of 5) but to a much less extent the subcortical afferents (~ 1 out of 5) in the STN expressed ChR2. Considering that the densities of VGLUT1 and VGLUT2 immunoreactive terminals were similar, the ratio of ChR2-positive glutamatergic afferents in the STN of *Thy1-ChR2-EYFP* line 18 of cortical origins to that of subcortical origins is about 4:1. In addition, ChR2 is also expressed by GABAergic afferents, as suggested by colocalisation of ChR2-EYFP with VGAT, a marker for GABAergic terminals. Similar density of VGAT and VGLUT1 immunoreactive puncta and the percentage of VGAT and VGLUT1 puncta colocalised with ChR2-EYFP suggest that as many GABAergic afferents in the STN express ChR2 as glutamatergic cortical afferents. Functional expression of ChR2 in glutamatergic and GABAergic afferents was confirmed by electrophysiological recordings that demonstrated the capability of photostimulation to evoke AMPA, NMDA and GABA currents in the STN neurons.

Electrophysiological studies (Paz et al., 2005), retrograde (Canteras et al., 1990; Feger et al., 1994) and anterograde labelling (Kita and Kita, 2012) in rodents suggest that cortical–STN innervations largely originate from layer V pyramidal neurons in motor cortex. In this and previous studies (Arenkiel et al., 2007) substantial ChR2 expression was observed in the layer V cortical neurons of *Thy1-ChR2-EYFP* mouse line 18, consistent with results presented here showing high proportion of VGLUT1-immunoreactive terminals in the STN was ChR2-positive. Subcortical excitatory projections in the STN predominantly arise from the intralaminar thalamus, particularly the centro-median parafascicular complex (Feger et al., 1994; Bevan et al., 1995). However, minimal somatic expression of ChR2 was detected within the PF of the transgenic ChR2-EYFP mouse line. Within other subcortical midbrain structures that project to the STN (Bevan and Bolam, 1995; Coizet et al., 2009), cellular immunostaining of ChR2-EYFP was similarly absent except for minor labelling in the SC and MEA (presumably also PPN to a much lesser extent). Although both GABAergic and glutamatergic projection neurons are found in the SC, GABAergic neurons mostly innervate locally within the nucleus (Lee and Hall, 2006; Sooksawate et al., 2011). MEA is largely noncholinergic and may also give rise to glutamatergic (and GABAergic) projections to the STN (Bevan and Bolam, 1995). Therefore these data suggest that the small proportion of ChR2-positive VGLUT2 terminals may largely originate from the

SC and/or MEA.

Since STN predominantly receives GABAergic projection from the GPe (Smith et al., 1998), most of VGAT terminals that were ChR2-positive are likely to arise from the nucleus. Indeed, ChR2-EYFP DAB staining was detected in many neuronal cell bodies across distributed regions of the GPe, suggesting that these neurons are the main origin of GABAergic projections to the STN. Although STN also receives GABAergic projection from the ventral pallidum, the innervation is known to be restricted only to the very medial pole of STN (Bevan et al., 1997). However, minor ChR2-positive GABAergic projection from the immunoreactive MEA remains a possibility (Bevan and Bolam, 1995).

The results from this study have several implications. First, the current study could be the first rigorous quantification of the relative abundance of different cortical and subcortical inputs to STN. Selectivity in stimulation of cortical-STN input, which has been difficult with traditional stimulation electrodes, is particularly important considering the unexpected finding that subcortical glutamatergic inputs to STN are just as numerous as cortical inputs to STN. Multiple sources of glutamatergic afferents often cause difficulty in interpreting results from various studies of synaptic phenomena in the STN. Although not exclusive, the abundant expression of ChR2 in cortical afferents compared to subcortical afferents in the STN of *Thy1-ChR2-EYFP* line 18 will significantly improve the specificity of cortical input stimulation.

Second, characterisation of ChR2 expression in the STN will facilitate more precise interrogation of the mechanisms underlying DBS. Previous study using *Thy1-ChR2-EYFP* line 18 mice demonstrated that optogenetic HFS of motor cortex and of afferents in the STN improved motor impairments in parkinsonian animals, suggesting that DBS exerts its effect through driving the cortical–STN input (Gradinaru et al., 2009). This study however reveals abundant expression of ChR2 in GABAergic terminals within the STN, implying that manipulation of GPe–STN input could in part contribute to the reversal of parkinsonian symptoms during DBS. This speculation is consistent with the observation that LFS of STN worsened motor symptoms in these parkinsonian animals similar to observations in PD patients, whereas LFS of motor cortex did not produce such effect (Gradinaru et al., 2009).

Indeed growing body of evidence suggests that abnormal GPe–STN transmission following dopamine depletion is critical for the manifestation of activity rate and pattern changes of extrastriatal basal ganglia in experimental PD due to its pivotal position in the GPe–STN reciprocal network and in the indirect pathway of basal ganglia circuitry, as well as its interaction with glutamatergic input in the STN (Bevan et al., 2007; Wilson and Bevan, 2011). The *Thy1-ChR2-EYFP* mouse line will be a useful transgenic model to probe into the cellular principles regulating cortical and GPe–STN inputs and their modulation by dopamine in health and experimental PD.

Despite the non-exclusive specificity of ChR2 expression in cortical afferents within the STN, long-term use of this transgenic mouse strain will be a highly efficient alternative to costly and labour-intensive methods for repeated ChR2 delivery to the same specific classes of neurons. Although variants of ChR2, such as ChETA or ChiEF, have been developed to address some of the issues associated with ChR2 (eg. relatively slower kinetics and minor calcium permeability), they have not been extensively tested and wild-type ChR2 remains a robust choice for highly specific method to manipulate neuronal activity (Gunaydin et al., 2010; Berndt et al., 2011; Lin et al., 2011).

CHAPTER 4

THE IMPACT OF HCN CHANNELS ON INHIBITORY SYNAPTIC INTEGRATION IN NEURONS OF THE SUBTHALAMIC NUCLEUS

4.1. Introduction

The firing patterns of STN neurons are highly correlated with normal movement and abnormal movement in PD and are generated through the dynamic, non-linear interplay between intrinsic and synaptic conductances (Crossman, 2000; Brown, 2003; Wichmann and Delong, 2003; Bevan et al., 2006). Apart from glutamatergic projections from the cortex and intralaminar thalamus (Bevan et al., 1995), the STN is innervated by GABAergic afferents that predominantly arise from the GPe (Smith et al., 1998). Although GPe neurons fire at relatively high frequency *in vivo* (Urbain et al., 2000) and their inputs can potently pattern the frequency and synchronisation of the STN activity (Bevan et al., 2002; Baufreton et al., 2005,2009), GPe and STN neuronal activities are rarely correlated under normal conditions (eg. Hallworth and Bevan, 2005; Mallet et al., 2008b). The intrinsic conductances that actively oppose inhibitory conductances might therefore play an important role. One potential candidate is the HCN channels because their role in the STN neurons is still poorly understood. Despite high levels of expression (Santoro et al., 2000; Notomi and Shigemoto, 2004), the channels do not contribute to the characteristic autonomous activity of STN neurons and their role in (certain forms of) synaptic integration appears minimal (Bevan and Wilson, 1999; Beurrier et al., 2000; Do and Bean, 2003; Baufreton et al., 2005). Thus, blockade of HCN channel function has no effect on firing rate or rhythmicity of STN cells or on the resetting of firing by single GABAergic synaptic inputs. The duration and degree of hyperpolarization produced by individual IPSPs are apparently not enough to strongly activate HCN channels (and deinactivate Ca_v3 channels; Baufreton et al., 2005). In contrast, in many classes of nerve cell HCN channels underlie a key conductance that contributes to intrinsic activity and sculpts the integration of synaptic inputs (Robinson and Siegelbaum, 2003; Baruscotti and DiFrancesco, 2004; Biel et al., 2009).

The molecular and biophysical properties of native HCN channels have been extensively characterised (Robinson and Siegelbaum, 2003; Baruscotti and DiFrancesco, 2004; Biel et al., 2009). Native HCN channels comprise homo- or hetero-tetramers of up to 4 subunits (HCN1–4), activate progressively with hyperpolarisation and are modulated directly by cyclic AMP. HCN channels invariably mediate depolarisation

because the equilibrium potential of their mixed cation current is ~ –30 mV. HCN channels subserve a range of neuronal functions. Thus, HCN channels contribute oscillatory properties to neurons and neuronal networks (Lüthi and McCormick, 1998; Bennett et al., 2000; Ludwig et al., 2003; Chan et al., 2004; Garden et al., 2008), regulate the location dependence of synaptic potential magnitude and time course (Magee, 1998, 1999; Williams and Stuart, 2000; Angelo et al., 2007), oppose bistability and Ca^{2+} channel-mediated electrogenesis (Pape and McCormick, 1989; Lüthi and McCormick, 1998; Williams et al., 2002; Tsay et al., 2007) and mediate homeostatic adjustments in intrinsic excitability (Fan et al., 2005).

In STN neurons, HCN channel currents can be readily detected upon prolonged hyperpolarization of the membrane potential by current pulses (Nakanishi et al., 1987; Bevan and Wilson, 1999; Beurrier et al., 2000). Upon removal of the hyperpolarization, prominent rebound bursts are seen in all STN neurons due to the deinactivation of low-voltage-gated Ca_v3 channels (Bevan et al., 2002; Hallworth et al., 2003). Therefore, these Ca^{2+} and non-specific cation currents are often present together, and their interaction may be functionally relevant to PD which involves excessive burst firing in the STN. Indeed, HCN channel dysregulation has been linked to certain neurological disorders including epilepsy and PD (Shah et al., 2004; Kole et al., 2007; Shin et al., 2008; Meurers et al., 2009; Chan et al., 2011).

The functional roles of HCN channels are related to a variety of factors including their subunit composition, compartmental expression pattern, voltage-dependence, kinetics and interaction with intrinsic and synaptic conductances (Robinson and Siegelbaum, 2003; Baruscotti and DiFrancesco, 2004; Biel et al., 2009). Therefore, in order to address the specific roles of HCN channels in STN neurons, following techniques were applied: 1) single cell molecular profiling to determine the subunit expression pattern 2) immunocytochemistry to determine the plasma membrane expression pattern 3) patch clamp recording to determine the biophysical properties of HCN channels and their role in burst firing 4) dynamic clamp to determine their role in the integration of inhibitory inputs, and 5) computational modelling to examine the interaction of HCN and other ion channels.

4.2. Materials and methods

This study utilised tissue prepared from male Sprague Dawley or Wistar rats (p16-adult) and adult C57BL/6 HCN2 wildtype and deficient mice (Ludwig et al., 2003). Procedures were performed in accordance with the policies of the Society for Neuroscience, the National Institutes of Health, the 1986 UK Animals (Scientific Procedures) Act and the Institutional Animal Care and Use Committees of Bordeaux, Northwestern and Sheffield Universities and the Graduate University for Advanced Studies, Okazaki, Japan.

4.2.1. Single cell molecular profiling

STN neurons (p16-25) were acutely isolated and subjected to molecular profiling using the single cell reverse transcription polymerase chain reaction technique (scRTPCR), as described previously (Tkatch et al., 2000; Ramanathan et al., 2008). The results of scRTPCR were expressed as a fraction of cells with detectable mRNA levels. The detection of mRNA was based on the presence of a clearly visible band of the appropriate size in an ethidium bromide-stained gel. In order to ensure consistent efficacy of reverse transcriptase all experiments were carried out with the same batch of enzyme. HCN1 mRNA (GenBank accession AF247450) was detected with a pair of primers ATGCCTCTCTTTGCTAACGC (position 1458) and TATTCCTCCAAGACCTCGTTGAA (position 1476), which gave a PCR product of 311 bp. HCN2 mRNA (GenBank accession AF247451) was detected with a pair of primers TTCCGCCAGAAGATCCACGATTA (position 1318) and GAACACGTGCGACTTACTCATAA (position 832), which gave a PCR product of 185bp. HCN3 mRNA (GenBank accession AF247452) was detected with a pair of primers GTCGGAGAACAGCCAGTGTAA (position 1496) and TGAGCGTCTAGCAGATCGAG (position 1928), which gave a PCR product of 452 bp. HCN4 mRNA (GenBank accession AF247453) was detected with a pair of primers ATCAACGGCATGGTGAATAACTC (position 1584) and TGCCCTGGTAGCGGTGTTC (position 1893), which gave a PCR product of 328 bp.

4.2.2. Immunohistochemical analysis of HCN2 subunit expression

The rabbit polyclonal HCN2 antibody used in this study was raised against glutathione S-transferase fusion proteins containing the C-terminus of rat HCN2 (amino acid residues 797-862), as described previously (Notomi and Shigemoto, 2004). For immunization, HCN2 fusion protein was purified by sodium dodecyl sulphate-polyacrylamide gel electrophoresis. The gel fragments containing the purified fusion protein were emulsified with Freund's complete (first immunization) or incomplete (second immunization) adjuvant (Nacalai tesque, Kyoto, Japan) and injected subcutaneously into rabbits (500 mg fusion protein per animal) at intervals of 4 weeks. From antisera collected 2 weeks after the second injection, HCN2 antibody was affinity purified, first using Protein G-Sepharose (Amersham Pharmacia Biotech, Uppsala, Sweden) and then CNBr-activated Sepharose 4B (Amersham Pharmacia Biotech) coupled to the HCN2 fusion protein. The specificity of immunostaining with the HCN2 antibody was verified using an HCN2 gene-deficient mouse (Ludwig et al., 2003) (Fig. 4.1). Adult wild-type and HCN2 gene-deficient (Ludwig et al., 2003) mice were deeply anaesthetised with pentobarbital, perfused with phosphate buffered saline (PBS; 0.01 M phosphate, pH 7.4) for 1 minute, followed by fixative containing 4% paraformaldehyde, 0.05% glutaraldehyde, and 15% saturated picric acid in 0.1 M phosphate buffer (PB; pH 7.4) for 15 minutes. Brains were removed and sections cut on a vibratome (VT1000s; Leica Microsystems) at a thickness of 50 μm. Sections were then incubated at 4°C with the HCN2 antibody (1.0 μg/ml) in PBS containing 0.1% Triton X-100, 0.25% -carrageenan, and 0.5% normal goat serum (NGS). After several washes in PBS the sections were incubated with biotinylated goat anti-rabbit IgG antibody (1:200, Vector Laboratories; Burlingame, USA) at room temperature for 1 hour and then with avidin–biotin–peroxidase complex (1:100 ABC-Elite in PBS; Vector Laboratories) at room temperature for 1 hour. Finally, sections were incubated in DAB (Dojindo, Kumamoto, Japan) and hydrogen peroxide to reveal immunoreactivity. Sections were then mounted on glass slides and prepared for light microscopic analysis.

Rats (p20-adult; Charles River) were deeply anaesthetised with ketamine and xylazine and perfused via the ascending aorta with PBS, followed by 300 ml of 4% paraformaldehyde and 0.05% glutaraldehyde in PB followed by 200 ml of PB. Brains

were then removed and sectioned in the sagittal plane on a vibratome (VT1000s; Leica Microsystems) at 70 μm. Sections were freeze-thawed, washed in PBS and then incubated in PBS containing 10% NGS for 2 h prior to antibody incubations in PBS containing 2% NGS. Sections were incubated in the HCN2 antibody described above at 0.5 μg/ml, for 48 h at 4°C. Sections for immunoperoxidase labelling were incubated in biotinylated goat anti-rabbit IgG (1:200; Vector Laboratories) for 2–3 h, followed by 2 h in avidin–biotin–peroxidase complex (1:100 ABC-Elite; Vector Laboratories), at room temperature. Bound peroxidase was then revealed by incubating the sections in DAB in the presence of hydrogen peroxide (Vector Laboratories). Sections for immunogold labelling were incubated in goat anti-rabbit IgG coupled to 1.4 nm gold particles (1:100; Nanoprobes, Yaphank, USA) for 3–4 h at room temperature. Bound gold particles were silver-enhanced using the HQ Silver kit (Nanoprobes). Sections were then postfixed in 1% osmium tetroxide in PB for 25 min (immunoperoxidase) or 10 min (immunogold) and dehydrated through a graded series of alcohol dilutions and embedded in resin (Durcupan ACM Fluka; Sigma-Aldrich) on glass slides.

Immunoreactive structures in the STN were examined using a light microscope equipped with 40–100× oil immersion objectives (Zeiss Axioskop, Zeiss, Oberkochen, Germany) and images were captured using a high-resolution digital camera (Zeiss Axiocam). The dimensions of immunoreactive neuronal somata and putative glial cell bodies were quantified from the digital images using Image J (National Institutes of Health, Bethesda, USA) and compared statistically using the Mann-Whitney *U* test (Prism 5, GraphPad Software). An α value of 0.05 was used as the criterion for determining statistically significant differences. Following light microscopic analysis, areas of the STN were excised, re-sectioned at 50–70 nm on an ultramicrotome (UCT, Leica Microsystems) and collected on pioloform-coated, single-slot copper grids. Ultrathin sections were then stained with 1 % uranyl acetate for 30 min followed by lead citrate for 2–3 min before being imaged and analysed with a Jeol 1200 (Jeol USA, Peabody, USA) or Tecnai G2 Spirit (FEI, Hillsboro, USA) transmission electron microscope. Electron microscopic analysis of structures expressing HCN2 was performed on rat DAB and immunogold labelled tissue. Tissue close to the surface of the block was analysed to minimise false negative labelling due to limited penetration of immunoreagents. The densities of immunogold particles overlying somatic and

dendritic compartments were quantified using Reconstruct (http://synapses.clm.utexas.edu/tools/reconstruct/reconstruct.stm). Given that the dendrites of STN neurons tend to decrease in diameter with distance from the soma (Kita et al., 1983; Afsharpour, 1985), proximal dendrites were defined arbitrarily as having a diameter > 1 μm and distal dendrites as having a diameter < 1 μm (two perpendicular diameters were measured for each dendrite and the minimum diameter was used for analysis). The distance of immunogold particles from the middle of the plasma membrane to the middle of the particle was measured. The best Gaussian fit to the data showed a peak position at 23.3 nm from the membrane with an SD of 9.9 nm. A gold particle was thus considered to be associated with the plasma membrane if it was located within an area that was up to 43 nm (peak + 2SD) of the cytoplasmic side of the plasma membrane. Immunoparticle densities were measured by calculating the number of gold particles per unit area. Nonspecific labelling was considered to be the density of nuclear labelling. The compartmental distribution of HCN2 labelling was compared statistically using the Kruskal-Wallis test with Dunnett's post hoc analysis (Prism 5, GraphPad Software) An α value of 0.05 was used as the criterion for determining statistically significant differences.

4.2.3. Electrophysiology

Slice preparation and recordings. Brain slices were prepared, maintained and then transferred to recording chamber as described previously (refer to section 3.2.2. Electrophysiology). Somatic recordings, made using borosilicate glass micropipettes, were obtained under visual guidance (Axioskop FS2, Zeiss) using computer-controlled manipulators (Luigs & Neumann) and a Multiclamp 700B amplifier and digidata 1440A digitizer controlled by PClamp 10 (Molecular Devices). Recording pipettes contained 135 mM K-$MeSO_4$, 3.8 mM NaCl, 1 mM $MgCl_2.6H_2O$, 10 mM HEPES, 0.1 mM Na_4EGTA, 0.4 mM Na_3GTP, and 2 mM $Mg_{1.5}$ATP. The resistance of filled pipettes (as measured in the bath) was 3–4 MΩ for voltage clamp experiments, and 5–12 MΩ for current clamp experiments.

Recordings were acquired using Clampex 10 software (Molecular Devices, Palo

Alto, CA) running on a PC connected to a Multiclamp 700B amplifier (Molecular Devices) *via* a Digidata 1322A digitizer (Molecular Devices). Recordings were low-pass filtered online at 10 kHz and sampled at 50 kHz. For current clamp recordings electrode capacitance was compensated on-line and voltage errors due to series resistance were either compensated on-line or corrected off-line. For voltage clamp recordings, electrode capacitance and series resistances of ~ 10–20 MΩ were electrically compensated. A liquid junction potential correction of 9 mV was subtracted from whole-cell recordings. Synthetic $GABA_A$R-mediated IPSPs were generated through the patch pipette using a synaptic module (SM-1) conductance injection amplifier (Cambridge Conductance, Cambridge, UK), as previously described (Baufreton et al., 2009).

Drugs. All drugs used were prepared as concentrated stock solutions and stored at –20˚C. On the day of the experiment drugs were diluted and applied either through the bath or local perfusion system. GABAergic and glutamatergic synaptic transmission was blocked for all experiments. NMDA, AMPA, $GABA_A$ and $GABA_B$ receptors were blocked with 50 μM APV (Ascent Scientific, Princeton, NJ), 20 μM DNQX (Ascent Scientific), 20 μM GABAzine (Ascent Scientific; SR 95531) and 2 μM CGP 55845 (Tocris Bioscience, Ellisville, USA), respectively. Na_v and HCN channels were blocked with 1 mM TTX (Ascent Scientific) and 20 μM 4-ethylphenylamino-1,2-dimethyl-6-methylaminopyrimidinium chloride (ZD7288; Ascent Scientific), respectively. Because ZD7288 may have non-specific effects (Chevaleyre and Castillo, 2002; Do and Bean, 2003; Felix et al., 2003), 2 mM Cs was also applied in some experiments to block HCN channels (Halliwell and Adams, 1982).

Data analysis. Data were analysed using Clampfit 10 (Molecular Devices), IgorPro 6 (Wavemetrics, Portland, OR), and Prism 5 (GraphPad Software). Line scan images were analysed with IgorPro 6. Maximum intensity projections of Z-series were generated with Image J (National Institutes of Health, Bethesda, USA). Numerical data are presented as mean ± SD. An α value of 0.05 was used as the criterion for determining statistically significant differences.

4.2.4. Computational modelling

In order to further investigate the impact of HCN channels on synaptic integration, a simplified compartmental model consisting of a single spherical somatic compartment and a four-compartment dendrite, of which each compartment was represented by a cylinder was constructed. The suffix i represents the location of each compartment, with 0 for the somatic compartment and 1–4 for each dendritic compartment. The diameter (d_i) and length (l_i) of each compartment are listed in Table 4.1. The membrane potential of the i-th compartment V_i was calculated from the following equation:

$$c_{\mathrm{m}} A_i \frac{dV_i}{dt} = -g^{\mathrm{axis}}_{i-1,i}(V_i - V_{i-1}) - g^{\mathrm{axis}}_{i+1,i}(V_i - V_{i+1}) - A_i I^{\mathrm{ion}}_i - I^{\mathrm{syn}}_i - I^{\mathrm{app}}_i$$

where c_m is unit membrane capacitance (c_m = 1 μF cm^{-2}) and A_i is the surface area of the i-th compartment ($\pi d_i l_i$). g^{axis} is the axial conductance between adjacent compartments and was determined from the cytoplasmic resistance R_{a} (150 Ωcm) (Gillies and Willshaw, 2006) and the dimensions of adjacent compartments according to the following equation:

$$g^{\mathrm{axis}}_{i-1,i} = \frac{1}{\frac{2R_{\mathrm{a}}}{\pi}\left(\frac{l_{i-1}}{d^2_{i-1}} + \frac{l_i}{d^2_i}\right)}$$

I^{ion}, I^{syn} and I^{app} are ionic current density, synaptic current and applied current, respectively. The ionic current density I^{ion} was determined by currents flowing through several ion channels including leak, Na_v, class 3 voltage dependent K^+ (K_v3), small conductance Ca^{2+}-dependent K^+ (SK), class 3 and 2.2 voltage dependent Ca^{2+} (Ca_v3 and $Ca_v2.2$, respectively) and HCN channels:

$$\begin{aligned} I^{\mathrm{ion}} = & -g_{\mathrm{leak}}(V - E_{\mathrm{leak}}) - g_{\mathrm{Nav}} m^3 h (V - E_{\mathrm{Na}}) - g_{\mathrm{Kv3}} n^4 (V - E_{\mathrm{K}}) - g_{\mathrm{SK}} r^2 (V - E_{\mathrm{K}}) \\ & - g_{\mathrm{Cav3}} p^2 q (V - E_{\mathrm{Ca}}) - g_{\mathrm{Cav2.2}} v w (V - E_{\mathrm{Ca}}) - g_{\mathrm{HCN}} f (V - E_{\mathrm{cation}}) \end{aligned}$$

Gating variables for each ion channel were described by an activation function and a time constant:

$$\frac{dx}{dt} = \frac{x_\infty(u) - x}{\tau_x(u)}$$

$$x_\infty(u) = \frac{1}{1 + \exp[(u - \theta_x)/k_x]}$$

$$\tau_x(u) = \tau_x^0 + \frac{\tau_x^1}{\exp[(u - \phi_x^1)/\sigma_x^1] + \exp[(u - \phi_x^2)/\sigma_x^2]}$$

where x represents the gating variable and u is membrane potential for a voltage-dependent channel or intracellular Ca^{2+} concentration for the SK channel. Intracellular calcium concentration obeyed the following equation (Otsuka et al., 2004):

$$\frac{d[Ca^{2+}]_i}{dt} = -\frac{\gamma_i}{ZF}(I_{Cav3} + I_{Cav2.2}) - K_{Ca}[Ca^{2+}]_i$$

where Z is the valence of calcium ion (2), F is the Faraday constant, K_{Ca} is the Ca^{2+} removal rate (2 ms) and γ_i is the ratio of surface area to volume for the i-th compartment. Parameters for Na_v, K_v3, Ca_v3 and SK channels were adopted from the model of Otsuka and colleagues (2004) with voltage-dependent functions shifted by −7.1 mV for Na_v and −5 mV for the others (θ_x, $\varphi_x{}^1$ and $\varphi_x{}^2$ are changed). Parameters for $Ca_v2.2$ channels were adopted from Tsay and colleagues (2007) except for a shift in voltage-dependence of −5 mV. The activation function of HCN channels was based on experimental data. The voltage-dependent time constant of Angelo et al. (2007) was adopted except that the time constant $\tau_x{}^1$ was increased from 1600 ms to 2400 ms. Parameters for each channel are detailed in Table 4.2. Equilibrium potentials (E) were set as follows: E_{leak} = −67 mV, E_{Na} = 50 mV, E_K = −90 mV and E_{cation} = −35 mV for the HCN channel. E_{Ca} was determined by the Nernst equation. To determine the impact of HCN channel expression and compartmental distribution 3 models were investigated: somatic, somatodendritic and deficient. Respectively, HCN conductance was restricted to the soma, uniformly expressed in each compartment or entirely absent. The total HCN conductance for each model ($\Sigma_i A_i g_{HCN,i}$) was equivalent for the somatic and somatodendritic models. The initial magnitude of conductances in each compartment are detailed in Table 4.1 and were chosen so that 1) model neurons exhibited typical membrane properties of STN neurons i.e., autonomous activity of ~ 10 Hz, voltage sag in response to hyperpolarising current injection (for models in which HCN channels were expressed) and rebound burst activity; 2) the impact of channel removal was

similar to that observed experimentally (Bevan et al., 1999; Beurrier et al., 2000; Hallworth et al., 2003); 3) APs were generated in the soma before propagating into the dendritic compartment, as observed experimentally (Atherton et al., 2008). The maximum conductance of each ion channel in each compartment is indicated in Table 4.1. I^{syn} represents excitatory and inhibitory synaptic currents. EPSCs were modelled as a compound of AMPA receptor-mediated and NMDA receptor-mediated components. The AMPA receptor-mediated EPSC was described by the model of Tsodyks and Markram (1997):

$$\begin{aligned} I_{\mathrm{AMPA}}^{\mathrm{syn}} &= g_{\mathrm{AMPA}} e (V - E_{\mathrm{AMPA}}) \\ \frac{de}{dt} &= -\frac{e}{\tau} + Ur\delta(t - t_{\mathrm{AP}}) \\ \frac{dr}{dt} &= \frac{1 - r - e}{\tau_{\mathrm{rec}}} \end{aligned}$$

where e and r represent effective and recovered ratios of neurotransmission, respectively. The decay constant of the EPSC τ and the recovery time constant τ_{rec} were set to 2.5 ms and 200 ms, respectively. The presynaptic release probability U was 0.2. t_{AP} represents the timing of the presynaptic AP.

The NMDA receptor-mediated EPSC was described by the model of Destexhe and colleagues (1998):

$$\begin{aligned} I_{\mathrm{NMDA}}^{\mathrm{ion}} &= g_{\mathrm{NMDA}} s F(V)(V - E_{\mathrm{NMDA}}) \\ \frac{ds}{dt} &= \alpha T(1 - s) - \beta s \\ F(V) &= \frac{1}{1 + 0.28 \exp(-0.062V)} \end{aligned}$$

where α^{-1} and β^{-1} are rise and decay time constants of the open ratio of receptors (s) and were set to 2.0 ms and 142.8 ms, respectively. The variable T represents presynaptic neurotransmitter release, which was set to 1 ms after the occurrence of an AP, and is otherwise 0. $F(V)$ is a postsynaptic-voltage-dependent function that represents voltage dependent Mg^{2+} block. The inhibitory postsynaptic current mediated by $GABA_A$ receptors was modelled similarly to AMPA receptors except that a decay time constant

of 8.0 ms was employed. Finally, simulation codes were written in C and numerical integration was carried out with the fourth order Runge-Kutta method. An integration time step of 0.05 ms was used although similar results were obtained with a time step of 0.01 ms.

	soma 0	**dend 1**	**dend 2**	**dend 3**	**dend 4**
diameter [μm]	10.0	2.0	1.5	1.0	0.5
length	10.0	100.0	100.0	100.0	100.0
g_{leak} **[mScm^{-2}]**	0.08	0.08	0.08	0.08	0.08
g_{Nav}	33.0	0.01	0.01	0.01	0.01
g_{Kv3}	69.0	0.01	0.01	0.01	0.01
g_{SK}	0.1	0.1	0.1	0.1	0.1
g_{Cav3}	0.6	0.6	0.6	0.6	0.6
$g_{Cav2.2}$	1.0	1.0	0.1	0.1	0.1
G_{HCN} **(somatic)**	1.2	0.0	0.0	0.0	0.0
G_{HCN} **(uniform)**	0.2	0.2	0.2	0.2	0.2
G_{HCN} **(deficient)**	0.0	0.0	0.0	0.0	0.0

Table 4.1. Morphological and electrical properties of the STN neuron model

Channel	Parameters	Values	Channel	Parameters	Values
Na_v	θ_m, k_m	−47.1, −8.0	$Ca_v2.2$	θ_w, k_w	−64.0, 10.0
Na_v	τ_m^0, τ_m^0	0.2, 3.0	$Ca_v2.2$	τ_w^0, τ_w^1	121.0, 0
Na_v	φ_m, σ_m	−58.0, −0.7	Ca_v3	θ_p, k_p	−61.0, −6.7
Na_v	θ_h, k_h	−50.5, 6.4	Ca_v3	τ_p^0, τ_p^1	5.0, 0.33
Na_v	τ_h^0, τ_h^1	0, 24.5	Ca_v3	φ_p^1, σ_p^1	−32.0, −10.0
Na_v	φ_h^1, σ_h^1	−55.0, −15.0	Ca_v3	φ_p^2, σ_p^2	−107.0, 15.0
Na_v	φ_h^2, σ_h^2	−55.0, 16.0	Ca_v3	θ_q, k_q	−95.0, 5.8
K_v3	θ_n, k_n	−46.0, −14.0	Ca_v3	τ_q^0, τ_q^1	0, 400.0
K_v3	τ_n^0, τ_n^0	0, 11.0	Ca_v3	φ_q^1, σ_q^1	−55.0, −15.0
K_v3	φ_n^1, σ_n^1	−45.0, −40.0	Ca_v3	φ_q^2, σ_q^2	−55.0, 16.0
K_v3	φ_n^2, σ_n^2	−45.0, 50.0	HCN	θ_f, k_f	-90.0, 8.0
SK	θ_r, k_r	0.17, −0.08	HCN	τ_f^0, τ_f^1	0, 2400.0
SK	τ_r^0, τ_r^1	2.0, 0.0	HCN	φ_f^1, σ_f^1	−68.0, −22.0
$Ca_v2.2$	θ_v, k_v	−7.0, −10.0	HCN	φ_f^2, σ_f^2	−68.0, 7.0
$Ca_v2.2$	τ_v^0, τ_v^1	3.0, 0			

Table 4.2. Channel parameters of the STN neuron model

4.3. Results

4.3.1. STN neurons express multiple HCN subunits

scRTPCR analysis was carried out to determine the pattern of HCN channel subunit mRNA expression in individual acutely isolated STN neurons (Fig. 4.1 *A*, *B*). Of 16 cells tested, 8 (50.0%) expressed detectable levels of HCN1 channel subunit mRNA, 13 (81.3%) expressed HCN2 and HCN3 subunit mRNA and 4 (25%) expressed HCN4 subunit mRNA (Fig. 4.1 *B*).

The STN has previously been shown to most strongly express HCN2 (Monteggia et al., 2000; Santoro et al., 2000; Notomi and Shigemoto, 2004). Light microscopic analysis confirmed that the rat and mouse STN was immunoreactive for HCN2 and demonstrated that STN immunoreactivity was abolished in HCN2 deficient mice (Fig. 4.1 *C–E*; Ludwig et al., 2003). Immunoreactivity was present in the somata of STN neurons, smaller diameter putative glial cells (minimum diameter of STN neurons = 9.6 ± 1.5 μm, n = 54; minimum diameter of putative glial cells = 6.6 ± 1.0 μm, n = 40; Mann-Whitney *U* test, $p < 0.05$) and fine dendritic- and axonal-like structures (Fig. 4.1 *C, D*). HCN2 immunoreactivity in other brain regions was also consistent with earlier reports (Monteggia et al., 2000; Santoro et al., 2000; Notomi and Shigemoto, 2004; data not shown).

Given that axons, terminals and perineuronal oligodendrocytes also express HCN2 subunits (Notomi and Shigemoto, 2004; Boyes et al., 2007) electron microscopic analysis of DAB labelled tissue was employed to determine the expression pattern of HCN2 in the somatodendritic compartment of STN neurons. Small and large diameter dendrites and neuronal somata were immunoreactive (Fig. 4.2 *A*). Labelled glial cells (putative perineuronal oligodendrocytes) were readily distinguished from the somata of STN neurons on the basis of their well-characterised ultrastructural properties including round/ovoid nuclei with relatively dense clumps of heterochromatin, electron dense cytoplasm filled with ribosomes and short strands of Golgi apparatus and endoplasmic reticulum (Ludwin et al., 1979; data not shown).

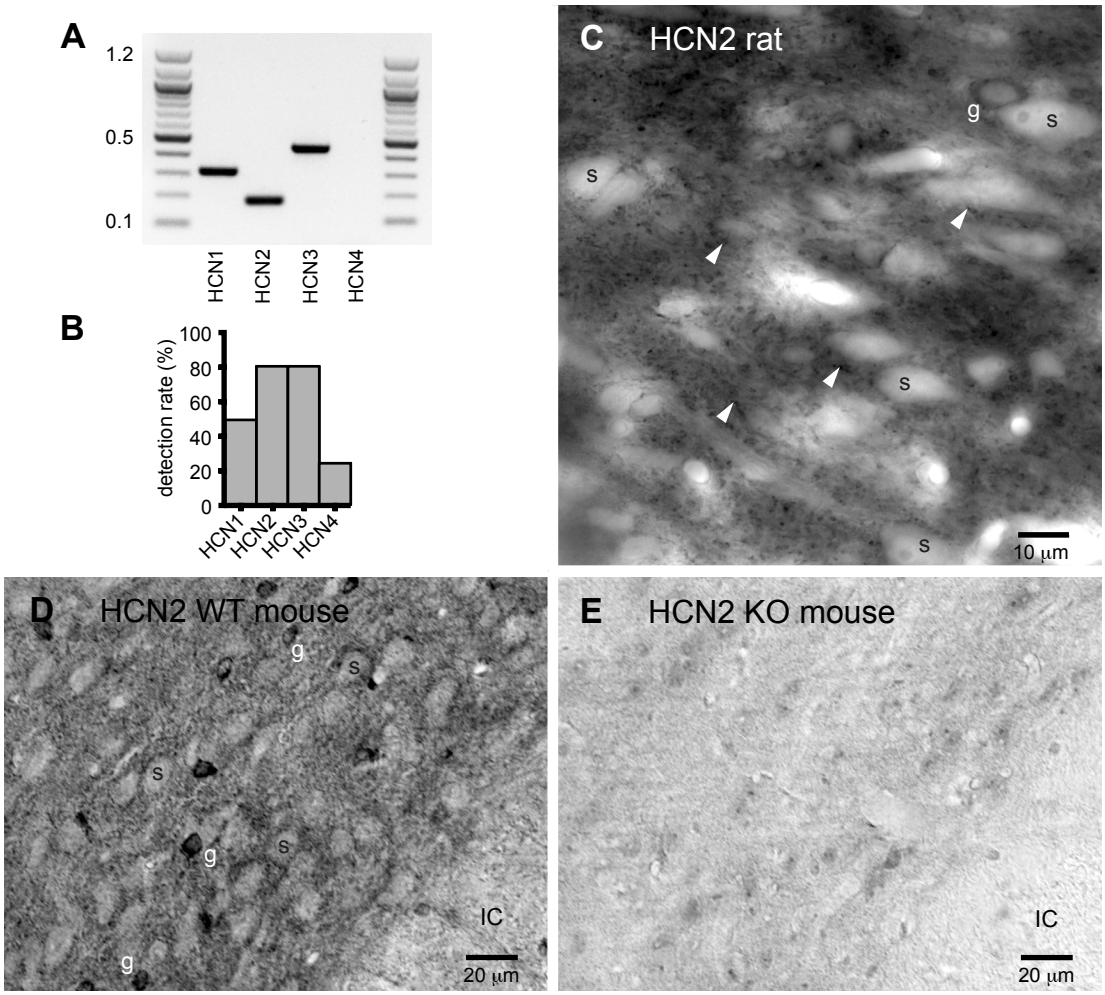

Figure 4.1. Expression of HCN channels

A, Gel from a single STN neuron that expressed HCN1, 2 and 3 mRNA. B, scRT-PCR detection rate of HCN1–4 subunits in STN neurons (n = 16). C, Light micrograph of rat STN HCN2 immunoreactivity visualised with DAB and intensified by post-fixation with osmium tetroxide. Arrowheads point to small immunoreactive elements in the neuropil. Neuronal somata (s) and small glial cells (g) were also weakly and strongly labelled, respectively. D–E, STN HCN2 immunoreactivity (as revealed by DAB without post-fixation with osmium tetroxide) in a wild type (WT) and HCN2 knockout (HCN2 KO) mouse. The pattern of labelling in the rat and WT mouse STN (labelled as for C) are similar. However, specific labelling was abolished in the STN of the HCN2 KO mouse.

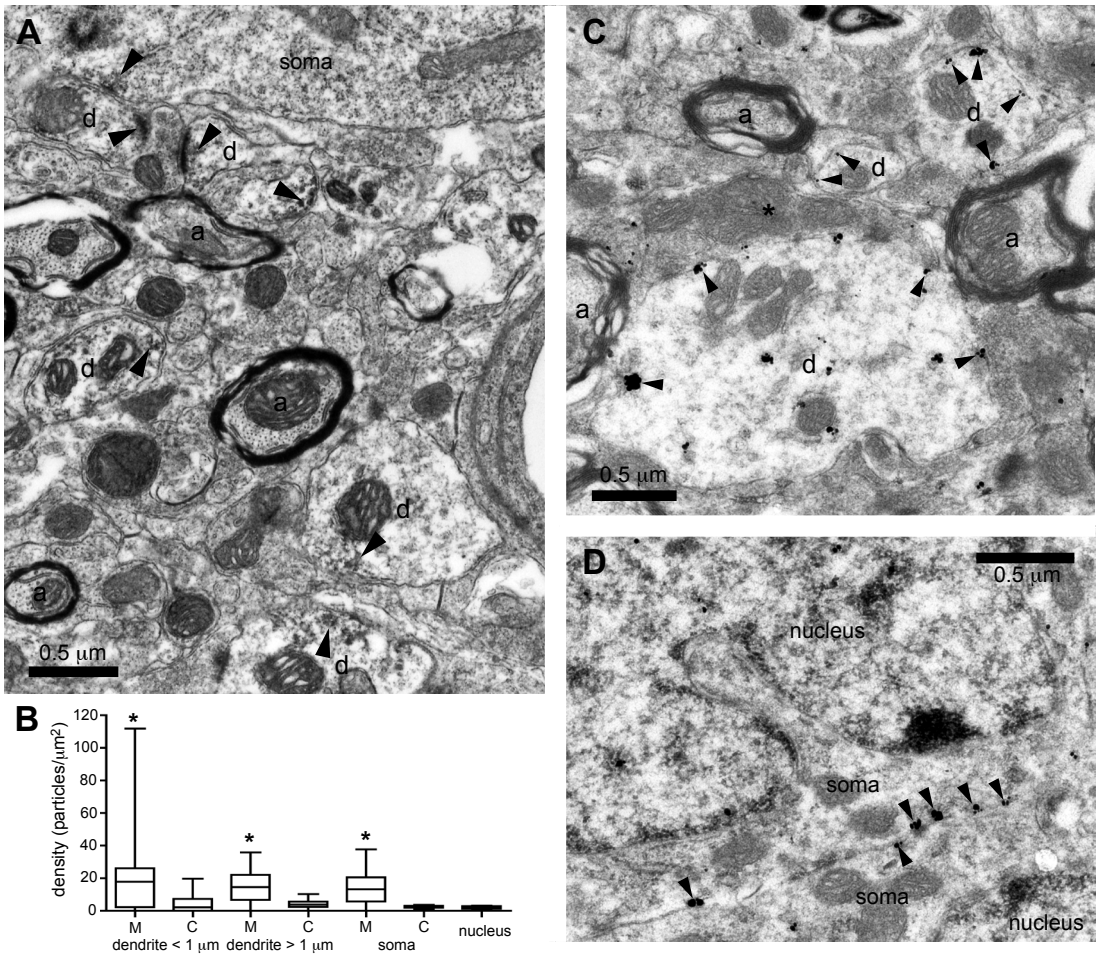

Figure 4.2. HCN2 immunoreactivity is expressed across the somatodendritic axis of STN neurons

A, Electron micrograph of STN HCN2 immunoreactivity visualised with DAB. Reaction product (arrowheads) was observed in the soma (s) of a STN neuron and dendrites (d) of varying diameters. B, The density of HCN2 immunogold particles overlying the somatodendritic membrane (M) was similar across the somatodendritic axis and significantly higher than the densities overlying cytoplasmic (C) or nuclear compartments. This sample was taken from p41 tissue. C–D, Selective association of HCN2 immunogold particles (arrowheads) with the plasma membrane of small (< 1 μm) and large (> 1 μm) diameter dendritic (d; C) and somatic (s; D) compartments of STN neurons. In C, a terminal (*) with the morphology of a globus pallidus terminal forms symmetrical synaptic contacts (arrows) with a large diameter immunoreactive dendrite. In these examples immunoreactivity was absent from myelinated axons (a) *, $p < 0.05$; box plot: box, 25%, 50% and 75%; whiskers, 10–90%.

In order to more precisely quantify the relative expression of HCN2 in each compartment of STN neurons immunogold labelling of HCN2 was analysed (c.f. Lörincz et al., 2002; Holderith et al., 2003; Boyes et al., 2007). Material from p20, p41 and p82 rats were studied to ensure that the expression patterns of HCN2 in juvenile animals (in which physiological measurements were mostly made) were similar to those associated with later stages of development. The pattern of HCN2 expression at the electron microscopic level was similar for material derived from each animal. Thus, the density of HCN2 expression overlying the somatic, large and small diameter dendritic plasma membrane of STN neurons was significantly higher than background labelling over neuronal nuclei in each sample (Fig. 4.2 *B–D*); Kruskal-Wallis and Dunn's multiple comparison tests, $p < 0.05$). In contrast the density of HCN2 expression overlying the cytoplasmic component of each compartment was not significantly different from background nuclear labelling (Fig. 4.2 *B–D*). In order to compare the specific membranous expression pattern of HCN2 across the somatodendritic axis background labelling was subtracted. The pattern of specific HCN2 expression in the somatic and large/small diameter dendritic membrane was not significantly different and this pattern was consistent for each sample [specific density of HCN2 labelling, particles per square micrometer; p20: soma = 6.3 ± 3.9 (n = 16), dendrite > 1.0 mm = 6.7 ± 7.2 (n = 20), dendrite < 1.0 mm = 9.2 ± 9.4 (n = 28); p41: soma = 10.5 ± 9.5 (n = 20), dendrite > 1.0 mm = 12.0 ± 9.1 (n = 21), dendrite < 1.0 mm = 18.5 ± 21.7 (n = 62); p82: soma = 6.9 ± 4.7 (n = 15); dendrite > 1.0 mm = 8.3 ± 5.7 (n = 11); dendrite < 1.0 mm = 9.0 ± 7.9 (n = 31); Kruskal-Wallis and Dunn's multiple comparison tests, N.S.)]. Together these data suggest that HCN2 subunits are expressed throughout the somatodendritic membrane of STN neurons and this expression pattern is stable over the developmental period of interest.

4.3.2. Voltage-dependence of HCN channel activation

Previous studies have suggested that HCN channels contribute minimally to autonomous activity of STN neurons or integration of single IPSPs emanating from the GPe (Bevan and Wilson, 1999; Beurrier et al., 2000; Do and Bean, 2003; Baufreton et al., 2005). In order to further characterise the activation of HCN channels at voltages

associated with and more hyperpolarised than the resting membrane potential (~ 70 mV), the voltage dependence of HCN channels was characterised under voltage clamp (Fig. 4.3). TTX was applied to improve voltage control. STN cells were held at –50 mV for 2 s before stepping to voltages between –50 mV and –120 mV. The cells were held at the test potential for 5 s and then stepped to –120 mV for 1 s to evoke a tail current (Fig. 4.3 *A*). In order to isolate HCN channel current, the experiments were repeated in the presence of ZD7288. Analysis of ZD7288-sensitive tail currents for the cell shown in Fig. 4.3 *A* revealed a small inward current that activated at membrane potentials hyperpolarised to ~ –60 mV. The half-maximal activation voltage ($V_{½}$) was estimated by sigmoidal fit to be –87.5 mV. Overall, for 8 cells tested, the ZD7288-sensitive current displayed minimal activation at –60 mV (1.1 ± 16.8 %) and a $V_{½}$ of –87.1 ± 4.2 mV (Fig. 4.3 *B*). Steady state currents (measured immediately prior to the step to –120 mV to measure tail currents) ranged from –13.4 ± 10.3 pA at –70 mV to –130.1 ± 98.6 pA at –120 mV (n = 8). The activation kinetics of HCN current were best fit by a double exponential (–90 mV: A_1 = 35.7 ± 12.3 %; t_1 = 430.9 ± 261.6 ms; A_2 = 64.3 ± 12.3 %; t_2 = 2270.0 ± 866.1 ms; n = 6). Together these data suggest that: 1) inputs that hyperpolarise the voltage below the range associated with autonomous activity lead to the activation of HCN channels; 2) STN HCN channels activate slowly with time constants ranging from several hundred ms to several secs.

4.3.3. HCN channels are recruited by and oppose $GABA_A$ receptor-mediated inhibition

In many types of neuron HCN channels are active at the resting membrane potential and participate in the integration of synaptic inputs (Lüthi and McCormick, 1998; Magee, 1999; Bennett et al., 2000; Williams and Stuart, 2000; Williams et al., 2002; Williams and Stuart, 2003; Ludwig et al., 2003; Chan et al., 2004; Shah et al., 2004; Fan et al., 2005; Angelo et al., 2007; Garden et al., 2008). Although STN HCN channels are apparently not active during autonomous activity, these neurons receive continuous and powerful $GABA_A$ receptor-mediated inhibition from the GPe (DeLong, 1990; Crossman, 2000; Hallworth and Bevan, 2005; Tachibana et al., 2008;

Figure 4.3. Voltage-dependence of HCN channel activation

A, representative example. A1, voltage clamp waveform used to measure voltage dependence of HCN channel activation. A2–4, currents measured under control conditions (A2), in the presence of ZD7288 (A3) and ZD7288-sensitive (A4) currents (inset shows tail currents evoked at –120 mV). A5, ZD7288-sensitive tail currents increased with progressive hyperpolarisation from –60 mV. B, Absolute and normalised (norm) ZD7288-sensitive tail currents for the sample population. Vm, membrane potential.

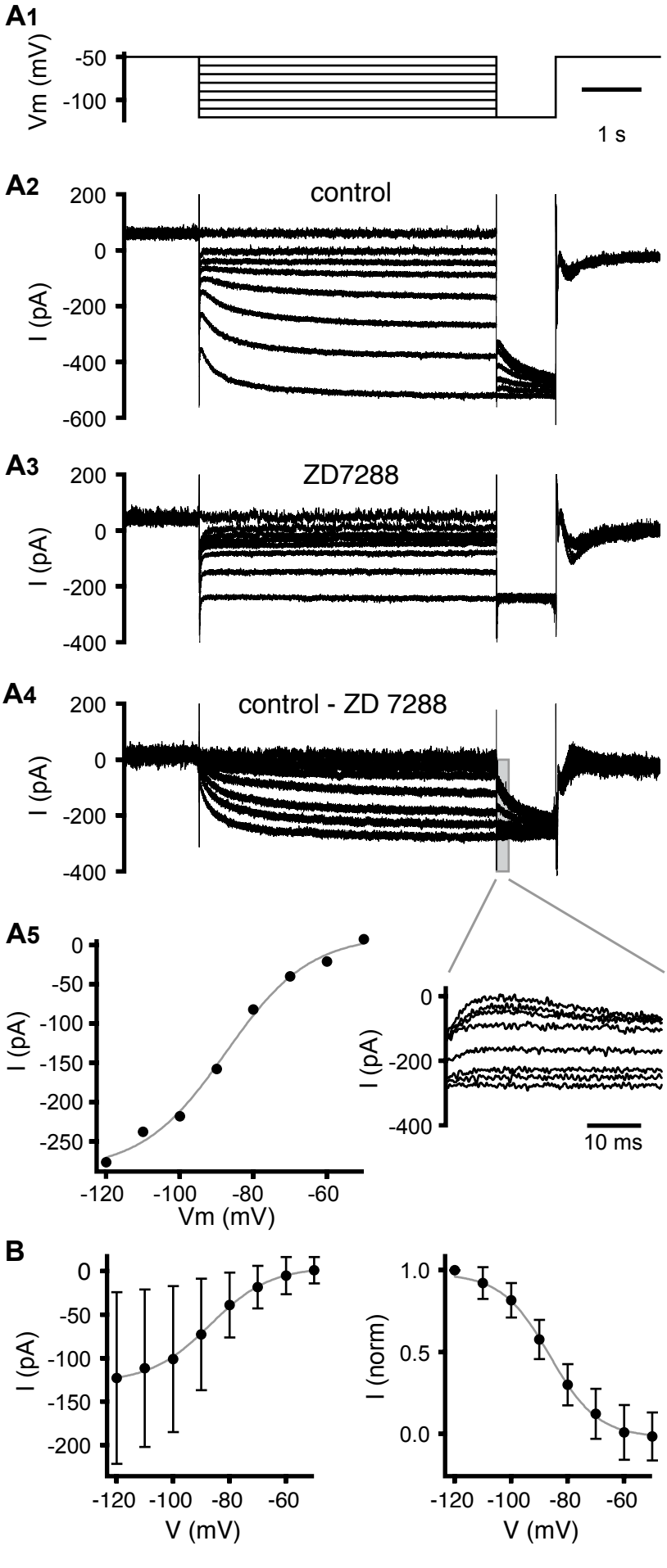
A1
Vm (mV)
-50
-100
1 s
A2
control
200
0
-200
-400
-600
I (pA)
A3
ZD7288
200
0
-200
-400
I (pA)
A4
control - ZD 7288
200
0
-200
-400
I (pA)
A5
0
-50
-100
-150
-200
-250
I (pA)
-120
-100
-80
-60
Vm (mV)
0
-200
-400
I (pA)
10 ms
B
0
-50
-100
-150
-200
I (pA)
-120
-100
-80
-60
V (mV)
1.0
0.5
0.0
I (norm)
-120
-100
-80
-60
V (mV)

Karachi et al., 2009). Given that the maximum instantaneous conductance arising from this pathway in rats is estimated to be several hundred nS and the equilibrium potential of $GABA_A$ receptor current is < –80 mV (Bevan et al., 2000, 2002; Baufreton et al., 2009), HCN channels may be strongly and dynamically recruited by GABAergic inhibition. Indeed at –80 mV HCN channels are 30.2 ± 12.6% activated and contribute approximately –30.6 ± 22.9 pA at steady state (n = 8). To test this hypothesis STN neurons were injected with a $GABA_A$ receptor mediated conductance derived from a 10 s voltage clamp record of a minimally stimulated GPe–STN axon (Fig. 4.4). Minimal stimulation was performed as described previously (Baufreton et al., 2009). The temporal pattern of minimal stimulation was derived from a GPe neuron recorded extracellularly in an awake restrained rat (Urbain et al., 2000). The record was chosen because the frequency and pattern of activity of the GPe neuron was close to the population mean (frequency = 33 Hz; CV = 0.65). Application of ZD7288 significantly reduced the number of APs generated (control = 14.0 ± 9.2; ZD7288 = 9.3 ± 8.3; n = 6; WSR test, $p < 0.05$) and significantly hyperpolarised the membrane potential (control = –71.9 ± 2.2 mV; ZD7288 = –74.5 ± 2.5 mV; n = 6; WSR test, $p < 0.05$) during the period of conductance injection. Both the peak and decay time course of IPSPs were clearly increased by blockade of HCN channels. Similar results were also obtained when HCN channels were blocked with 2 mM Cs^+ in each of 3 neurons tested (APs: control = 29.0 ± 14.0; Cs^+ = 18.7 ± 10.1; n = 3) (Vm: control = –71.2 ± 3.2 mV; Cs^+ = –73.5 ± 3.1 mV).

In order to determine how the distribution of HCN channels might influence the integration of inhibitory inputs across the somatodendritic axis, the effect of the same inhibitory conductance waveform was analysed for models in which HCN channel conductance was present at the soma or across the somatodendritic axis or was absent. The inhibitory conductance waveform was applied to the soma (not shown) or most distal dendritic compartment (Fig. 4.5). In either case the somatodendritic model was associated with greater spiking activity and was slightly more depolarised than the somatic model (somatic conductance injection; somatic HCN model: spikes = 59, mean V_o = –71.0 mV, mean V_4 = –69.9 mV; somatodendritic HCN model: spikes = 65, mean V_o = –70.7 mV, mean V_4 = –69.2 mV) (dendritic conductance injection; somatic HCN model: spikes = 41, mean V_o = –67.8 mV, mean V_4 = –72.7 mV; somatodendritic

Figure 4.4. The impact of $GABA_A$ receptor-mediated inhibition is enhanced by blockade of HCN channels

A1, Response of a STN neuron under control conditions (black) and in the presence of ZD7288 (red) to an *in vivo*-like $GABA_A$ receptor-mediated synaptic conductance waveform (blue). A2, Zoom of epoch highlighted by blue rectangle in A1. Blockade of HCN channels increased inhibition of autonomously generated action potentials (control example 31 action potentials; ZD7288 example 25 action potentials) and the degree of hyperpolarisation produced by the $GABA_A$ receptor-mediated synaptic conductance both in the representative example (A) and sample population (B; individual cells denoted by distinct colours; sample mean and SD also indicated). Vm, membrane potential; *, $p < 0.05$.

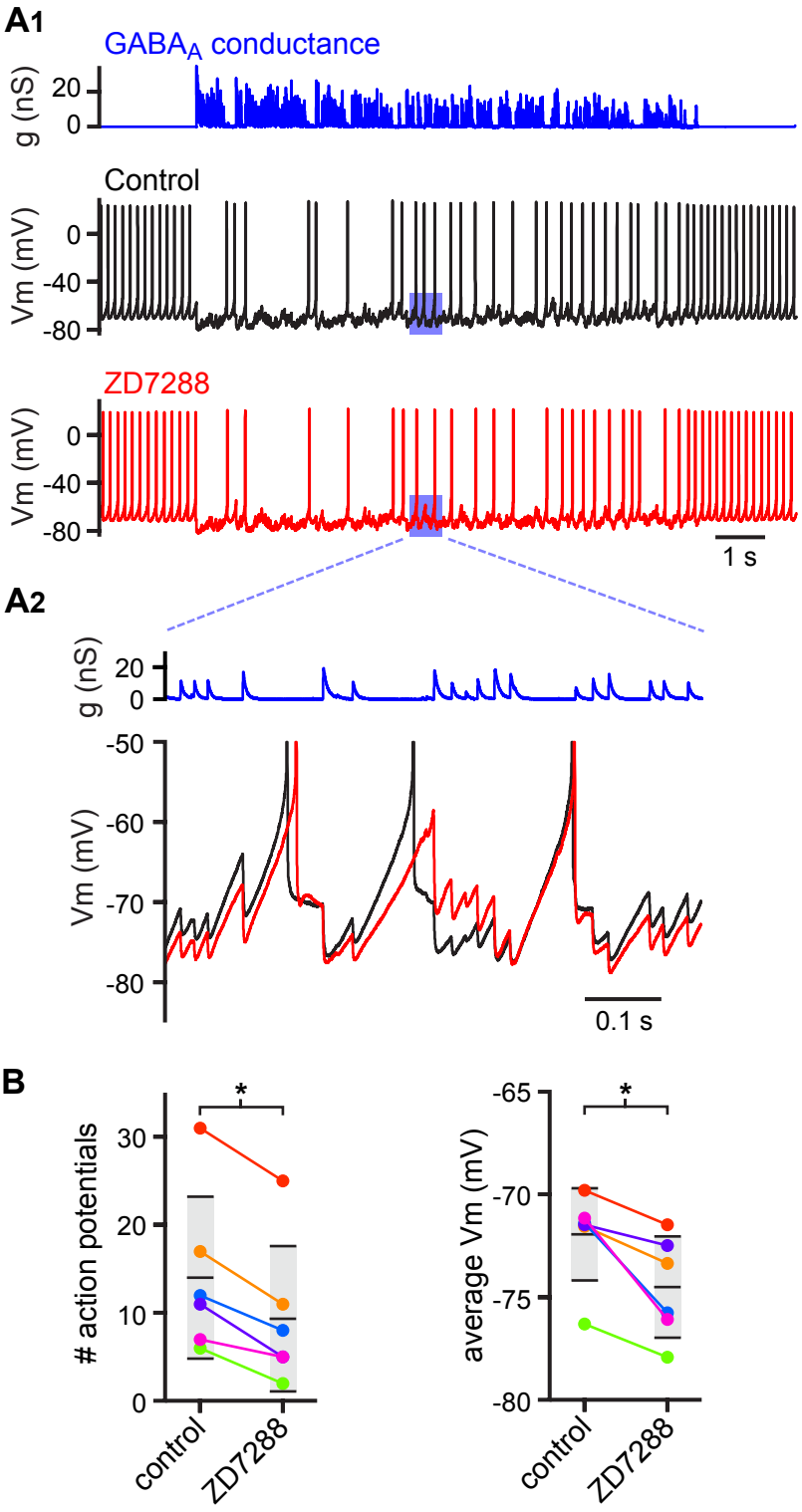
A1
GABA$_A$ conductance
g (nS)
20
0
Control
Vm (mV)
0
-40
-80
ZD7288
Vm (mV)
0
-40
-80
1 s
A2
g (nS)
20
0
-50
-60
-70
-80
Vm (mV)
0.1 s
B
action potentials
30
20
10
0
*
control
ZD7288
average Vm (mV)
-65
-70
-75
-80
*
control
ZD7288

Figure 4.5. HCN channels distributed across the somatodendritic axis most effectively counteract GABAergic inhibition

A, Somatic (black) and 4th (most distal) dendritic compartment (gray) responses of each STN neuron model to a $GABA_A$ receptor mediated-synaptic conductance (upper panel) applied to the 4th dendritic compartment. The number of action potentials generated during GABAergic inhibition was 41, 54 and 30 for the somatic, somatodendritic and deficient models, respectively. B, Zoom of the epoch 2–2.4 s from the traces in A. During the period of inhibition the somatic and 4th dendritic compartments of the somatodendritic model (blue) were relatively depolarised compared to the somatic (green) and deficient (red) models. Whole-cell HCN and Na_v channel currents were also greatest for the somatodendritic model. Vm, membrane potential.

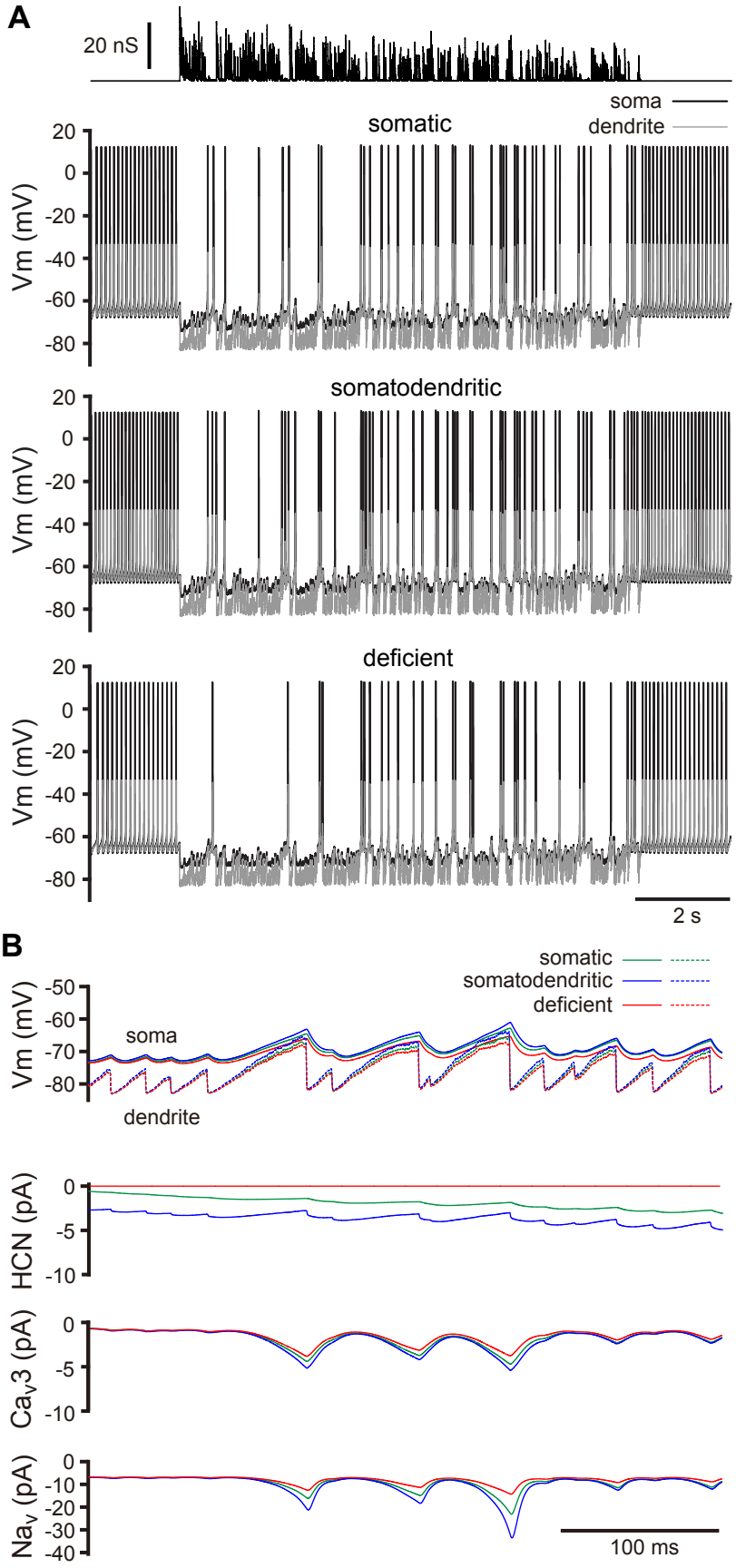
A
20 nS
soma
dendrite
somatic
somatodendritic
deficient
Vm (mV)
20
0
-20
-40
-60
-80
2 s
B
somatic
somatodendritic
deficient
soma
dendrite
-50
-60
-70
-80
HCN (pA)
0
-5
-10
Cav3 (pA)
Nav (pA)
-30
-40
100 ms

HCN model: spikes = 54, mean V_o = –67.4 mV, mean V_4 = –71.9 mV). As predicted, the deficient model was relatively inhibited and more hyperpolarised than either of the models expressing HCN channels (somatic conductance injection; HCN deficient model: spikes = 51, mean V_0 = –71.8 mV, mean V_4 = –70.6 mV) (dendritic conductance injection; HCN deficient model: spikes = 30, mean V_0 = –68.6 mV, mean V_4 = –73.1 mV).

In order to determine how HCN channels interact with other channels to oppose synaptic inhibition and promote AP generation, the magnitude of HCN, Na_v and Ca_v3 channel currents were compared for each model during the somatic (not shown) or dendritic (Fig. 4.5 *B*) application of the $GABA_A$ receptor-mediated inhibitory conductance. In each case the somatodendritic model was associated with larger depolarising Na_v and HCN channel currents than the somatic model and similar Ca_v3 channel currents (somatic conductance injection; somatic model: I_{Nav} = –17.0 pA, I_{HCN} = –2.0 pA, I_{Cav3} = –3.7 pA; somatodendritic model: I_{Nav} = –18.5 pA, I_{HCN} = –2.8 pA, I_{Cav3} = –3.8 pA) (dendritic conductance injection; somatic model: I_{Nav} = –14.6 pA, I_{HCN} = –1.3 pA, I_{Cav3} = –2.4 pA; somatodendritic model: I_{Nav} = –17.7 pA, I_{HCN} = –2.7 pA, I_{Cav3} = –2.4 pA). Na_v and to a lesser extent Ca_v3 channel current was also smallest for the HCN deficient model presumably due to weaker activation of the channels at the relatively hyperpolarised voltages associated with the HCN deficient model (somatic conductance injection; deficient model: I_{Nav} = –14.9 pA, I_{HCN} = 0 pA, I_{Cav3} = –3.5 pA) (dendritic conductance injection; deficient model: I_{Nav} = –11.5 pA, I_{HCN} = 0 pA, I_{Cav3} = –2.3 pA).

One reason for larger HCN channel current in the somatodendritic model appears to be the effect of APs, which more effectively reduce the electrochemical gradient for HCN channel current and deactivate somatic compared to dendritic HCN channels. The effect on HCN channel current was further augmented by the slow kinetics of HCN channel activation following spike-generated deactivation (Fig. 4.5 *B*). Indeed, when back propagation of APs into dendritic compartments was enhanced by increasing dendritic Na_v channel conductance from 0.01 to 1.0 mS.cm^{-2} in each dendritic compartment (while reducing somatic conductance to 28 mS.cm^{-2} to maintain the same whole-cell Na_v channel conductance) the relative capability of the

somatodendritic model compared to the somatic model to counteract inhibition was eliminated (somatic conductance injection; somatic HCN model: spikes = 54, mean V_o = –70.9 mV, mean V_4 = –69.2 mV; somatodendritic HCN model: spikes = 54, mean V_o = –71.0 mV, mean V_4 = –69.1 mV) (dendritic conductance injection; somatic HCN model: spikes = 36, mean V_o = –67.8 mV, mean V_4 = –72.2 mV; somatodendritic HCN model: spikes = 36, mean V_o = –67.8 mV, mean V_4 = –72.0 mV). However, the relative susceptibility of the HCN deficient model to inhibition was not abolished (somatic conductance injection; HCN deficient model: spikes = 47, mean V_o = –71.7 mV, mean V_4 = –70.0 mV) (dendritic conductance injection; HCN deficient model: spikes = 26, mean V_o = –68.7 mV, mean V_4 = –72.8 mV).

Together the data demonstrate that 1) HCN channels distributed throughout the somatodendritic compartment (similar to the distribution observed experimentally) most effectively opposed synaptic inhibition directed to the somatic or dendritic compartment 2) the relative capability of somatodendritic HCN channels to counteract inhibition was associated with larger Na_v and HCN channel currents.

4.3.4. HCN channels limit the deinactivation of Ca_v3 channels in STN neurons

Several studies suggest that HCN channels play a pivotal role in the regulation of Ca_v channel mediated electrogenesis (Pape and McCormick, 1989; Lüthi and McCormick, 1998; Kole et al., 2007; Tsay et al., 2007). In STN neurons hyperpolarisation below the voltages associated with autonomous activity can lead to the deinactivation of Ca_v3, which at the offset of hyperpolarisation can trigger rebound burst activity (Beurrier et al., 1999; Bevan and Wilson, 1999; Otsuka et al., 2001; Bevan et al., 2002; Hallworth et al., 2003; Hallworth and Bevan 2005; Kass and Mintz, 2006). By opposing hyperpolarisation HCN channels may therefore limit the propensity for low-voltage-activated Ca^{2+} channel-mediated rebound burst firing.

The response of STN neurons to the offset of 500 ms moderate hyperpolarising current under control conditions and in the presence of ZD7288 was characterised

(Fig. 4.6). Rebound activity was compared for both matching voltage at the end of the current step (~ –85 mV) and matching hyperpolarising current (~ –15 pA). The latency to the generation of the first AP following the offset of hyperpolarising current was greatly increased for both comparisons following blockade of HCN channels (Fig. 4.6; latency following –15 pA injection: control = 85.5 ± 16.9 ms; ZD7288 = 364.4 ± 342.3 ms; n = 6; WSR test, $p < 0.05$) (Fig. 4.6; latency following hyperpolarisation to –85 mV: control = 57.1 ± 23.6 ms; ZD7288 = 364.4 ± 342.3 ms; n = 6; WSR test, $p < 0.05$). The duration and frequency of rebound activity, defined as activity exceeding the mean autonomous firing frequency + 3 SD, was also significantly increased by ZD7288 for matching current (Fig. 4.6; duration of rebound activity following –15 pA injection: control = 453.6 ± 461.4 ms; ZD7288 = 1537.6 ± 990.1 ms; n = 6; WSR test, $p < 0.05$) (Fig. 4.6; maximum frequency of rebound activity following –15 pA injection: control = 30.9 ± 47.8 Hz; ZD7288 = 98.3 ± 61.4 Hz; n = 6; WSR test, $p < 0.05$) (Fig. 4.6; mean frequency of rebound activity following –15 pA injection: control = 14.6 ± 17.4 Hz; ZD7288 = 38.1 ± 26.1 Hz; n = 6; WSR test, $p < 0.05$) but not for voltage (data not shown). Rebound activity following the termination of –15 pA current injection was also delayed (control = 244.7 ± 72.8 ms; Cs^+ = 360.0 ± 44.9 ms; n = 4) but enhanced in intensity (maximum frequency; control = 7.8 ± 10.4 Hz; Cs^+ = 92.4 ± 39.3 Hz; n = 4) (mean frequency: control = 7.8 ± 9.9 Hz; Cs^+ = 34.2 ± 4.6 Hz; n = 4) and duration (control = 138.9 ± 173.2 ms; Cs^+ = 2553.0 ± 3306 ms; n = 4) by application of 2 mM Cs^+ in a manner similar to that produced by ZD7288 in each of 4 neurons tested. Together these data confirm that HCN channels accelerate depolarisation following the offset of hyperpolarising current and by restricting hyperpolarisation during current application reduce the intensity of rebound burst activity.

In order to determine the impact of HCN channels on the specific contribution of Ca_v3 channels a synaptic $GABA_A$ receptor conductance (peak conductance of 80 nS at 40 Hz for 5 seconds) was applied to the soma of the original somatic, somatodendritic and deficient models and the Ca_v3 channel conductance following the termination of inhibition was studied (Fig. 4.7). Simulations supported experimental observations that deficiency of HCN channels causes GABAergic inhibition to more effectively hyperpolarize STN neurons, which in turn leads to more complete deinactivation of Ca_v3 channels and thus relatively powerful Ca_v3 channel-mediated rebound burst firing at

Figure 4.6. Blockade of HCN channels increases the intensity of rebound burst firing

A, Response of a STN neuron under control conditions (black) and in the presence of ZD7288 (red) to hyperpolarising current injection. A1, from top to bottom, responses to –15 pA, –25 pA and –15 pA, respectively. A2, Instantaneous frequency plots for each trace. Dashed line represents the mean instantaneous frequency + 3 SD associated with autonomous activity. The degree of hyperpolarisation and frequency of subsequent rebound activity in response to –15 pA were greatly enhanced by ZD7288. Application of –25 pA and–15 pA under control conditions and in the presence of ZD7288 produced similar degrees of hyperpolarisation and rebound activity, respectively. B, Population data. Individual cells are represented by distinct colours. Population mean and SD are also indicated. Action potentials truncated at 0 mV; fq, frequency; Vm, membrane potential; *, $p < 0.05$.

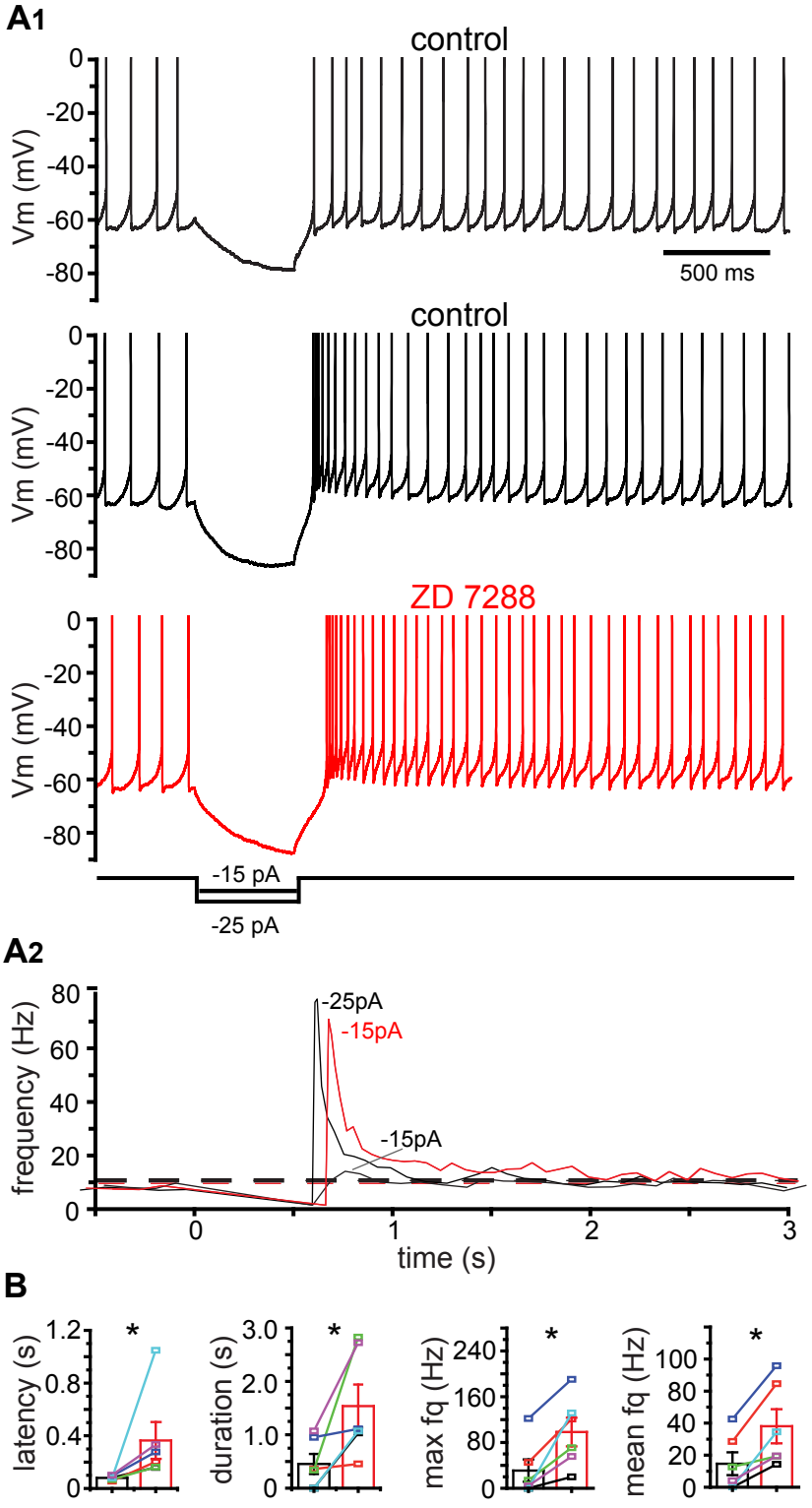
A1
control
Vm (mV)
0
-20
-40
-60
-80
500 ms
control
ZD 7288
-15 pA
-25 pA
A2
frequency (Hz)
80
60
40
20
0
-25pA
-15pA
-15pA
0
1
2
3
time (s)
B
latency (s)
1.2
0.8
0.4
0
duration (s)
3.0
2.0
1.0
0
max fq (Hz)
240
160
80
0
mean fq (Hz)
100
80
40
20
0
*

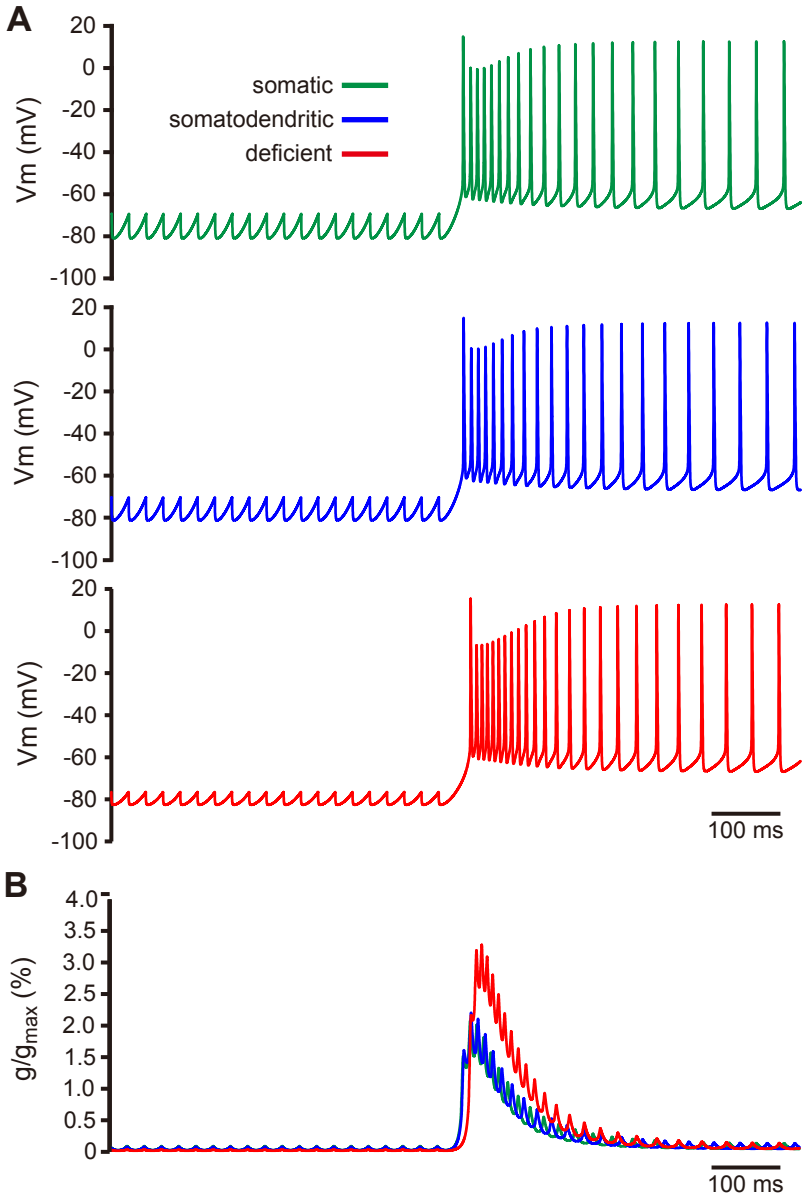

Figure 4.7. HCN channels reduce the propensity for Ca_v3 channel-mediated rebound burst firing

A, Somatic responses of the somatic, somatodendritic and deficient STN HCN models at the end and offset of somatic $GABA_A$ receptor synaptic conductance injection. The effectiveness of $GABA_A$ receptor-mediated hyperpolarization and subsequent rebound burst firing is enhanced by deficiency of HCN channels. B, Conductance (expressed as % g/gmax) of Ca_v3 channels for the 3 models at the end and offset of somatic $GABA_A$ receptor synaptic conductance injection. During inhibition the conductance of Ca_v3 channels is smallest in the HCN deficient model. At the offset of inhibition the conductance of Ca_v3 channels is largest in the HCN deficient model. Vm, membrane potential.

the offset of inhibition (Fig. 4.7). This effect was amplified by hypothetically increasing Ca_v3 channel conductance to 2–5 times of the original (not shown). Together, the experimental and modelling data suggest that STN HCN channels limit the capability of $GABA_A$-receptor mediated inhibition to generate low-voltage-activated Ca^{2+} channel-mediated rebound burst firing in STN neurons.

4.4. Discussion

Cellular and subcellular expression of HCN subunits

Regional mRNA and protein expression studies have shown that the STN is associated with a high level of HCN2 and 3 and lower levels of HCN1 and 4 expression (Monteggia et al., 2000; Santoro et al., 2000; Notomi and Shigemoto, 2004). Using single cell molecular profiling, this study showed that the detection rates of HCN subunit expression in individual neurons approximated the regional pattern. Thus, individual STN (and other) neurons express a variety of HCN subunits, which could underlie homomeric channels with heterogenous, distinct biophysical properties and/or heteromeric channels with homogenous, intermediate properties (Robinson and Siegelbaum, 2003; Baruscotti and DiFrancesco, 2004; Biel et al., 2009).

Immunocytochemical detection of HCN2 subunits revealed that STN neurons express HCN2 channel subunits across their somatodendritic plasma membrane. However, the sampling approach used here (and in most studies) might fail to detect heterogeneous cellular and/or subcellular expression patterns. Uniform (Angelo et al., 2007), decreasing (Bullis et al., 2007) and increasing (Magee, 1998, 1999; Williams and Stuart, 2000; Lörincz et al., 2002) somatodendritic expression with distance from the soma have been reported in other neurons using high resolution immunoelectron microscopy (Notomi and Shigemoto, 2004; Lörincz et al., 2002) and/or cell-attached patch clamp recording (Magee, 1998, 1999; Williams and Stuart, 2000; Angelo et al., 2007; Bullis et al., 2007). In pyramidal cells where both approaches have been applied, the data were concordant implying that immunocytochemical detection of

HCN channels is highly correlated with functional expression. Distinct compartmental expression patterns of HCN channels may confer neuron specific cellular and subcellular computational properties (London and Häusser, 2005).

Voltage dependence and kinetics of STN HCN channels

In order to determine the voltage range at which STN HCN channels are activated the response of STN neurons to current and voltage steps were compared before and during application of ZD7288 or Cs^+. In contrast to other autonomously active [eg. GPe neurons (Chan et al., 2004) and striatal cholinergic interneurons (Bennett et al., 2000)] and inactive neurons [e.g. cortical pyramidal neurons (Magee 1998, 1999; Shah et al., 2004; Kole et al., 2007; Tsay et al., 2007)], STN HCN channels are barely activated at the resting membrane potential and contribute little to their intrinsic activity or excitability. Thus loss of HCN channel function was not accompanied by a reduction in the frequency of spontaneous firing (Bennett et al., 2000; Chan et al., 2004), hyperpolarisation (Magee 1998, 1999; Shah et al., 2004; Kole et al., 2007; Tsay et al., 2007), emergence of bistable states (Williams et al., 2002) or an enhancement in excitability (Magee 1998, 1999; Shah et al., 2004; Kole et al., 2007; Tsay et al., 2007), as reported for other neurons. Only hyperpolarisation below the peak of single spike afterhyperpolarisation sufficiently activated HCN channels to modify the integrative properties of STN neurons.

Although the half activation voltage of STN HCN channel current overlaps that reported for homo- and/or hetero-meric HCN1–4 subunit-containing channels the slow kinetics of activation are consistent with slower gating homo- and/or hetero-meric channels containing HCN2–4 subunits and inconsistent with more rapidly gating homomeric HCN1 channels (Robinson and Siegelbaum, 2003; Baruscotti and DiFrancesco, 2004; Biel et al., 2009).

STN HCN channels counteract GABAergic inhibition and reduce the propensity of rebound burst firing

Studies which maintained natural chloride homeostasis have shown that $GABA_A$ receptor-mediated inhibition can hyperpolarise STN neurons 20 mV below the voltage range of autonomous STN activity, which in turn leads to deinactivation of low-voltage-activated Ca^{2+} channels and rebound burst firing (Bevan et al., 2000, 2002; Hallworth and Bevan, 2005). By using hyperpolarising current injection or the dynamic clamp technique to impose physiologically relevant patterns of GABAergic inhibition, blockade of HCN channels greatly enhanced inhibition of autonomous activity, the degree of hyperpolarisation and thus the propensity for rebound burst firing. Computational modelling revealed that somatodendritic HCN channel expression, similar to that observed experimentally, most effectively counteracted inhibition directed either towards the soma or dendrite.

Previous studies have shown that dendritic HCN channels may be positioned to reduce local temporal summation of synaptic potentials and/or local regenerative potentials engaged by synaptic input (Magee 1998, 1999; Shah et al., 2004; Angelo et al., 2007; Bullis et al., 2007; Kole et al., 2007; Tsay et al., 2007). Findings described here further suggest that dendritic HCN channels may be protected from deactivation by back propagating APs compared to somatic channels closer to the initiation site. This protective effect may be particularly critical in STN neurons, which express HCN channels that activate slowly following AP-driven deactivation. The degree to which APs attenuate in the extensive small caliber dendrites of STN neurons is unknown but may be considerable: 1) dendritic, in contrast to axosomatic, Na_v channels do not contribute to autonomous firing implying their density is relatively low (Atherton et al., 2008); 2) the velocity of back propagation is slow implying that it is relatively passive in nature (Atherton et al., 2008); 3) AP-associated dendritic Ca^{2+} transients decline precipitously with distance from the soma implying that the amplitude of dendritic potentials is small (unpublished observations).

The depolarisation produced by HCN channels was supplemented by increased activation of Na_v and Ca_v3 channels. Na_v channels are the primary driver of autonomous firing in STN neurons (Bevan and Wilson, 1999; Beurrier et al., 2000; Do and Bean,

2003) and although Ca_v3 channels were largely inactivated a small fraction of channels may contribute a tiny window current that promotes activity (Dreyfus et al., 2010).

Computational modelling further suggested that the impact of HCN channel currents on rebound burst firing is due to its limitation of the deinactivation of Ca_v3 channels. Previous studies showed that about 75% of STN neurons display short (<100 ms) rebound burst driven by Ca_v3 channels (Bevan and Wilson, 1999; Beurrier et al., 2000; Song et al., 2000; Do and Bean, 2003; Hallworth et al., 2003). Some neurons, however, exhibit longer rebound bursts (>100 ms) due to the additional recruitment of low-voltage-gated $Ca_v1.2–1.3$ channels. Therefore, the effect of HCN channels on rebound bursts possibly also includes similar interaction with $Ca_v1.2–1.3$ channels in a proportion of STN neurons.

Functional implications

At rest, tonically active GPe neurons inhibit the somatodendritic domain of STN neurons largely through the synaptic activation of $GABA_A$ receptors (Hallworth and Bevan, 2005; Tachibana et al., 2008; Baufreton et al., 2009; Karachi et al., 2009). Data from this study suggest that the compartmental distribution and biophysical properties of STN HCN channels are conformed to maintain STN neurons in a voltage range where autonomous spiking activity is promoted and low-voltage-activated Ca^{2+} channels are largely inactivated. By opposing $GABA_A$-receptor-mediated synaptic inhibition, which predominantly arises from the GPe, HCN channels may reduce the capability of GPe-STN to inhibit, reset, and synchronise firing in STN neurons (Baufreton et al., 2009). This interaction between intrinsic and synaptic conductances is a possible factor contributing to the decorrelated nature of GPe-STN network observed both *ex vivo* and *in vivo* (Baufreton et al., 2009). By maintaining STN activity, HCN channels may help to prevent involuntary movements that are produced by interruptions in STN activity (Crossman et al., 1984; DeLong, 1990; Wichmann et al., 1994; Baunez et al., 1995). By reducing low-voltage-activated Ca^{2+} channel-dependent burst firing STN HCN channels may help to prevent tremor, akinesia and bradykinesia that are associated with excessive burst firing in PD (Bergman et al., 1994; Magill et al., 2001;

Levy et al., 2002; Brown, 2003). However, it is possible that a small proportion of STN neurons are not capable of generating low-voltage-activated Ca^{2+} channel-dependent rebound burst firing (Bevan et al., 2000). The functional implication of HCN channel expression in these neurons remain to be determined. Although there is no direct evidence thus far suggesting that burst firings in parkinsonian STN *in vivo* is mediated by classical rebound bursts mediated by low-voltage-activated Ca^{2+} channels, the loss of depolarising effect of postsynaptic dopamine action (Baufreton et al., 2003; Zhu et al., 2002a; Zhu et al., 2002b; Loucif et al., 2008; Ramanathan et al., 2008) could lead to more hyperpolarised membrane potential of STN neurons that promotes the deinactivation of these calcium channels.

The mechanisms through which the distribution, number and gating of STN HCN channels are dynamically regulated are unknown but data from thalamic and cortical neurons suggest that intrinsic homeostatic signalling pathways and neuromodulatory tone are critical for maintenance of normal thalamocortical HCN channel function (Pape and McCormick, 1989; Lüthi and McCormick, 1998; Shah et al., 2004; Fan et al., 2005). It is therefore speculated that in PD, aberrant afferent activity together with alterations in dopaminergic neuromodulation (Bergman et al., 1994; François et al., 2000; Raz et al., 2000; Magill et al., 2001; Levy et al., 2002; Brown, 2003; Shen and Johnson, 2005; Baufreton and Bevan 2008; Ramanathan et al., 2008) could represent conditions for the dysregulation of STN HCN channels and thus the emergence of pathological burst firing in STN neurons. The pathophysiological role of HCN channels has indeed been recently demonstrated in the parkinsonian GPe, in which excessive burst firing occurs due to the loss of HCN channel pacemaking function (Chan et al., 2011). Whether the acute loss of dopaminergic neuromodulation, or chronic adaptive changes in the PD network could lead to the dysregulation of HCN channels, remain to be determined.

CHAPTER 5

GENERAL DISCUSSION

5.1. Summary and concluding remarks

The overall objective of the research presented in this thesis was to further elucidate the mechanisms underlying the regulation of GABAergic inhibition in the STN in health and PD. To accomplish this objective, complementary molecular and cellular electrophysiological, imaging, computational and optogenetic approaches were applied to the rat and mouse STN.

In idiopathic and experimental PD, the GPe and STN exhibit hypo- and hyper-activity, respectively, and abnormal synchronous rhythmic burst firing. Motor symptoms are intimately related to changes in the frequency and pattern of neuronal activity in the reciprocally connected GPe and STN as well as associated brain networks. Following lesion of midbrain dopamine neurons beta band synchronisation emerges slowly before reaching its peak in the STN at 2 to 3 weeks later (Mallet et al., 2008a). This process suggests that adaptive changes in cellular and network properties contribute to the evolution of parkinsonian STN activity.

The primary objective of my thesis therefore focused on the possibility of altered GPe–STN connectivity following chronic dopamine depletion. GPe–STN transmission in control and 6-OHDA-lesioned rodents was compared 2–3 weeks post-operative. Electrophysiological recordings showed that 1) the frequency (but not the amplitude) of mIPSCs increased by ~ 70%; 2) the amplitude of evoked IPSCs and isoguvacine-evoked current increased by ~ 60% and ~ 70%, respectively. Quantitative PCR analysis revealed that levels of mRNA encoding α1, β2 and γ2 $GABA_A$ receptor subunits increased by 15–30%. In addition, immunocytochemical approach demonstrated the increase in the density of postsynaptic gephyrin and γ2 subunit co-immunoreactive structures by ~ 40%, whereas the density of VGAT and bassoon co-immunoreactive axon terminals was unchanged. The number of ultrastructurally defined synapses per GPe–STN terminal doubled with no alteration in terminal/synapse size or target preference. Therefore, loss of dopamine leads, through an increase in the number of synaptic connections per GPe–STN terminal, to substantial strengthening of the GPe–STN pathway. This alteration may be a homeostatic response to oppose hyperactivity but could also maladaptively contribute to the manifestation of hypersynchronous rhythmic burst firing in the parkinsonian STN.

Suppression of the abnormal hypersynchronous activity pattern by STN DBS at high frequency (>100 Hz) has been a highly effective treatment for motor symptoms in PD. The mechanisms of DBS action are, however, poorly defined. The first study described in this thesis suggests that the generation and/or exacerbation of pathological oscillations in the STN could in part be attributed to the strengthening of GPe–STN transmission, which makes it a plausible therapeutic target of DBS. Indeed recent optogenetic studies using *Thy1-ChR2* transgenic mice (line 18; Gradinaru et al., 2009) suggests that DBS exerts its effect through manipulating cortical activity and undefined afferents within the STN.

The following objective of this thesis was hence to characterise the ChR2 expression in the STN of this mouse line, in which ChR2 is expressed in multiple brain regions. Immunocytochemical analysis revealed that the majority (~ 80%) of ChR2-expressing glutamatergic afferents in the STN are from the cortex. Stereological quantification estimated that the ratio of ChR2-expressing cortical afferents to subcortical afferents is about 4:1. In addition, as many GABAergic afferents as cortical afferents also express ChR2. Consistent with the expression pattern in STN, strong and widespread cellular labelling of ChR2-EYFP was observed within Layer V motor cortex and GPe. Electrophysiological recordings confirmed functional ChR2 expression by glutamatergic and GABAergic afferents in the STN. Together these data suggested that DBS might exert its therapeutic effect through disrupting not just cortical input as previously suggested but presumably also through manipulating GABAergic input arising from the GPe. In addition, *Thy1-ChR2* mouse line 18 is a useful optogenetic tool to study the regulation of cortical and GPe input and their interaction in normal and parkinsonian STN.

Given that the GPe potently regulates the frequency and pattern of STN activity, the basis of decorrelation between GPe and STN activity under normal conditions requires further characterisation. The third study in my thesis, investigated the poorly understood role of HCN channels in inhibitory synaptic integration within STN neurons. Molecular profiling using single-cell PCR technique showed that individual STN neurons express mRNA encoding multiple HCN subunits, with HCN2 and HCN3 being the most abundant. Light and electron microscopic analysis showed that HCN2

subunits are strongly expressed and uniformly distributed across the somatodendritic plasma membrane. Voltage- and dynamic-clamp analysis and computational modelling demonstrated that HCN channels are activated by $GABA_A$ receptor-mediated inputs and thus limit synaptic hyperpolarisation and deinactivation of low-voltage-activated Ca^{2+} channels. Consistent with the subcellular pattern of HCN expression observed experimentally, computational modelling also showed that uniform distribution of HCN channels across the somatodendritic axis most effectively counteracts GABAergic inhibition. Together the data demonstrate that HCN channels in STN neurons oppose $GABA_A$ receptor-mediated inhibition arising from the GPe and thus maintain single-spike autonomous activity rather than rebound burst firing.

In conclusion, the first study in the thesis proposed that abnormally synchronous rhythmic bursting activity in the STN may at least in part arise from strengthening of the GABAergic inhibition due to augmentation in GPe–STN synaptic connectivity. Although loss of dopaminergic neuromodulation in PD directly contributes to the abnormal activity in the basal ganglia, long-term alterations in cellular and network properties could also be important. This study demonstrated that adaptive changes in synaptic connectivity following chronic dopamine depletion does not only occur at the level of striatum as previously shown, but also in the STN within the "indirect" pathway. Given that GPe neurons that project to the STN exhibit anti-phase rhythmic activities (<30 Hz) in relation to STN neurons (Mallet et al., 2012) and that GPe–STN input may enhance the sensitivity of STN neurons to cortical idling rhythms (Baufreton et al., 2005) in PD, strengthening of these GPe inputs is likely to cause or reinforce pathological oscillations in the STN. Together with disruptions in autonomous firing reported in STN neurons (Zhu et al., 2002a; Wilson et al., 2006), these adaptations appear to reflect homeostatic compensatory response to STN hyperactivity that ultimately may be maladaptive by contributing to abnormal activity patterns.

If enhanced GPe–STN transmission is a key underlying pathophysiological cause of abnormal activity pattern in the STN and its target nuclei in the basal ganglia, correcting or abolishing the maladaptive output may potentially be beneficial for improving motor symptoms in PD. The second study identified a transgenic ChR2 mouse model that will facilitate precise interrogation of the neuronal circuits underlying

motor dysfunction in PD. The abundant presence of ChR2-expressing GABAergic (besides cortical) afferents in the STN suggests that the recently reported therapeutic benefit of STN HFS in this model of PD (Gradinaru et al., 2009) could not be solely due to driving of cortical–STN connections. Considering the critical role of GPe–STN synaptic transmission in pathological condition as implied in the first study of the thesis, optogenetic manipulation of GPe–STN input presumably in part accounted for the correction of motor impairments upon STN photostimulation in the previous study (Gradinaru et al., 2009). In the future, hypotheses regarding the interactions between GPe and cortical inputs and intrinsic properties of STN in health and experimental PD can be tested using this mouse line. Combined with the use of other optogenetic tools, various manipulation strategies can be employed to identify the most relevant mechanisms underlying DBS therapeutic effect on motor impairments in PD.

Finally, the last study of the thesis provides us insights on the underlying instrinsic mechanism of STN neurons that actively opposes the impact of GABAergic inhibition under normal conditions. The selective role of HCN channels in regulating inhibitory synaptic input in part explains why GPe–STN network activity is often not seen correlated. In other brain regions, non-uniform distribution of HCN channels is thought to be important for cellular and subcellular computation of glutamatergic input integration. Work from the third study here shows that uniform distribution of the channels across the somatodendritic axis also serves important computational function in synaptic integration, i.e. to most effectively counteract GABAergic inhibition (arising from the GPe). As a result, HCN channels may act to reduce the capability of GPe input to inhibit, synchronise and/or generate rebound burst firing in the STN neurons. In PD, abnormal afferent activity or altered dopaminergic neuromodulation could potentially represent conditions for disruption of the channel function, thereby contributing to the emergence of rhythmic, synchronised burst firing in the STN.

5.2. Technical considerations

The experimental results presented in this thesis should be interpreted with consideration of a number of technical issues arising from the methods employed.

6-OHDA-treated model of Parkinson's Disease

6-OHDA is a neurotoxin that has been intensively used to generate rodent model of PD associated with SNc dopaminergic cell death for more than 40 years (Ungerstedt, 1968). The most common model involves unilateral 6-OHDA injection into the nigra or MFB, resulting in rapid cell death. Syndrome that develops following dopamine depletion shares many similarities with PD, although some pathological features are not reproduced (Schwarting and Huston 1996, Dauer and Przedborski, 2003; Yuan et al., 2005). Prominent pathophysiological characteristics of PD and primate PD models, including changes in the firing rates and patterns within the cortex and basal ganglia have however been reproduced in 6-OHDA-treated models (Magill et al., 2001; Mallet et al., 2008a,b). Although the unilateral 6-hydroxydopamine (6-OHDA) model is more frequently used in rats, substantial and stable unilateral 6-OHDA-induced lesions that are functionally assessable can also be established in mice (Iancu et al., 2005). Thus, mice were also utilised as experimental PD models in this thesis (Chapter 2) where use of rats was not practical.

A main difference between nigral and MFB 6-OHDA lesion models is that the latter also causes destruction of dopaminergic neurons in the ventral tegmental area (VTA), which does not closely mimic PD pathology. However, inaccurate/incomplete nigral targeting of the 6-OHDA injection sometimes results in the sparing of a proportion of dopaminergic neurons. The axons of residual dopaminergic neurons in the midbrain might undergo sprouting and reinnervate the striatum, thereby causing a behavioural recovery (Perese et al., 1989; Carman et al., 1991). Considering these factors, both nigral and MFB 6-OHDA-lesioned rodents were employed in current studies.

6-OHDA-induced toxicity is relatively selective for monoaminergic neurons because it is preferentially taken up by dopamine and noradrenergic transporters (Luthman et al., 1989). To target specifically the death of dopaminergic neurons in these studies, 6-OHDA was used in conjunction with desipramine, a selective noradrenaline reuptake inhibitor. Because SNc dopaminergic neurons are known to

innervate contralateral basal ganglia structures (Fass and Butcher, 1981), the use of non-lesion side of the unilateral 6-OHDA-treated animals as control was avoided. However, quantification of dopaminergic denervation in the ipsilateral STN and GPe was not performed and therefore it is not known to what extent the loss of direct dopamine innervation is correlated with the enhancement of GPe–STN transmission in 6-OHDA-lesioned animals.

Electrophysiology

Patch clamp recordings were performed in our studies to examine the properties of synaptic input to STN neurons. Theoretical and experimental studies have suggested that a typical problem associated with somatic voltage clamp is that it exerts limited control over the dendritic arbor (Bar-Yehuda and Korngreen, 2008; Williams and Mitchell, 2008; Poleg-Polsky and Diamond, 2011). HCN currents recorded from the soma (Chapter 4) may therefore arise mostly from somatic HCN channel activity. The fine caliber dendrites of STN neurons nonetheless prevented local access for patch clamp recording. Because voltage clamp does not uniformly control voltage across the somatodendritic axis, electrical measurement of dendritic synaptic ion channel activity might be restricted. For this reason measurement of kinetics and voltage-dependence of instrinsic HCN channels were inevitably compromised, but the voltage-dependent contribution of STN HCN channels was shown to be similar under current (data not shown) and voltage clamp.

Additionally, the expected poor space clamp cannot avoid synaptic inputs distant from the soma from driving the membrane potential away from the holding potential. Measurements of the amplitude, kinetics, slope conductance and reversal potential of synaptic inputs are distorted in a dendritic distance-dependent manner (Williams and Mitchell, 2008). In Chapter 2, the incomplete voltage control of synaptic events at the dendrites might partially mask augmentation of the GPe–STN inputs following chronic dopamine depletion. This possibility is consistent with the electron microscopic studies revealing a greater fold of increase in GABAergic synapses than that suggested by electrophysiological recordings. However, because GPe–STN projections

are predominantly targeted to the somata (31%) and the proximal dendrites (39%) of STN neurons (Smith et al., 1990), the space clamp problem in the measurement of $GABA_A$-receptor mediated currents was relatively less severe. Since the recording conditions were consistent in each experiment, issues related to space clamp would be the same across recordings and hence not affect the qualitative results of these experiments.

Confocal Microscopy

The use of fluorescent and confocal microscopy in immunocytochemical studies is accompanied by several technical limitations (Semwogerere and Weeks, 2005; Pawley, 2006). Since confocal microscopy employs focused laser beam and pin-hole to minimise light diffraction, the optical resolution achieved by high numerical aperture (NA) objective lens is improved compared to conventional epifluorescence microscopy, but still considerably limited. With 63× and 1.4 NA objective lens used in Chapter 3 study, the maximum *xy* resolution achieved was above ~ 200 nm, whereas the distance between two adjacent synapses can be as close as 50 nm as observed in electron microscopy. Therefore, in determining the density of pre and post-synaptic immunoreactive puncta, some of the closely positioned synapses might not have been resolved as separate structures. Because the increase in GPe–STN transmission is mediated by upregulation of functional synapses without proliferation of presynaptic terminals, new synapses might be formed in close proximity to existing synapses. It is possible that the increase in GABAergic synaptic density observed was underestimated due to the limited optical resolution.

Furthermore, the optical *z*-resolution is relatively worse than the lateral *xy* resolution. With the same 63× and 1.4 NA objective lens, *z* resolution obtained was above ~ 800 nm. This could potentially confound the colocalisation studies described in either Chapter 2 or 3, because structures that are physically separate might be observed as overlapping in the *xy* plane of an image. Additionally, because refractive index is different for different wavelengths, chromatic shift occurs when lights travel through the specimen, although this problem was largely corrected by the objectives

used. To address these issues, specimens were imaged in small step size (0.3–0.4 μm) and immunoreactive structures were examined throughout their *z*-axis spanning to assure reliable pattern of colocalisation.

Another confocal microscopy issue concerns with photobleaching of fluorescent molecules tagging structures of interest. Photobleaching is a process in which molecular structure of a dye is altered due to absorption of excitation light, thus rendering this dye less or non-fluorescent. This potentially results in apparent reduction in the size/intensity of immunofluorescent structures. In worse situation, structures with weaker fluorescence fail to be detected. However, the visibility of immunofluorescent structures remained stable across a broad range of excitation wavelength intensity. In order to minimise bleaching, 1) Prolong Gold antifade reagent (Invitrogen) was used; 2) image acquisition settings were optimised such that: the power of confocal lasers that emit excitation wavelengths and the laser scanning dwell time on each pixel was minimised, whereas photomultiplier gain was maximised, while maintaining high signal-to-noise ratio. No apparent fluorescent fading of specimens was observed after imaging was completed.

Last but not least, spherical aberration is a typical problem in confocal imaging. It occurs mainly because light passing through the periphery of the lens is not brought into focus at the same plane as that travelling through lens centre, due to different degree of refraction. This problem can be worsened by the use of thin coverslips that individually have uneven thickness. To minimise loss of resolution due to spherical aberration, high-precision coverslips (170 ± 5 μm) were used in studies involving imaging of fine synaptic structures.

Electron microscopy

Electron microscopy offers much higher resolution images than confocal microscopy and the ability to observe ultrastructural details. Although state-of-the-art super-resolution microscopy system (eg. structured illumination microscopy, SIM) that can produce up to two times the resolution of confocal microscopes has been recently developed (Sigrist and Sabatini, 2012), the thickness of fixed tissue sections often

greatly diminishes the resolving power of the system due to high degree of light diffraction passing through the specimens (Gustafsson et al., 2008). Because of this issue my attempt to better resolve immunofluorescent synaptic structures in the STN slice (Chapter 2) using super-resolution microscopy (Nikon SIM; Nikon, Tokyo, Japan) did not yield significantly improved results (not shown). Immunoelectron microscopy was therefore performed, but also not without its caveats. Due to a common problem in tissue penetration of antibodies, the identification of immunoreactive structures is limited to the superficial layer of ultrathin sections. At this depth stereological counting could be performed to quantify the number of terminals and synapses within these structures (Chapter 2). However, GPe–STN terminals are often large in size (Smith et al., 1998; Baufreton et al., 2009) and spans many sections beyond that held by a grid, making the quantification very difficult and labour-intensive. Consequently, semi-quantitative method was used instead, by analysing the number of synapses per identified GPe terminals on single sections. Although this method is confounded by the fact that larger structures are more likely to be counted and hence oversampled, the similar length of GABAergic synapses in control and parkinsonian STN samples (Chapter 2) suggests that their size is not altered by chronic dopamine depletion.

In Chapter 4, because immunoperoxidase DAB labelling can variably diffuse over long distances and difficult to quantify (Courtoy et al., 1983), immunogold labelling was used to characterise the quantitative distribution of HCN channels. Given that gold particles (~ 30 nm) are bound to secondary antibodies but not the antigen itself, they appear 15–30 nm away from the antigen (Hermann et al., 1996). This poses a problem when determining whether the immunoreactive HCN channels are membranous or not. Thus, mean distance of the structures from the membrane + 2SD was used to define their subcellular localisation (i.e. membranous versus cytoplasmic) (Lörincz et al., 2002). Absolute density of HCN channels was determined because 1) the binding of immunogold may not be linear to channel density 2) silver enhancement of gold particles for enhanced detection causes variation in particle size and coagulation (Robinson et al., 2000).

Reverse transcriptase PCR

Two types of reverse transcriptase PCR were employed to gauge the levels of gene expression in the STN: real-time quantitative PCR and single-cell end-point PCR. The former technique described in Chapter 2 is relatively much more sensitive and precise (Valasek and Repak, 2005), but considerable starting material for the reaction process is required and hence microdissected STN tissue was used instead of single isolated neurons. Because glial cells are often known to express $GABA_A$ receptors (Vélez-Fort et al., 2011), expression of the same RNAs of interest in the glia might cause underestimation of expression level changes in STN neurons. Relative quantification was performed using a comparative quantification (ΔΔCT) method because absolute RNA levels were not of interest. The method is based on the assumption that the difference in threshold cycles (ΔCT) between the gene of interest and the housekeeping gene is proportional to the relative expression level of the gene of interest. To optimise the accuracy of the obtained data, the reaction efficiencies of different primers were tested so that they were similar. Additionally, because not all proposed housekeeping genes may retain constant expression levels after chronic dopamine depletion, the weighted average of 5 housekeeping genes based on their relative stability was used. In Chapter 4, single cell PCR was used instead because previous studies have examined HCN subunit expressions in the whole STN (Monteggia et al., 2000; Santoro et al., 2000; Notomi and Shigemoto, 2004). Although relative quantification of HCN subunits would be desirable, the amount of RNA materials collected from isolated single neurons was not sufficient for quantitative PCR procedure.

5.3. Future studies

There is a number of investigations that can be further pursued based on the findings detailed in this thesis.

Even though substantial dopaminergic neurodegeneration occurs within few hours of 6-OHDA injection into the nigra (Jeon et al., 1995; Zuch et al., 2000), pathological synchrony at beta band in the STN emerges 3 days afterward and intensifies to its peak at 2–3 weeks (Mallet et al., 2008a). At this time point, the

number of functional GPe–STN synapses is significantly upregulated, without presynaptic terminal proliferation (Chapter 2). However, the precise timecourse of aberrant GPe–STN connectivity in experimental PD has not been defined and is likely to be functionally relevant to the manifestation of abnormal activity frequency and pattern within the GPe–STN network. It would be interesting to see if the alterations in GPe–STN connectivity are correlated with the evolution of beta band activity in experimental PD. If the upregulation of GPe-STN synapses directly contributes to emergence of the abnormal activity pattern, the maladaptive alteration should occur gradually over 2 to 3 weeks and stabilise after that time point. However, it is possible that different mechanisms are employed at different time points of increased GPe–STN transmission, including enhanced synaptic release probability, increased Cl^{-1} extrusion, increased number of $GABA_A$ receptors per synapse, altered $GABA_A$ receptor subunit composition, and proliferation of GPe–STN synaptic terminals. Defining the timecourse and nature of altered GPe–STN transmission will help us focus on relevant underlying mechanisms for the treatment of parkinsonism.

In addition, determining the pathophysiological events that trigger the enhancement of GPe–STN synaptic transmission will enable us to lay down the principles regulating GPe–STN interactions in health and disease. GABAergic synaptic plasticity is often triggered by elevated intracellular Ca^{2+} through NMDA receptors and/or intrinsic Ca_v channels (Maffei, 2011). In PD, STN neurons are hyperactive and more strongly entrained by cortical inputs (Mallet et al., 2008a; Moran et al., 2011), suggesting that hyperactivation of STN NMDA receptors and/or Ca_v channels potentially leads to upregulation of GPe–STN synaptic transmission. Rectifying these triggers might therefore reverse alteration in GPe–STN connections and diminish pathological activity in the STN.

Defining the molecular mechanisms underlying the increased GPe–STN transmission are also of future research interests. Most forms of synaptic plasticity are triggered by changes in intracellular Ca^{2+} that regulate a variety of signalling pathways in neurons. Excessive activation of NMDA receptors and/or hyperactivity of STN neurons in PD may lead to elevation of intracellular Ca^{2+}, which in turn activates signalling cascades that upregulate synaptic number/strength. Whether the increase

in postsynaptic Ca^{2+} are indeed necessary for plasticity should be determined. Current literature suggests that synaptic potentiation is typically mediated through the Ca^{2+}-dependent activation of protein kinases (in some cases phosphatases) (Mayford, 2007; Tretter and Moss, 2008). Notably, NMDA receptor activation can lead to enhanced trafficking and exocytosis of GABA receptor subunits into the plasma membrane mediated through Ca^{2+} calmodulin-dependent kinase II (CAMKII) (Marsden et al., 2007). Gephyrin clustering of GABA receptors to form functional synapses is dependent on phosphorylation by glycogen synthase kinase 3β (Tyagarajan et al., 2011). Using specific activators and inhibitors of these kinases/phospathases, their role in mediating increased GPe–STN transmission in the STN can be determined.

In addition, downstream intracellular signalling cascades that regulate a variety of cellular processes including transcription, translation, trafficking, exocytosis, endocytosis, recycling, and degradation of molecules involved, are also potential intervention points for preventing synaptic plasticity (Smith and Kittler, 2010). In particular, interaction of GABARAP with NSF, a protein critical for intracellular membrane trafficking events, may be important for the increased production of GABAergic synapses (Kittler et al., 2001; Luscher et al., 2011). Reduced endocytosis of GABA receptor subunits may also contribute to their increased surface expression. In addition, formation and maintenance of $GABA_A$ receptors clusters at inhibitory synapses could be augmented. This is possibly mediated through the binding of synaptic adhesion molecule neuroligin 2 that activates collybistin's clustering of gephyrin-dependent $GABA_A$ receptors at the membrane (Poulopoulos et al., 2009). At different time points of activity pattern changes in PD, presynaptic mechanisms might be involved in enhancement of GPe–STN transmission, such as changes in vesicle pool properties, proliferation of presynaptic terminals, and regulation by presynaptic NMDA or $GABA_B$ receptor (Takesian et al., 2010; Fioravante and Regehr, 2011; Maffei, 2011; Mathew and Hablitz, 2011). In long term, maintenance of potentiated transmission also often involve enhancement of gene transcription and translation mediated by transcription factors like c-fos and CREB (Loebrich and Nedivi, 2009). Phosphorylation of CREB in response to membrane depolarisation and elevated intracellular Ca^{2+} level can lead to c-fos gene activation which regulates activity-dependent transcription in neurons (Sheng et al., 1990). Taken together, defining the role of postsynaptic Ca^{2+} increase,

the relevant signalling cascades, and the molecular processes underlying GABAergic plasticity in experimental PD, using a combination of *ex vivo* electrophysiological and molecular approaches, should enable us to more precisely and effectively correct aberrant GPe–STN transmission in experimental PD.

In addition, findings in this thesis (Chapter 3) suggest that the *Thy1-ChR2* mouse line 18 is a useful optogenetic tool to investigate the phenomenon of enhanced GPe–STN transmission in experimental PD. By specifically manipulating the activity of predominantly cortical afferents *ex vivo* and *in vivo*, this model can be used to test the hypothesis that hyperactivation of NMDA receptor due to enhanced cortical-STN transmission triggers the synaptic plasticity of GPe–STN input. The molecular mechanisms underlying the NMDA receptor-mediated GABAergic plasticity can also subsequently be probed in this model.

Once the triggers (or molecular processes) underlying enhancement of GPe–STN transmission are identified *ex vivo*, *in vivo* studies will be useful to investigate the interventions leading lead to prevention/reversal of motor symptoms in PD. For instance, the effect of blocking NMDA receptor hyperactivation before, during or after 6-OHDA injection into the nigra, on GPe–STN transmission and motor behaviours can be studied. This can be achieved by conditional knockout of NR1 subunit (required to form functional NMDA receptor channel; Traynelis et al., 2010) in the STN neurons, through viral gene delivery combined with Cre/LoxP recombination system in transgenic mice (Kühn and Torres, 2002).

Understanding the neuronal principles underlying the pathophysiology of motor symptoms in PD will also help us define the therapeutic mechanisms of DBS. Despite advanced knowledge of HFS impact on neural activity (eg. Deniau et al., 2010), it is still not clear how the effects induced by stimulation contribute to its beneficial outcome. One possibility is that that DBS exerts therapeutic effect through manipulating afferent activities in the STN. Particularly, high frequency driving of synaptic transmission may attenuate its capability to pattern pathological activity due to heavy synaptic depression (Baufreton and Bevan, 2008). Thus, $GABA_A$-receptor-mediated transmission in the STN exhibit activity-dependent depression, such that even brief period (1–2 s) of high frequency stimulation (50 Hz) heavily reduced IPSC

amplitude (Baufreton and Bevan, 2008). The synaptic depression is predicted to be enhanced in the absence of dopamine because presynaptic dopamine action reduces phasic GABAergic transmission in the STN (Baufreton and Bevan, 2008). The ChR2 transgenic mouse line will allow us to specifically probe into the activity-dependent plasticity of GPe–STN (or predominantly cortical inputs) at HFS and LFS in *ex vivo* recordings. Given the proliferation of GPe–STN transmission may be a maladaptive alteration that promotes synchronised, rhythmic neuronal discharge in the STN, abolishing this input (through synaptic depression) is predicted to suppress the emergence of pathological activity pattern in the STN during DBS. This could in part explain recent report demonstrating that HFS of GPe improves motor symptoms in PD patients (Vitek et al., 2004) and reduces bursting in the STN and GPi (Vitek et al., 2012). Therefore, direct high-frequency photoactivation of GPe neurons in the *Thy1-ChR2* transgenic mice should deliver similar beneficial motor outcome. Considering the heterogenous effect of STN DBS, it would also be interesting to study the way in which STN neurons, under the effect of DBS, integrate beta-band rhythms from the GPe. The ChR2 mouse line 18 should enable us to explore this question, by specifically stimulating GPe–STN input at low frequency while recording response in the STN neurons under electrical HFS of the nucleus. In combination with the use of other micro-opsins, viral vectors and transgenic mouse lines, *ex vivo* and *in vivo* optogenetic approaches will facilitate our search for the most effective mechanisms for correcting symptoms in experimental PD.

The selective role of HCN channels in opposing the impact of GABAergic inhibition on STN activity (Chapter 4) suggests that dysregulation of the channel function may potentially promote the emergence of abnormal activity patterns. Indeed, loss of HCN channels in the parkinsonian GPe pathologically enhances burst firing (Chan et al., 2011). Therefore, our research group has probed into the possibility of altered HCN channel function in 6-OHDA-lesioned rodents. Although preliminary electrophysiological and anatomical data suggest downregulation of HCN channel function, a larger number of observations from current and voltage clamp recordings did not reveal significant difference from normal animals (unpublished). Several reasons might explain the negative results: 1) the magnitude of HCN currents varies considerably from one cell to another 2) somatic voltage-clamp recordings

might not sufficiently reveal changes in channel function in the dendritic structures of STN neurons due to poor space clamp 3) alteration in HCN currents could be masked by changes in other overlapping conductances 4) whole-cell patch clamp results in intracellular dialysis due to the relatively much larger volume of internal recording solution, therefore perturbing the internal ionic and/or messenger components important for normal HCN channel function.

For more robust characterisation of HCN (dys)regulation in the parkinsonian STN, perforated patch clamp technique, which does not involve rupture of the patch membrane, could be performed to minimise the dialysis of the cell. HCN currents should also be isolated through the use of specific channel blocker such as ZD7288. Furthermore, electron microscopic studies (eg. immunogold labelling of HCN subunits) will help to define the ultrastructural changes, if any, of the subcellular distribution and expression level of HCN channels across the somatodendritic axis of STN neurons. The loss of HCN channel function in the STN could potentially represent a novel therapeutic target for PD. In that case, restoring normal function of HCN channels, or suppressing the enhanced function of low-voltage-gated Ca_v3 channels (deinactivated by more powerful GPe-STN patterning due to reduced opposing HCN currents), is predicted to diminish excessive synchronous burst firing in the STN and alleviate motor symptoms in PD.

Considering that HCN channels participate minimally in autonomous firing of STN neurons (Bevan and Wilson, 1999; Beurrier et al., 2000; Do and Bean, 2003; Baufreton et al., 2005) and that autonomous firing is disrupted in models of PD (Zhu et al., 2002a), abnormal STN activity pattern could not be solely due to dysregulation of HCN channels. The ionic mechanism(s) responsible for the reduced pacamaking in STN neurons is still unknown. One potential candidate is ATP-sensitive potassium (KATP) channels. KATP channels are inwardly rectifying potassium channels that are inhibited by intracellular ATP (Zeng et al., 2007; Hibino et al., 2010). Their role in central neurons is not well understood but they are mainly thought to remain closed except under conditions of severe metabolic deprivation to limit cellular excitability. In parkinsonism, ATP deficiency due to increased patterning by cortical inputs and/or hyperactivity of STN neurons (Mallet et al., 2008b; Wichmann et al., 2011)

could therefore hypothetically represent conditions for excessive activation of KATP channels, leading to additional K^+ efflux and compensatory reduction in excitability. Understanding the mechanistic involvement of KATP and/or other ion channels in the disruption of autonomous firing in STN neurons may further unravel novel therapeutic strategies that target (mal)adaptive changes in the parkinsonian basal ganglia.

BIBLIOGRAPHY

Adamantidis AR, Zhang F, Aravanis AM, Deisseroth K, De Lecea L (2007) Neural substrates of awakening probed with optogenetic control of hypocretin neurons. Nature 450:420-4.

Afsharpour S (1985) Light microscopic analysis of Golgi-impregnated rat subthalamic neurons. J Comp Neurol 236:1-13.

Albin RL, Young AB, Penney JB (1989) The functional-anatomy of basal ganglia disorders. Trends Neurosci 12:366-75.

Albin RL, Young AB, Penney JB (1995) The functional-anatomy of disorders of the basal ganglia. Trends Neurosci 18:63-4.

Alexander GE, Delong MR, Strick PL (1986) Parallel organization of functionally segregated circuits linking basal ganglia and cortex. Annu Rev Neurosci 9:357-81.

Andersen CL, Jensen JL, Ørntoft TF (2004) Normalisation of real-time quantitative reverse transcription-PCR data: a model-based variance estimation approach to identify genes suited for normalisation, applied to bladder and colon cancer data sets. Cancer Res 64:5245-50.

Angelo K, London M, Christensen SR, Häusser M (2007) Local and global effects of I(h) distribution in dendrites of mammalian neurons. J Neurosci. 27:8643-53.

Aravanis AM, Wang L-P, Zhang F, Meltzer LA, Mogri MZ, Schneider MB, Deisseroth K (2007) An optical neural interface: in vivo control of rodent motor cortex with integrated fiberoptic and optogenetic technology. J Neural Eng 4:S143-56.

Arenkiel BR, Peca J, Davison IG, Feliciano C, Deisseroth K, Augustine GJ, Ehlers MD, Feng G (2007) In vivo light-induced activation of neural circuitry in transgenic mice expressing channelrhodopsin-2. Neuron 54:205-18.

Atherton JF, Ramanathan S, Wokosin DL, Bevan MD (2008) Autonomous initiation and propagation of action potentials in neurons of the subthalamic nucleus. J Physiol 586:5679-700.

Aziz TZ, Peggs D, Agarwal E, Sambrook MA, Crossman AR (1992) Subthalamic nucleotomy alleviates parkinsonism in the 1-methyl-4-phenyl-1,2,3,6-tetrahydropyridine (MPTP)-exposed primate. Br J Neurosurg 6:575-82.

Bar-Yehuda D, Korngreen A (2008) Space-clamp problems when voltage clamping neurons expressing voltage-gated conductances. J Neurophysiol 99:1127-36.

Baron MS, Vitek JL, Bakay RAE, Green J, Kaneoke Y, Hashimoto T, Turner RS, Woodard JL, Cole SA, McDonald WM, Delong MR (1996) Treatment of advanced Parkinson's disease by posterior GPi pallidotomy: 1-year results of a pilot study. Ann Neurol 40:355-66.

Baruscotti M, DiFrancesco D (2004) Pacemaker channels. Ann N Y Acad Sci 1015:111-21.

Baufreton J, Atherton JF, Surmeier DJ, Bevan MD (2005) Enhancement of excitatory synaptic integration by GABAergic inhibition in the subthalamic nucleus. J Neurosci 25:8505-17.

Baufreton J, Bevan MD (2008) D2-like dopamine receptor-mediated modulation of activity-dependent plasticity at GABAergic synapses in the subthalamic nucleus. J Physiol 586:2121-42.

Baufreton J, Garret M, Rivera A, de la Calle A, Gonon F, Dufy B, Bioulac B, Taupignon A (2003) D5 (Not D1) dopamine receptors potentiate burst-firing in neurons of the subthalamic nucleus by modulating an L-type calcium conductance. J Neurosci 23:816-25.

Baufreton J, Kirkham E, Atherton JF, Menard A, Magill PJ, Bolam JP, Bevan MD (2009) Sparse but selective and potent synaptic transmission from the globus pallidus to the subthalamic nucleus. J Neurophysiol. 102:532-45.

Baunez C, Nieoullon A, Amalric M (1995) In a rat model of parkinsonism, lesions of the subthalamic nucleus reverse increases of reaction time but induce a dramatic premature responding deficit. J Neurosci 15:6531-41.

Benabid AL (2003) Deep brain stimulation for Parkinson's disease. Curr Opin Neurobiol 13:696-706.

Benabid AL, Chabardes S, Torres N, Piallat B, Krack P, Fraix V, Pollak P. (2009) Functional neurosurgery for movement disorders: a historical perspective. Prog Brain Res 175:379-91.

Bennett BD, Callaway JC, Wilson CJ (2000) Intrinsic membrane properties underlying spontaneous tonic firing in neostriatal cholinergic interneurons. J Neurosci 20:8493-503.

Bergman H, Wichmann T, Karmon B, DeLong MR (1994) The primate subthalamic nucleus. II. Neuronal activity in the MPTP model of parkinsonism. J Neurophysiol 72:507-20.

Berke JD, Okatan M, Skurski J, Eichenbaum HB (2004) Oscillatory entrainment of striatal neurons in freely moving rats. Neuron 43:883-96.

Berndt A, Schoenenberger P, Mattis J, Tye KM, Deisseroth K, Hegemann P, Oertner TG (2011) High-efficiency channelrhodopsins for fast neuronal stimulation at low light levels. PNAS 108:7595-600.

Beurrier C, Bioulac B, Audin J, Hammond C (2001) High-frequency stimulation produces a transient blockade of voltage-gated currents in subthalamic neurons. J Neurophysiol 85:1351-6.

Beurrier C, Bioulac B, Hammond C (2000) Slowly inactivating sodium current (INaP) underlies single-spike activity in rat subthalamic neurons. J Neurophysiol 83:1951-7.

Beurrier C, Congar P, Bioulac B, Hammond C (1999) Subthalamic nucleus neurons switch from single-spike activity to burst-firing mode. J Neurosci 19:599-609.

Bevan MD, Bolam JP (1995) Cholinergic, GABAergic, and glutamate-enriched inputs from the mesopontine tegmentum to the subthalamic nucleus in the rat. J Neurosci 15:7105-20.

Bevan MD, Hallworth NE, Baufreton J (2007) GABAergic control of the subthalamic nucleus. Prog Brain Res 160:173-88.

Bevan MD, Magill PJ, Hallworth NE, Bolam JP, Wilson CJ (2002) Regulation of the

timing and pattern of action potential generation in rat subthalamic neurons *in vitro* by GABA-A IPSPs. J Neurophysiol 87:1348-62.

Bevan MD, Atherton JF, Baufreton J (2006) Cellular principles underlying normal and pathological activity in the subthalamic nucleus. Curr Opin Neurobiol 16:621-8.

Bevan MD, Clarke NP, Bolam JP (1997) Synaptic integration of functionally diverse pallidal information in the entopeduncular nucleus and subthalamic nucleus in the rat. J Neurosci 17:308-24.

Bevan MD, Francis CM, Bolam JP (1995) The glutamate-enriched cortical and thalamic input to neurons in the subthalamic nucleus of the rat - convergence with GABA-positive terminals. J Comp Neurol 361:491-11.

Bevan MD, Magill PJ, Terman D, Bolam JP, Wilson CJ (2002) Move to the rhythm: oscillations in the subthalamic nucleus-external globus pallidus network. Trends Neurosci 25:525-31.

Bevan MD, Wilson CJ (1999) Mechanisms underlying spontaneous oscillation and rhythmic firing in rat subthalamic neurons. J Neurosci 19:7617-28.

Bevan MD, Wilson CJ, Bolam JP, Magill PJ (2000) Equilibrium potential of GABA(A) current and implications for rebound burst firing in rat subthalamic neurons *in vitro*. J Neurophysiol 83:3169-72.

Biel M, Wahl-Schott C, Michalakis S, Zong X (2009) Hyperpolarisation-activated cation channels: from genes to function. Physiol Rev 89:847-85.

Boraud T, Bezard E, Guehl D, Bioulac B, Gross C (1998) Effects of L-DOPA on neuronal activity of the globus pallidus externalis (GPe) and globus pallidus internalis (GPi) in the MPTP-treated monkey. Brain Res 787:157-60.

Bouali-Benazzouz R, Tai CH, Chetrit J, Benazzouz A (2009) Intrapallidal injection of 6-hydroxydopamine induced changes in dopamine innervation and neuronal activity of globus pallidus. Neurosci 164:588-96.

Boyes J, Bolam JP, Shigemoto R, Stanford IM (2007) Functional presynaptic HCN channels in the rat globus pallidus. Eur J Neurosci 25:2081-92.

Brown P (2007) Abnormal oscillatory synchronisation in the motor system leads to impaired movement. Curr Opin Neurobiol 17:656-64.

Brown P (2003) Oscillatory nature of human basal ganglia activity: relationship to the pathophysiology of Parkinson's disease. Mov Disord 18:357-63.

Bullis JB, Jones TD, Poolos NP (2007) Reversed somatodendritic I(h) gradient in a class of rat hippocampal neurons with pyramidal morphology. J Physiol 579:431-43.

Burbaud P, Gross C, Benazzouz A, Coussemacq M, Bioulac B (1995) Reduction of apomorphine-induced rotational behavior by subthalamic lesion in 6-OHDA lesioned rats is associated with a normalisation of firing rate and discharge pattern of pars reticulata neurons. Exp Brain Res 105:48-58.

Canteras NS, Shammahlagnado SJ, Silva BA, Ricardo JA (1990) Afferent connections of the subthalamic nucleus - a combined retrograde and anterograde horseradish-peroxidase study in the rat. Brain Res 513:43-59.

Carman LS, Gage FH, Shults CW (1991) Partial lesion of the substantia-nigra -

relation between extent of lesion and rotational behavior. Brain Res 553:275-83.
Chan CS, Shigemoto R, Mercer JN, Surmeier DJ (2004) HCN2 and HCN1 channels govern the regularity of autonomous pacemaking and synaptic resetting in globus pallidus neurons. J Neurosci 24:9921-32.
Chan CS, Glajch KE, Gertler TS, Guzman JN, Mercer JN, Lewis AS, Goldberg AB, Tkatch T, Shigemoto R, Fleming SM, Chetkovich DM, Osten P, Kita H, Surmeier DJ (2011) HCN channelopathy in external globus pallidus neurons in models of Parkinson's disease. Nat Neurosci 14:85-92.
Chen CC, Lin WY, Chan HL, Hsu YT, Tu PH, Lee ST, Chiou SM, Tsai CH, Lu CS, Brown P (2011) Stimulation of the subthalamic region at 20 Hz slows the development of grip force in Parkinson's disease. Exp Neurol 231:91-6.
Chen CC, Litvak V, Gilbertson T, Kühn A, Lu CS, Lee ST, Tsai CH, Tisch S, Limousin P, Hariz M, Brown P (2007) Excessive synchronisation of basal ganglia neurons at 20 Hz slows movement in Parkinson's disease. Exp Neurol 205:214-21.
Chen G, Kittler JT, Moss SJ, Yan Z (2006) Dopamine D3 receptors regulate $GABA_A$ receptor function through a phosphodependent endocytosis mechanism in nucleus accumbens. J Neurosci 26:2513-21.
Chen L, Yung WH (2005) Tonic activation of presynaptic GABA(B) receptors on rat pallidosubthalamic terminals. Acta Pharmacol Sin 26:10-6.
Chevaleyre V, Castillo PE (2002) Assessing the role of Ih channels in synaptic transmission and mossy fiber LTP. Proc Natl Acad Sci USA 99:9538-43.
Coizet V, Graham JH, Moss J, Bolam JP, Savasta M, McHaffie JG, Redgrave P, Overton PG (2009) Short-latency visual input to the subthalamic nucleus is provided by the midbrain superior colliculus. J Neurosci 29:5701-9.
Cooper AJ, Stanford IM (2001) Dopamine D2 receptor mediated presynaptic inhibition of striatopallidal GABA(A) IPSCs in vitro. Neuropharmacol 41:62-71.
Cossette M, Levesque M, Parent A (1999) Extrastriatal dopaminergic innervation of human basal ganglia. Neurosci Res 34:51-4.
Costa RM, Lin S-C, Sotnikova TD, Cyr M, Gainetdinov RR, Caron MG, Nicolelis MAL (2006) Rapid alterations in corticostriatal ensemble coordination during acute dopamine-dependent motor dysfunction. Neuron 52:359-69.
Courtemanche R, Fujii N, Graybiel AM (2003) Synchronous, focally modulated beta-band oscillations characterize local field potential activity in the striatum of awake behaving monkeys. J Neurosci 23:11741-52.
Courtoy PJ, Picton DH, Farquhar MG (1983) Resolution and limitations of the immunoperoxidase procedure in the localization of extracellular-matrix antigens. J Histochem Cytochem 31:945-51.
Cragg SJ, Baufreton J, Xue Y, Bolam JP, Bevan MD (2004) Synaptic release of dopamine in the subthalamic nucleus. Eur J Neurosci 20:1788-802.
Crossman AR (2000) Functional anatomy of movement disorders. J Anat 196:519-25.
Crossman AR, Sambrook MA, Jackson A (1984) Experimental hemichorea/hemiballismus in the monkey. Studies on the intracerebral site of action in a drug-induced dyskinesia. Brain 107:579-96.

Cruz AV, Mallet N, Magill PJ, Brown P, Averbeck BB (2011) Effects of dopamine depletion on information flow between the subthalamic nucleus and external globus pallidus. J Neurophysiol 106: 2012-23.

Dawson TM, Dawson VL (2003) Molecular pathways of neurodegeneration in Parkinson's disease. Science 302:819-22.

Dauer W, Przedborski S (2003) Parkinson's disease: Mechanisms and models. Neuron 39:889-909.

Day M, Wang Z, Ding J, An X, Ingham CA, Shering AF, Wokosin D, Ilijic E, Sun Z, Sampson AR, Mugnaini E, Deutch AY, Sesack SR, Arbuthnott GW, Surmeier DJ. (2006) Selective elimination of glutamatergic synapses on striatopallidal neurons in Parkinson disease models. Nat Neurosci 9:251-9.

Degos B, Deniau JM, Thierry AM, Glowinski J, Pezard L, Maurice N (2005) Neuroleptic-induced catalepsy: Electrophysiological mechanisms of functional recovery induced by high-frequency stimulation of the subthalamic nucleus. J Neurosci 25:7687-96.

Deisseroth K (2010) Controlling the brain with light. Sci Am 303:48-55.

Deisseroth K (2011) Optogenetics. Nat Methods 8:26-9.

Deisseroth K, Feng G, Majewska AK, Miesenbock G, Ting A, Schnitzer MJ (2006) Next-generation optical technologies for illuminating genetically targeted brain circuits. J Neurosci 26:10380-6.

DeLong MR (1990) Primate models of movement disorders of basal ganglia origin. Trends Neurosci 13:281-5.

Dejean C, Gross CE, Bioulac B, Boraud T (2008) Dynamic changes in the cortex-basal ganglia network after dopamine depletion in the rat. J Neurophysiol 100:385-96.

Deniau JM, Degos B, Bosch C, Maurice N (2010) Deep brain stimulation mechanisms: beyond the concept of local functional inhibition. Eur J Neurosci 32:1080-91.

Deniau JM, Mailly P, Maurice N, Charpier S (2007) The pars reticulata of the substantia nigra: a window to basal ganglia output. Prog Brain Res 160:151-72.

Destexhe A, Mainen ZF, Sejnowski TJ (1998) Kinetic models of synaptic transmission. In: Methods in neural modelling (Koch C, Segev I, eds), pp 1-25. Cambridge, MA: MIT.

Do MT, Bean BP (2003) Subthreshold sodium currents and pacemaking of subthalamic neurons: modulation by slow inactivation. Neuron 39:109-20.

Dobie FA, Craig AM (2011) Inhibitory synapse dynamics: coordinated presynaptic and postsynaptic mobility and the major contribution of recycled vesicles to new synapse formation. J Neurosci 31:10481-93.

Dorval AD, Kuncel AM, Birdno MJ, Turner DA, Grill WM (2010) Deep brain stimulation alleviates parkinsonian bradykinesia by regularizing pallidal activity. J Neurophysiol 104:911-21.

Dorval AD, Russo GS, Hashimoto T, Xu W, Grill WM, Vitek JL (2008) Deep brain stimulation reduces neuronal entropy in the MPTP-primate model of Parkinson's

disease. J Neurophysiol 100:2807-18.
Dreyfus FM, Tscherter A, Errington AC, Renger JJ, Shin HS, Uebele VN, Crunelli V, Lambert RC, Leresche N (2010) Selective T-type calcium channel block in thalamic neurons reveals channel redundancy and physiological impact of I(T) window. J Neurosci 30:99-109.
Drouot X, Oshino S, Jarraya B, Besret L, Kishima H, Remy P, Dauguet J, Lefaucheur JP, Dolle F, Conde F, Bottlaender M, Peschanski M, Keravel Y, Hantraye P, Palfi S (2004) Functional recovery in a primate model of Parkinson's disease following motor cortex stimulation. Neuron 44:769-78.
Engel AK, Fries P (2010) Beta-band oscillations - signalling the status quo? Curr Opin Neurobiol 20:156-65.
Eusebio A, Chen CC, Lu CS, Lee ST, Tsai CH, Limousin P, Hariz M, Brown P (2008) Effects of low-frequency stimulation of the subthalamic nucleus on movement in Parkinson's disease. Exp Neurol 209:125-30.
Eyre MD, Renzi M, Farrant M, Nusser Z (2012) Setting the time course of inhibitory synaptic currents by mixing multiple GABA(A) receptor α subunit isoforms. J Neurosci 32:5853-67.
Fallon JH, Moore RY (1978) Catecholamine innervation of basal forebrain .4. topography of dopamine projection to basal forebrain and neostriatum. J Comp Neurol 180:545-80.
Fan Y, Fricker D, Brager DH, Chen X, Lu HC, Chitwood RA, Johnston D (2005) Activity-dependent decrease of excitability in rat hippocampal neurons through increases in I(h). Nat Neurosci 8:1542-51.
Farries MA, Kita H, Wilson CJ (2010) Dynamic Spike Threshold and Zero Membrane Slope Conductance Shape the Response of Subthalamic Neurons to Cortical Input. J Neurosci 30:13180-91.
Fass B, Butcher LL (1981) Evidence for a crossed nigrostriatal pathway in rats. Neurosci Lett 22:109-13.
Fedorov LM, HaegelKronenberger H, Hirchenhain J (1997) A comparison of the germline potential of differently aged ES cell lines and their transfected descendants. Transgenic Res 6:223-31.
Feger J, Bevan M, Crossman AR (1994) The projections from the parafascicular thalamic nucleus to the subthalamic nucleus and the striatum arise from separate neuronal populations - a comparison with the corticostriatal and corticosubthalamic efferents in a retrograde fluorescent double-labeling study. Neurosci 60:125-32.
Feldbauer K, Zimmermann D, Pintschovius V, Spitz J, Bamann C, Bamberg E (2009) Channelrhodopsin-2 is a leaky proton pump. PNAS 106:12317-22.
Felix R, Sandoval A, Sánchez D, Gómora JC, De la Vega-Beltrán JL, Treviño CL, Darszon A. (2003) ZD7288 inhibits low-threshold Ca^{2+} channel activity and regulates sperm function. Biochem & Biophys Res Comm 311:187-92.
Fenno L, Yizhar O, Deisseroth K (2011) The development and application of optogenetics. annual review of neuroscience 34:389-412.

Filion M, Tremblay L (1991) Abnormal spontaneous activity of globus-pallidus neurons in monkeys with MPTP-induced parkinsonism. Brain Res 547:142-51.
Fioravante D, Regehr WG (2011) Short-term forms of presynaptic plasticity. Curr Opin Neurobiol 21:269-74.
Flores G, Liang JJ, Sierra A, Martinez-Fong D, Quirion R, Aceves J, Srivastava LK (1999) Expression of dopamine receptors in the subthalamic nucleus of the rat: Characterization using reverse transcriptase polymerase chain reaction and autoradiography. Neurosci 91:549-56.
François C, Savy C, Jan C, Tande D, Hirsch EC, Yelnik J (2000) Dopaminergic innervation of the subthalamic nucleus in the normal state, in MPTP-treated monkeys, and in Parkinson's disease patients. J Comp Neurol 425:121-29.
Fujiyama F, Kuramoto E, Okamoto K, Hioki H, Furuta T, Zhou LG, Nomura S, Kaneko T (2004) Presynaptic localisation of an AMPA-type glutamate receptor in corticostriatal and thalamostriatal axon terminals. Eur J Neurosci 20:3322-30.
Fujiyama F, Unzai T, Nakamura K, Nomura S, Kaneko T (2006) Difference in organization of corticostriatal and thalamostriatal synapses between patch and matrix compartments of rat neostriatum. Eur J Neurosci 24:2813-24.
Galati S, Stanzione P, D'Angelo V, Fedele E, Marzetti F, Sancesario G, Procopio T, Stefani A (2009) The pharmacological blockade of medial forebrain bundle induces an acute pathological synchronisation of the cortico-subthalamic nucleus-globus pallidus pathway. J Physiol 587: 4405-23.
Galvan A, Wichmann T (2008) Pathophysiology of parkinsonism. Clin Neurophysiol 119:1459-74.
Garcia L, Audin J, D'Alessandro G, Bioulac B, Hammond C (2003) Dual effect of high-frequency stimulation on subthalamic neuron activity. J Neurosci 23:8743-51.
Garcia L, D'Alessandro G, Fernagut PO, Bioulac B, Hammond C (2005) Impact of high-frequency stimulation parameters on the pattern of discharge of subthalamic neurons. J Neurophysiol 94:3662-9.
Garden DL, Dodson PD, O'Donnell C, White MD, Nolan MF (2008) Tuning of synaptic integration in the medial entorhinal cortex to the organization of grid cell firing fields. Neuron 60:875-89.
Gatev P, Darbin O, Wichmann T (2006) Oscillations in the basal ganglia under normal conditions and in movement disorders. Mov Disord 21:1566-77.
Gerfen CR, Surmeier DJ (2011) Modulation of striatal projection systems by dopamine. Annu Rev Neurosci 34:441-66.
Gillies A, Willshaw D (2006) Membrane channel interactions underlying rat subthalamic projection neuron rhythmic and bursting activity. J Neurophysiol 95:2352-65.
Gittis AH, Hang GB, LaDow ES, Shoenfeld LR, Atallah BV, Finkbeiner S, Kreitzer AC (2011) Rapid target-specific remodelling of fast-spiking inhibitory circuits after loss of dopamine. Neuron 71:858–68.
Grill WM, Cantrell MB, Robertson MS (2008) Antidromic propagation of action

potentials in branched axons: implications for the mechanisms of action of deep brain stimulation. J Comput Neurosci 24:81-93.

Goetz T, Arslan A, Wisden W, Wulff P (2007) GABA(A) receptors: structure and function in the basal ganglia. Prog Brain Res 160:21-41.

Goffin D, Ali AB, Rampersaud N, Harkavyi A, Fuchs C, Whitton PS, Nairn AC, Jovanovic JN (2010) Dopamine-dependent tuning of striatal inhibitory synaptogenesis. J Neurosci 30:2935-50.

Gotz T, Kraushaar U, Geiger J, Lubke J, Berger T, Jonas P (1997) Functional properties of AMPA and NMDA receptors expressed in identified types of basal ganglia neurons. J Neurosci 17:204-15.

Guo Y, Rubin JE, McIntyre CC, Vitek JL, Terman D (2008) Thalamocortical relay fidelity varies across subthalamic nucleus deep brain stimulation protocols in a data-driven computational model. J Neurophysiol 99:1477-92.

Gustafsson MGL, Shao L, Carlton PM, Wang CJR, Golubovskaya IN, Cande WZ, Agard DA, Sedat JW (2008) Three-dimensional resolution doubling in wide-field fluorescence microscopy by structured illumination. Biophys 94:4957-70.

Gradinaru V, Mogri M, Thompson KR, Henderson JM, Deisseroth K (2009) Optical deconstruction of parkinsonian neural circuitry. Science 324:354-59.

Groenewegen HJ, Berendse HW (1990) Connections of the subthalamic nucleus with ventral striatopallidal parts of the basal ganglia in the rat. J Comp Neurol 294:607-22.

Gunaydin LA, Yizhar O, Berndt A, Sohal VS, Deisseroth K, Hegemann P (2010) Ultrafast optogenetic control. Nat Neurosci 13:387-392.

Halliwell JV, Adams PR (1982) Voltage-clamp analysis of muscarinic excitation in hippocampal neurons. Brain Res 250:71-92.

Hallworth NE, Bevan MD (2005) Globus pallidus neurons dynamically regulate the activity pattern of subthalamic nucleus neurons through the frequency-dependent activation of postsynaptic $GABA_A$ and $GABA_B$ receptors. J Neurosci 25:6304-15.

Hallworth NE, Wilson CJ, Bevan MD (2003) Apamin-sensitive small conductance calcium-activated potassium channels, through their selective coupling to voltage-gated calcium channels, are critical determinants of the precision, pace, and pattern of action potential generation in rat subthalamic nucleus neurons *in vitro*. J Neurosci 23: 7525-42.

Hammond C, Bergman H, Brown P (2007) Pathological synchronisation in Parkinson's disease: networks, models and treatments. Trends Neurosci 30:357-64.

Hashimoto T, Elder CM, Okun MS, Patrick SK, Vitek JL (2003) Stimulation of the subthalamic nucleus changes the firing pattern of pallidal neurons. J Neurosci 23:1916-23.

Helmich RC, Janssen MJR, Oyen WJG, Bloem BR, Toni I (2011) Pallidal dysfunction drives a cerebellothalamic circuit into Parkinson tremor. Ann Neurol 69:269-81.

Henchcliffe C, Beal MF (2008) Mitochondrial biology and oxidative stress in

Parkinson disease pathogenesis. Nat Clin Pract Neurol 4:600-9.
Hermann R, Walther P, Muller M (1996) Immunogold labeling in scanning electron microscopy. Histochem Cell Biol 106:31-9.
Hernandez-Lopez S, Tkatch T, Perez-Garci E, Galarraga E, Bargas J, Hamm H, Surmeier J (2000) D-2 dopamine receptors in striatal medium spiny neurons reduce L-type Ca2+ currents and excitability via a novel PLC beta 1-IP3-calcineurin-signaling cascade. J Neurosci 20:8987-95.
Hibino H, Inanobe A, Furutani K, Murakami S, Findlay I, Kurachi Y (2010) Inwardly Rectifying Potassium Channels: Their Structure, Function, and Physiological Roles. Physiol Rev 90:291-366.
Holderith NB, Shigemoto R, Nusser Z (2003) Cell type-dependent expression of HCN1 in the main olfactory bulb. Eur J Neurosci 18:344-54.
Holgado AJ, Terry JR, Bogacz R (2010) Conditions for the generation of beta oscillations in the subthalamic nucleus-globus pallidus network. J Neurosci 30:12340-52.
Humphries MD, Gurney K (2012) Network effects of subthalamic deep brain stimulation drive a unique mixture of responses in basal ganglia output. Eur J Neurosci 36:2240-51.
Hur EE, Zaborszky L (2005) VGLUT2 afferents to the medial prefrontal and primary somatosensory cortices: A combined retrograde tracing in situ hybridization. J Comp Neurol 483:351-73.
Hutchison WD, Dostrovsky JO, Walters JR, Courtemanche R, Boraud T, Goldberg J, Brown P (2004) Neuronal oscillations in the basal ganglia and movement disorders: Evidence from whole animal and human recordings. J Neurosci 24:9240-3.
Iancu R, Mohapel P, Brundin P, Paul G (2005) Behavioral characterization of a unilateral 6-OHDA-lesion model of Parkinson's disease in mice. Behav Brain Res 162:1-10.
Ikarashi Y, Takahashi A, Ishimaru H, Arai T, Maruyama Y (1997) Regulation of dopamine D-1 and D-2 receptors on striatal acetylcholine release in rats. Brain Res Bull 43:107-15.
Ingham CA, Hood SH, Mijnster MJ, Baldock RA, Arbuthnott GW (1997) Plasticity of striatopallidal terminals following unilateral lesion of the dopaminergic nigrostriatal pathway: a morphological study. Exp Brain Res 116:39-49.
Jenkinson N, Brown P (2011) New insights into the relationship between dopamine, beta oscillations and motor function. Trends Neurosci (in press).
Jeon BS, Jacksonlewis V, Burke RE (1995) 6-hydroxydopamine lesion of the rat substantia-nigra - time-course and morphology of cell-death. Neurodegener 4:131-7.
Jin X-T, Pare J-F, Smith Y (2012) GABA transporter subtype 1 and GABA transporter subtype 3 modulate glutamatergic transmission via activation of presynaptic GABAB receptors in the rat globus pallidus. Eur J Neurosci 36:2482-92.
Johnson MD, McIntyre CC (2008) Quantifying the Neural Elements Activated and Inhibited by Globus Pallidus Deep Brain Stimulation. J Neurophysiol 100:2549-

63.
Karachi C, Grabli D, Baup N, Mounayar S, Tandé D, François C, Hirsch EC (2009) Dysfunction of the subthalamic nucleus induces behavioral and movement disorders in monkeys. Mov Disord 24:1183-92.
Kass JI, Mintz IM (2006) Silent plateau potentials, rhythmic bursts, and pacemaker firing: three patterns of activity that coexist in quadristable subthalamic neurons. Proc Natl Acad Sci USA 103:183-8.
Kita H, Chang HT, Kitai ST (1983) The morphology of intracellularly labeled rat subthalamic neurons: a light microscopic analysis. J Comp Neurol 215:245-57.
Kitai ST, Deniau JM (1981) Cortical inputs to the subthalamus - intracellular analysis. Brain Res 214:411-5.
Kita T, Kita H (2012) The subthalamic nucleus is one of multiple innervation sites for long-range corticofugal axons: a single-axon tracing study in the rat. J Neurosci 32:5990-9.
Kittler JT, Rostaing P, Schiavo G, Fritschy JM, Olsen R, Triller A, Moss SJ (2001) The subcellular distribution of GABARAP and its ability to interact with NSF suggest a role for this protein in the intracellular transport of GABA(A) receptors. Mol Cell Neurosci 18:13-25.
Kole MH, Bräuer AU, Stuart GJ (2007) Inherited cortical HCN1 channel loss amplifies dendritic calcium electrogenesis and burst firing in a rat absence epilepsy model. J Physiol 578:507-25.
Kordower JH, Chu Y, Hauser RA, Freeman TB, Olanow CW (2008) Lewy body-like pathology in long-term embryonic nigral transplants in Parkinson's disease. Nat Med 14:504-6.
Kravitz AV, Freeze BS, Parker PRL, Kay K, Thwin MT, Deisseroth K, Kreitzer AC (2010) Regulation of parkinsonian motor behaviours by optogenetic control of basal ganglia circuitry. Nature 466:622-6.
Kreitzer AC (2009) Physiology and Pharmacology of Striatal Neurons. Annu Rev Neurosci 32:127-47.
Kubota Y, Hatada S, Kondo S, Karube F, Kawaguchi Y (2007) Neocortical inhibitory terminals innervate dendritic spines targeted by thalamocortical afferents. J Neurosci 27:1139-50.
Kühn AA, Kempf F, Bruecke C, Doyle LG, Martinez-Torres I, Pogosyan A, Trottenberg T, Kupsch A, Schneider G-H, Hariz MI, Vandenberghe W, Nuttin B, Brown P (2008) High-frequency stimulation of the subthalamic nucleus suppresses oscillatory beta activity in patients with Parkinson's disease in parallel with improvement in motor performance. J Neurosci 28:6165-73.
Kühn AA, Tsui A, Aziz T, Ray N, Bruecke C, Kupsch A, Schneider G-H, Brown P (2009) Pathological synchronisation in the subthalamic nucleus of patients with Parkinson's disease relates to both bradykinesia and rigidity. Exp Neurol 215:380-7.
Kühn AA, Kupsch A, Schneider GH, Brown P (2006) Reduction in subthalamic 8-35 Hz oscillatory activity correlates with clinical improvement in Parkinson's

disease. Eur J Neurosci 23:1956-60.
Kühn R, Torres RM (2002) Cre/loxP recombination system and gene targeting. In: Transgenesis techniques principles and protocols (Clarke AR, ed). New York, NY: Springer.
Kurotani T, Yamada K, Yoshimura Y, Crair MC, Komatsu Y (2008) State-dependent bidirectional modification of somatic inhibition in neocortical pyramidal cells. Neuron 57:905-16.
Lee P, Hall WC (2006) An in vitro study of horizontal connections in the intermediate layer of the superior colliculus. J Neurosci 26:4763-8.
Levy R, Hutchison WD, Lozano AM, Dostrovsky JO (2002) Synchronised neuronal discharge in the basal ganglia of parkinsonian patients is limited to oscillatory activity. J Neurosci 22:2855-61.
Levy R, Lang AE, Dostrovsky JO, Pahapill P, Romas J, Saint-Cyr J, Hutchison WD, Lozano AM (2001) Lidocaine and muscimol microinjections in subthalamic nucleus reverse parkinsonian symptoms. Brain 124:2105-18.
Lewis AS, Chetkovich DM (2011) HCN channels in behavior and neurological disease: too hyper or not active enough? Mol Cell Neurosci 46:357-67.
Li J-Y, Englund E, Holton JL, Soulet D, Hagell P, Lees AJ, Lashley T, Quinn NP, Rehncrona S, Björklund A, Widner H, Revesz T, Lindvall O, Brundin P (2008) Lewy bodies in grafted neurons in subjects with Parkinson's disease suggest host-to-graft disease propagation. Nat Med 14:501-3.
Li S, Arbuthnott GW, Jutras MJ, Goldberg JA, Jaeger D (2007) Resonant antidromic cortical circuit activation as a consequence of high-frequency subthalamic deep-brain stimulation. J Neurophysiol 98:3525-37.
Lin JY (2011) A user's guide to channelrhodopsin variants: features, limitations and future developments. Exp Physiol 96:19-25.
Lindvall O, Björklund A (1979) Dopaminergic innervation of the globus pallidus by collaterals from the nigrostriatal pathway. Brain Res 172:169-73.
Litvak V, Jha A, Eusebio A, Oostenveld R, Foltynie T, Limousin P, Zrinzo L, Hariz MI, Friston K, Brown P (2011) Resting oscillatory cortico-subthalamic connectivity in patients with Parkinson's disease. Brain 134:359-74.
Loebrich S, Nedivi E (2009) The function of activity-regulated genes in the nervous system. Physiol Rev 89:1079-103.
London M, Häusser M (2005) Dendritic computation. Annu Rev Neurosci 28:503-32.
Loucif KC, Wilson CL, Baig R, Lacey AG, Stanford IA (2005) Functional interconnectivity between the globus pallidus and the subthalamic nucleus in the mouse brain slice. J Physiol (Lond) 567:977-87.
Loucif AJC, Woodhall GL, Sehirli US, Stanford IM (2008) Depolarisation and suppression of burst firing activity in the mouse subthalamic nucleus by dopamine D1/D5 receptor activation of a cyclic-nucleotide gated non-specific cation conductance. Neuropharmacol 55:94-105.
Lörincz A, Notomi T, Tamás G, Shigemoto R, Nusser Z (2002) Polarized and compartment-dependent distribution of HCN1 in pyramidal cell dendrites. Nat

Neurosci 5:1185-93.
Loucif AJ, Woodhall GL, Sehirli US, Stanford IM (2008) Depolarisation and suppression of burst firing activity in the mouse subthalamic nucleus by dopamine D1/D5 receptor activation of a cyclic-nucleotide gated non-specific cation conductance. Neuropharmacology 55:94-105.
Ludwig A, Budde T, Stieber J, Moosmang S, Wahl C, Holthoff K, Langebartels A, Wotjak C, Munsch T, Zong X, Feil S, Feil R, Lancel M, Chien KR, Konnerth A, Pape HC, Biel M, Hofmann F (2003) Absence epilepsy and sinus dysrhythmia in mice lacking the pacemaker channel HCN2. EMBO J 22:216-24.
Ludwin SK (1979) The perineuronal satellite oligodendrocyte. Acta Neuropathol 47:49-53.
Luscher B, Fuchs T, Kilpatrick CL (2011) $GABA_A$ receptor trafficking-mediated plasticity of inhibitory synapses. Neuron 70:385-409.
Lüthi A, McCormick DA (1998) Periodicity of thalamic synchronised oscillations: the role of Ca2+-mediated upregulation of Ih. Neuron 20: 553-63.
Luthman J, Fredriksson A, Sundstrom E, Jonsson G, Archer T (1989) Selective lesion of central dopamine or noradrenaline neuron systems in the neonatal rat - motor behavior and monoamine alterations at adult stage. Behav Brain Res 33:267-77.
Maffei A (2011) The many forms and functions of long term plasticity at gabaergic synapses. Neural Plast 2011:254724.
Magee JC (1998) Dendritic hyperpolarisation-activated currents modify the integrative properties of hippocampal CA1 pyramidal neurons. J Neurosci 18:7613-24.
Magee JC (1999). Dendritic lh normalises temporal summation in hippocampal CA1 neurons. Nat Neurosci 2:508-14.
Magill PJ, Bolam JP, Bevan MD (2000) Relationship of activity in the subthalamic nucleus-globus pallidus network to cortical electroencephalogram. J Neurosci 20:820-33.
Magill PJ, Bolam JP, Bevan MD (2001) Dopamine regulates the impact of the cerebral cortex on the subthalamic nucleus-globus pallidus network. Neuroscience 106:313-30.
Magill PJ, Sharott A, Bevan MD, Brown P, Bolam JP (2004) Synchronous unit activity and local field potentials evoked in the subthalamic nucleus by cortical stimulation. J Neurophysiol 92:700-14.
Magill PJ, Sharott A, Bolam JP, Brown P (2006) Delayed synchronisation of activity in cortex and subthalamic nucleus following cortical stimulation in the rat. J Physiol (Lond) 574:929-46.
Magill PJ, Sharott A, Harnack D, Kupsch A, Meissner W, Brown P (2005) Coherent spike-wave oscillations in the cortex and subthalamic nucleus of the freely moving rat. Neurosci 132:659-64.
Mallet N, Pogosyan A, Sharott A, Csicsvari J, Bolam JP, Brown P, Magill PJ (2008a) Disrupted dopamine transmission and the emergence of exaggerated beta

oscillations in subthalamic nucleus and cerebral cortex. J Neurosci 28:4795-806.

Mallet N, Pogosyan A, Márton LF, Bolam JP, Brown P, Magill PJ (2008b) Parkinsonian beta oscillations in the external globus pallidus and their relationship with subthalamic nucleus activity. J Neurosci 28:14245-58.

Mallet N, Micklem BR, Henny P, Brown MT, Williams C, Bolam JP, Nakamura KC, Magill PJ (2012) Dichotomous organization of the external globus pallidus. Neuron 74:1075-86.

Maltête D, Jodoin N, Karachi C, Houeto JL, Navarro S, Cornu P, Agid Y, Welter ML (2007) Subthalamic stimulation and neuronal activity in the substantia nigra in Parkinson's disease. J Neurophysiol 97:4017-22.

Marsden KC, Beattie JB, Friedenthal J, Carroll RC (2007) NMDA receptor activation potentiates inhibitory transmission through GABA receptor-associated protein-dependent exocytosis of GABA(A) receptors. J Neurosci 27:14326-37.

Mathew SS, Hablitz JJ (2011) Presynaptic nmda receptors mediate IPSC potentiation at GABAergic synapses in developing rat neocortex. Plos One 6:e17311.

Matsumoto M, Hikosaka O (2009) Two types of dopamine neuron distinctly convey positive and negative motivational signals. Nature 459:837-41.

Mattson MP (2007) Calcium and neurodegeneration. Aging Cell 6:337-50.

Maurice N, Thierry AM, Glowinski J, Deniau JM (2003) Spontaneous and evoked activity of substantia nigra pars reticulata neurons during high-frequency stimulation of the subthalamic nucleus. J Neurosci 23:9929-36.

Mayer ML, Westbrook GL, Guthrie PB (1984) Voltage-dependent block by Mg-2+ of NMDA responses in spinal-cord neurons. Nature 309:261-3.

Mayford M (2007) Protein kinase signaling in synaptic plasticity and memory. Curr Opin Neurobiol 17:313-7.

McCarthy MM, Moore-Kochlacs C, Gu X, Boyden ES, Han X, Kopell N (2011) Striatal origin of the pathologic beta oscillations in Parkinson's disease. PNAS 108:11620-5.

McIntire SL, Reimer RJ, Schuske K, Edwards RH, Jorgensen EM (1997) Identification and characterization of the vesicular GABA transporter. Nature 389:870-6.

Meissner W, Leblois A, Hansel D, Bioulac B, Gross CE, Benazzouz A, Boraud T (2005) Subthalamic high frequency stimulation resets subthalamic firing and reduces abnormal oscillations. Brain 128:2372-82.

Mendez I, Vinuela A, Astradsson A, Mukhida K, Hallett P, Robertson H, Tierney T, Holness R, Dagher A, Trojanowski JQ, Isacson O (2008) Dopamine neurons implanted into people with Parkinson's disease survive without pathology for 14 years. Nat Med 14:507-9.

Meurers BH, Dziewczapolski G, Bittner A, Shi T, Kamme F, Shults CW (2009) Dopamine depletion induced up-regulation of HCN3 enhances rebound excitability of basal ganglia output neurons. Neurobiol Dis 34:178-88.

Micheva KD, Busse B, Weiler NC, O'Rourke N, Smith SJ (2010) Single-synapse analysis of a diverse synapse population: proteomic imaging methods and markers.

Neuron. 68:639-53.
Miocinovic S, Parent M, Butson CR, Hahn PJ, Russo GS, Vitek JL, McIntyre CC (2006) Computational analysis of subthalamic nucleus and lenticular fasciculus activation during therapeutic deep brain stimulation. J Neurophysiol 96:1569-80.
Monakow KH, Akert K, Kunzle H (1978) Projections of the precentral motor cortex and other cortical areas of the frontal lobe to the subthalamic nucleus in the monkey. Exp Brain Res 33:395-403.
Monteggia LM, Eisch AJ, Tang MD, Kaczmarek LK, Nestler EJ (2000) Cloning and localisation of the hyperpolarisation-activated cyclic nucleotide-gated channel family in rat brain. Brain Res Mol Brain Res 81:129-39.
Moran RJ, Mallet N, Litvak V, Dolan RJ, Magill PJ, Friston KJ, Brown P (2011) Alterations in brain connectivity underlying beta oscillations in parkinsonism. PLoS Comput Biol 7: e1002124.
Moriizumi T, Nakamura Y, Kitao Y, Kudo M (1987) Ultrastructural analyses of afferent terminals in the subthalamic nucleus of the cat with a combined degeneration and horseradish-peroxidase tracing method. J Comp Neurol 265:159-74.
Morris ME (2000) Movement disorders in people with Parkinson disease: A model for physical therapy. Phys Ther 80:578-97.
Nagy A, Rossant J, Nagy R, Abramownewerly W, Roder JC (1993) Derivation of completely cell culture-derived mice from early-passage embryonic stem-cells. PNAS 90:8424-8.
Nakanishi H, Kita H, Kitai ST (1987) Electrical membrane-properties of rat subthalamic neurons in an in vitro slice preparation. Brain Res 437:35-44.
Nambu A (2007) Globus pallidus internal segment. Prog Brain Res 160:135-50.
Ni ZG, Bouali-Benazzouz R, Gao DM, Benabid AL, Benazzouz A (2000) Changes in the firing pattern of globus pallidus neurons after the degeneration of nigrostriatal pathway are mediated by the subthalamic nucleus in the rat. Eur J Neurosci 12:4338-44.
Notomi T, Shigemoto R (2004) Immunohistochemical localisation of Ih channel subunits, HCN1-4, in the rat brain. J Comp Neurol 471:241-76.
Nowak LG, Bullier J (1998) Axons, but not cell bodies, are activated by electrical stimulation in cortical gray matter II. Evidence from selective inactivation of cell bodies and axon initial segments. Exp Brain Res 118:489-500.
Nusser Z, Cull-Candy S, Farrant M (1997) Differences in synaptic GABA(A) receptor number underlie variation in GABA mini amplitude. Neuron 19:697-709.
Oorschot DE (1996) Total number of neurons in the neostriatal, pallidal, subthalamic, and substantia nigral nuclei of the rat basal ganglia: A stereological study using the cavalieri and optical disector methods. J Comp Neurol 366:580-99.
Otsuka T, Abe T, Tsukagawa T, Song WJ (2004) Conductance-based model of the voltage-dependent generation of a plateau potential in subthalamic neurons. J Neurophysiol 92:255-64.
Otsuka T, Murakami F, Song WJ (2001) Excitatory postsynaptic potentials trigger

a plateau potential in rat subthalamic neurons at hyperpolarised states. J Neurophysiol 86:1816-25.

Ouardouz M, Sastry BR (2000) Mechanisms underlying LTP of inhibitory synaptic transmission in the deep cerebellar nuclei. J Neurophysiol 84:1414-21.

Poulopoulos A, Aramuni G, Meyer G, Soykan T, Hoon M, Papadopoulos T, Zhang M, Paarmann I, Fuchs C, Harvey K, Jedlicka P, Schwarzacher SW, Betz H, Harvey RJ, Brose N, Zhang W, Varoqueaux F (2009) Neuroligin 2 drives postsynaptic assembly at perisomatic inhibitory synapses through gephyrin and collybistin. Neuron 63:628-42.

Papadopoulos T, Soykan T (2011) The role of collybistin in gephyrin clustering at inhibitory synapses: facts and open questions. Front Cell Neurosci 5:11.

Pape HC, McCormick DA (1989) Noradrenaline and serotonin selectively modulate thalamic burst firing by enhancing a hyperpolarisation-activated cation current. Nature 340:715-8.

Patel NK, Heywood P, O'Sullivan K, McCarter R, Love S, Gill SS (2003) Unilateral subthalamotomy in the treatment of Parkinson's disease. Brain 126:1136-45.

Pawley J (2006) Fundamental limits in confocal microscopy. In: Handbook of Biological Confocal Microscopy. (Pawley J, ed), pp 20-42. New York, NY: SpingerScience+Business Media, LLC.

Paz JT, Deniau JM, Charpier S (2005) Rhythmic bursting in the cortico-subthalamo-pallidal network during spontaneous genetically determined spike and wave discharges. J Neurosci 25:2092-101.

Perese DA, Ulman J, Viola J, Ewing SE, Bankiewicz KS (1989) A 6-hydroxydopamine-induced selective parkinsonian rat model. Brain Res 494:285-93.

Pfaffl MW, Tichopad A, Prgomet C, Neuvians TP (2004) Determination of stabhousekeeping genes, differentially regulated target genes and sample integrity: BestKeeper – Excel-based tool using pair-wise correlations. Biotechnology Letters 26:509–15.

Plenz D, Kital ST (1999) A basal ganglia pacemaker formed by the subthalamic nucleus and external globus pallidus. Nature 400:677-82.

Poleg-Polsky A, Diamond JS (2011) Imperfect Space Clamp Permits Electrotonic Interactions between Inhibitory and Excitatory Synaptic Conductances, Distorting Voltage Clamp Recordings. Plos One 6:e19463.

Poulopoulos A, Aramuni G, Meyer G, Soykan T, Hoon M, Papadopoulos T, Zhang M, Paarmann I, Fuchs C, Harvey K, Jedlicka P, Schwarzacher SW, Betz H, Harvey RJ, Brose N, Zhang W, Varoqueaux F (2009) Neuroligin 2 drives postsynaptic assembly at perisomatic inhibitory synapses through gephyrin and collybistin. Neuron 63:628-42.

Ramanathan S, Tkatch T, Atherton JF, Wilson CJ, Bevan MD (2008) D2-like dopamine receptors modulate SK_{Ca} channel function in subthalamic nucleus neurons through inhibition of $Ca_v2.2$ channels. J Neurophysiol 99:442-59.

Raz A, Vaadia E, Bergman H (2000) Firing patterns and correlations of spontaneous discharge of pallidal neurons in the normal and the tremulous 1-methyl-4-

phenyl-1,2,3,6-tetrahydropyridine vervet model of parkinsonism. J Neurosci 20:8559-71.
Redgrave P, Marrow L, Dean P (1992) Topographical organization of the nigrotectal projection in rat - evidence for segregated channels. Neurosci 50:571-95.
Redgrave P, Prescott TJ, Gurney K (1999) The basal ganglia: A vertebrate solution to the selection problem? Neurosci 89:1009-23.
Redgrave P, Vautrelle N, Reynolds JNJ (2011) Functional properties of the basal ganglia's re-entrant loop architecture: selection and reinforcement. Neurosci 198:138-51.
Reese R, Leblois A, Steigerwald F, Poetter-Nerger M, Herzog J, Mehdorn HM, Deuschl G, Meissner WG, Volkmann J (2011) Subthalamic deep brain stimulation increases pallidal firing rate and regularity. Exp Neurol 229:517-21.
Remple MS, Bradenham CH, Kao CC, Charles PD, Neimat JS, Konrad PE (2011) Subthalamic nucleus neuronal firing rate increases with Parkinson's disease progression. Mov Disord 26:1657-62.
Robinson JM, Takizawa T, Vandre DD (2000) Enhanced labeling efficiency using ultrasmall immunogold probes: Immunocytochemistry. J Histochem Cytochem 48:487-92.
Robinson RB, Siegelbaum SA (2003) Hyperpolarisation-activated cation currents: from molecules to physiological function. Annu Rev Physiol 65:453-80.
Rommelfanger KS, Wichmann T (2010) Extrastriatal dopaminergic circuits of the basal ganglia. Front Neuroanat 4:139.
Rubin JE, Terman D (2004) High frequency stimulation of the subthalamic nucleus eliminates pathological thalamic rhythmicity in a computational model. J Comput Neurosci 16:211-35.
Ryan LJ, Sanders DJ (1993) Subthalamic nucleus lesion regularizes firing patterns in globus-pallidus and substantia-nigra pars-reticulata neurons in rats. Brain Res 626:327-31.
Samii A, Nutt JG, Ransom BR (2004) Parkinson's disease. Lancet 363:1783-93.
Santaniello S, Montgomery EB, Jr., Gale JT, Sarma SV (2012) Non-stationary discharge patterns in motor cortex under subthalamic nucleus deep brain stimulation. Front Integr Neurosci 6:35.
Santoro B, Chen S, Lüthi A, Pavlidis P, Shumyatsky GP, Tibbs GR, Siegelbaum SA (2000) Molecular and functional heterogeneity of hyperpolarisation-activated pacemaker channels in the mouse CNS. J Neurosci 20:5264-75.
Schwarting RKW, Huston JP (1996) The unilateral 6-hydroxydopamine lesion model in behavioral brain research. Analysis of functional deficits, recovery and treatments. Prog Neurobiol 50:275-331.
Schallert T, Fleming SM, Leasure JL, Tillerson JL, Bland ST (2000) CNS plasticity and assessment of forelimb sensorimotor outcome in unilateral rat models of stroke, cortical ablation, parkinsonism and spinal cord injury. Neuropharmacology 39:777-87.
Semwogerere D, Weeks E (2005) Confocal microscopy. In: Encyclopedia of

Biomaterials and Biomedical Engineering (Bowlin GL, Wnek GE, eds). New York, NY: Informa Healthcare.

Shah MM, Anderson AE, Leung V, Lin X, Johnston D (2004) Seizure-induced plasticity of h channels in entorhinal cortical layer III pyramidal neurons. Neuron 44:495-508.

Sharott A, Magill PJ, Bolam JP, Brown P (2005a) Directional analysis of coherent oscillatory field potentials in the cerebral cortex and basal ganglia of the rat. J Physiol (Lond) 562:951-63.

Sharott A, Magill PJ, Harnack D, Kupsch A, Meissner W, Brown P (2005b) Dopamine depletion increases the power and coherence of beta-oscillations in the cerebral cortex and subthalamic nucleus of the awake rat. Eur J Neurosci 21:1413-22.

Shen KZ, Johnson SW (2000) Presynaptic dopamine D2 and muscarine M3 receptors inhibit excitatory and inhibitory transmission to rat subthalamic neurones in vitro. J Physiol 525:331-41.

Shen KZ, Johnson SW (2005) Dopamine depletion alters responses to glutamate and GABA in the rat subthalamic nucleus. Neuroreport 16:171-4.

Sheng M, McFadden G, Greenberg ME (1990) Membrane depolarisation and calcium induce c-fos transcription via phosphorylation of transcription factor CREB. Neuron 4:571-82.

Shi LH, Luo F, Woodward DJ, Chang JY (2006) Basal ganglia neural responses during behaviorally effective deep brain stimulation of the subthalamic nucleus in rats performing a treadmill locomotion test. Synapse 59:445-57.

Shin M, Brager D, Jaramillo TC, Johnston D, Chetkovich DM (2008) Mislocalisation of h channel subunits underlies h channelopathy in temporal lobe epilepsy. Neurobiol Dis 32:26-36.

Shin RM, Masuda M, Miura M, Sano H, Shirasawa T, Song WJ, Kobayashi K, Aosaki T (2003) Dopamine D4 receptor-induced postsynaptic inhibition of GABAergic currents in mouse globus pallidus neurons. J Neurosci 23:11662-72.

Shink E, Bevan MD, Bolam JP, Smith Y (1996) The subthalamic nucleus and the external pallidum: Two tightly interconnected structures that control the output of the basal ganglia in the monkey. Neurosci 73:335-57.

Sigrist SJ, Sabatini BL (2012) Optical super-resolution microscopy in neurobiology. Curr Opin Neurobiol 22:86-93.

Silver N, Best S, Jiang J, Thein SL (2006) Selection of housekeeping genes for gene expression studies in human reticulocytes using real-time PCR. BMC Mol Biol 7:33.

Smith Y, Bevan MD, Shink E, Bolam JP (1998) Microcircuitry of the direct and indirect pathways of the basal ganglia. Neuroscience 86:353-87.

Smith Y, Bolam JP, Vonkrosigk M (1990) Topographical and synaptic organization of the GABA-containing pallidosubthalamic projection in the rat. Eur J Neurosci 2:500-11.

Smith KR, Kittler JT (2010) The cell biology of synaptic inhibition in health and disease. Curr Opin Neurobiol 20:550-6.

Smith Y, Raju DV, Pare JF, Sidibe M (2004) The thalamostriatal system: a highly specific network of the basal ganglia circuitry. Trends Neurosci 27:520-7.
Song WJ, Baba Y, Otsuka T, Murakami F (2000) Characterization of Ca2(+) channels in rat subthalamic nucleus neurons. J Neurophysiol 84:2630-7.
Sooksawate T, Isa K, Behan M, Yanagawa Y, Isa T (2011) Organization of GABAergic inhibition in the motor output layer of the superior colliculus. Eur J Neurosci 33:421-32.
Stephenson-Jones M, Ericsson J, Robertson B, Grillner S (2012) Evolution of the basal ganglia: Dual-output pathways conserved throughout vertebrate phylogeny. J Comp Neurol 520:2957-73.
Stephenson-Jones M, Samuelsson E, Ericsson J, Robertson B, Grillner S (2011) Evolutionary conservation of the basal ganglia as a common vertebrate mechanism for action selection. Curr Biol 21:1081-91.
Surmeier DJ, Guzman JN, Sanchez-Padilla J, Schumacker PT (2011) The role of calcium and mitochondrial oxidant stress in the loss of substantia nigra pars compacta dopaminergic neurons in Parkinson's disease. Neurosci 198:221-31.
Tachibana Y, Iwamuro H, Kita H, Takada M, Nambu A (2011) Subthalamo-pallidal interactions underlying parkinsonian neuronal oscillations in the primate basal ganglia. Eur J Neurosci 34:1470-84.
Tachibana Y, Kita H, Chiken S, Takada M, Nambu A (2008) Motor cortical control of internal pallidal activity through glutamatergic and GABAergic inputs in awake monkeys. Eur J Neurosci 27: 238-53.
Takakusaki K, Saitoh K, Harada H, Kashiwayanagi M (2004) Role of basal ganglia-brainstem pathways in the control of motor behaviors. Neurosci Res 50:137-51.
Takesian AE, Kotak VC, Sanes DH (2010) Presynaptic GABA(B) Receptors regulate experience-dependent development of inhibitory short-term plasticity. J Neurosci 30:2716-27.
Tang JKH, Moro E, Lozano AM, Lang AE, Hutchison WD, Mahant N, Dostrovsky JO (2005) Firing rates of pallidal neurons are similar in Huntington's and Parkinson's disease patients. Exp Brain Res 166:230-6.
Terman D, Rubin JE, Yew AC, Wilson CJ (2002) Activity patterns in a model for the subthalamopallidal network of the basal ganglia. J Neurosci 22:2963-76.
Thanvi BR, Lo TCN (2004) Long term motor complications of levodopa: clinical features, mechanisms, and management strategies. Postgrad Med J 80:452-8.
Tkatch T, Baranauskas G, Surmeier DJ (2000) Kv4.2 mRNA abundance and A-type K(+) current amplitude are linearly related in basal ganglia and basal forebrain neurons. J Neurosci 20:579-88.
Traynelis SF, Wollmuth LP, McBain CJ, Menniti FS, Vance KM, Ogden KK, Hansen KB, Yuan H, Myers SJ, Dingledine R (2010) Glutamate Receptor Ion Channels: Structure, Regulation, and Function. Pharmacol Rev 62:405-96.
tom Dieck S, Sanmartí-Vila L, Langnaese K, Richter K, Kindler S, Soyke A, Wex H, Smalla KH, Kämpf U, Fränzer JT, Stumm M, Garner CC, Gundelfinger ED (1998) Bassoon, a novel zinc-finger CAG/glutamine-repeat protein selectively localised

at the active zone of presynaptic nerve terminals. J Cell Biol 142:499-509.
Tretter V, Moss SJ (2008) GABAA receptor dynamics and constructing GABAergic synapses. Front Mol Neurosci 1:7.
Tsay D, Dudman JT, Siegelbaum SA (2007) HCN1 channels constrain synaptically evoked Ca2+ spikes in distal dendrites of CA1 pyramidal neurons. Neuron 56:1076-89.
Tseng KY, Kasanetz F, Kargieman L, Riquelme LA, Murer MG (2001a) Cortical slow oscillatory activity is reflected in the membrane potential and spike trains of striatal neurons in rats with chronic nigrostriatal lesions. J Neurosci 21:6430-9.
Tseng KY, Kasanetz F, Kargieman L, Pazo JH, Murer MG, Riquelme LA (2001b) Subthalamic nucleus lesions reduce low frequency oscillatory firing of substantia nigra pars reticulata neurons in a rat model of Parkinson's disease. Brain Res 904:93-103.
Tsodyks MV, Markram H (1997) The neural code between neocortical pyramidal neurons depends on neurotransmitter release probability. Proc Natl Acad Sci U S A 94:719-23.
Turrigiano GG (1999) Homeostatic plasticity in neuronal networks: the more things change, the more they stay the same. Trends Neurosci 22:221-7.
Tyagarajan SK, Fritschy JM (2010) $GABA_A$ receptors, gephyrin and homeostatic synaptic plasticity. J Physiol 588:101–6.
Tyagarajan SK, Ghosh H, Yevenes GE, Nikonenko I, Ebeling C, Schwerdel C, Sidler C, Zeilhofer HU, Gerrits B, Muller D, Fritschy J-M (2011) Regulation of GABAergic synapse formation and plasticity by GSK3 beta-dependent phosphorylation of gephyrin. PNAS 108:379-84.
Urbain N, Gervasoni D, Souliere F, Lobo L, Rentero N, Windels F, Astier B, Savasta M, Fort P, Renaud B, Luppi PH, Chouvet G (2000) Unrelated course of subthalamic nucleus and globus pallidus neuronal activities across vigilance states in the rat. Eur J Neurosci 12:3361–74.
Ungerstedt U (1968) 6-hydroxydopamine induced degeneration of central monoamine neurons. Eur J Pharmacol 5:107–10.
Valasek MA, Repa JJ (2005) The power of real-time PCR. Adv Physiol Educ 29:151-9.
Vandesompele J, De Preter K, Pattyn F, Poppe B, Van Roy N, De Paepe A, Speleman F (2002) Accurate normalisation of real-time quantitative RT-PCR data by geometric averaging of multiple internal control genes. Genome Biol 3:RESEARCH0034.
Velez-Fort M, Audinat E, Angulo MC (2012) Central Role of GABA in Neuron-Glia Interactions. Neuroscientist 18:237-50.
Vila M, Périer C, Féger J, Yelnik J, Faucheux B, Ruberg M, Raisman-Vozari R, Agid Y, Hirsch EC (2000) Evolution of changes in neuronal activity in the subthalamic nucleus of rats with unilateral lesion of the substantia nigra assessed by metabolic and electrophysiological measurements. Eur J Neurosci 12:337-44.
Vitek JL, Hashimoto T, Peoples J, DeLong MR, Bakay RAE (2004) Acute stimulation in the external segment of the globus pallidus improves parkinsonian motor signs. Mov Disord 19:907-15.

Vitek JL, Zhang J, Hashimoto T, Russo GS, Baker KB (2012) External pallidal stimulation improves parkinsonian motor signs and modulates neuronal activity throughout the basal ganglia thalamic network. Exp Neurol 233:581-6.

Walker HC, Huang H, Gonzalez CL, Bryant JE, Killen J, Cutter GR, Knowlton RC, Montgomery EB, Guthrie BL, Watts RL (2012) Short latency activation of cortex during clinically effective subthalamic deep brain stimulation for Parkinson's disease. Mov Disord 27:864-873.

Wang L, Kitai ST, Xiang Z (2006) Activity-dependent bidirectional modification of inhibitory synaptic transmission in rat subthalamic neurons. J Neurosci 26:7321-7.

Watabe-Uchida M, Zhu L, Ogawa SK, Vamanrao A, Uchida N (2012) Whole-Brain Mapping of Direct Inputs to Midbrain Dopamine Neurons. Neuron 74:858-73.

Watanabe K, Kita T, Kita H (2009) Presynaptic actions of D2-like receptors in the rat cortico-striato-globus pallidus disynaptic connection in vitro. J Neurophysiol 101:665-71.

Weinberger M, Mahant N, Hutchison WD, Lozano AM, Moro E, Hodaie M, Lang AE, Dostrovsky JO (2006) Beta oscillatory activity in the subthalamic nucleus and its relation to dopaminergic response in Parkinson's disease. J Neurophysiol 96:3248-56.

West MJ (1999) Stereological methods for estimating the total number of neurons and synapses: issues of precision and bias. Trends Neurosci 22: 51–61.

Wichmann T, Bergman H, DeLong MR (1994) The primate subthalamic nucleus. III. Changes in motor behavior and neuronal activity in the internal pallidum induced by subthalamic inactivation in the MPTP model of parkinsonism. J Neurophysiol 72:521-30.

Wichmann T, Bergman H, Starr PA, Subramanian T, Watts RL, DeLong MR (1999) Comparison of MPTP-induced changes in spontaneous neuronal discharge in the internal pallidal segment and in the substantia nigra pars reticulata in primates. Exp Brain Res 125:397-409.

Wichmann T, DeLong MR (2003) Pathophysiology of Parkinson's disease: the MPTP primate model of the human disorder. Ann N Y Acad Sci 991:199-213.

Wichmann T, DeLong MR, Guridi J, Obeso JA (2011) Milestones in research on the pathophysiology of Parkinson's disease. Mov Disord 26:1032-41.

Wichmann T, Kliem MA, Soares J (2002) Slow oscillatory discharge in the primate basal ganglia. J Neurophysiol 87:1145-8.

Williams D, Tijssen M, van Bruggen G, Bosch A, Insola A, Di Lazzaro V, Mazzone P, Oliviero A, Quartarone A, Speelman H, Brown P (2002a) Dopamine-dependent changes in the functional connectivity between basal ganglia and cerebral cortex in humans. Brain 125:1558-69.

Williams SR, Christensen SR, Stuart GJ, Häusser M (2002) Membrane potential bistability is controlled by the hyperpolarisation-activated current I(H) in rat cerebellar Purkinje neurons in vitro. J Physiol 539:469-83.

Williams SR, Stuart GJ (2000). Site independence of EPSP time course is mediated by

dendritic I(h) in neocortical pyramidal neurons. J Neurophysiol 83:3177-82.
Williams SR, Mitchell SJ (2008) Direct measurement of somatic voltage clamp errors in central neurons. Nat Neurosci 11:790-8.
Williams SR, Stuart GJ (2003) Voltage- and site-dependent control of the somatic impact of dendritic IPSPs. J Neurosci 23:7358-67.
Wilson CJ, Bevan MD (2011) Intrinsic dynamics and synaptic inputs control the activity patterns of subthalamic nucleus neurons in health and in Parkinson's disease. Neurosci 198:54-68.
Wilson CJ, Beverlin B, 2nd, Netoff T (2011) Chaotic desynchronization as the therapeutic mechanism of deep brain stimulation. Frontiers in systems neuroscience 5:50.
Wilson CL, Cash D, Galley K, Chapman H, Lacey MG, Stanford IM (2006) Subthalamic nucleus neurones in slices from 1-methyl-4-phenyl-1,2,3,6-tetrahydropyridine-lesioned mice show irregular, dopamine-reversible firing pattern changes, but without synchronous activity. Neuroscience 143:565-72.
Wilson CL, Puntis M, Lacey MG (2004) Overwhelmingly asynchronous firing of rat subthalamic nucleus neurones in brain slices provides little evidence for intrinsic interconnectivity. Neurosci 123:187-200.
Wisden W, Laurie DJ, Monyer H, Seeburg PH (1992) Distribution of 13 $GABA_A$ receptor subunit mRNAs in the brain. I. Telencephalon, diencephalon, mesencephalon. J Neurosci 12:1040–62.
Xiang ZX, Wang L, Kitai ST (2005) Modulation of spontaneous firing in rat subthalamic neurons by 5-HT receptor subtypes. J Neurophysiol 93:1145-57.
Yizhar O, Fenno LE, Davidson TJ, Mogri M, Deisseroth K (2011) Optogenetics in Neural Systems. Neuron 71:9-34.
Yu TS, Wang SD, Liu JC, Yin HS (2001) Changes in the gene expression of GABA(A) receptor alpha1 and alpha2 subunits and metabotropic glutamate receptor 5 in the basal ganglia of the rats with unilateral 6-hydroxydopamine lesion and embryonic mesencephalic grafts. Exp Neurol 168:231-41.
Yuan H, Sarre S, Ebinger G, Michotte Y (2005) Histological, behavioural and neurochemical evaluation of medial forebrain bundle and striatal 6-OHDA lesions as rat models of Parkinson's disease. J Neurosci Methods 144:35-45.
Zaidel A, Arkadir D, Israel Z, Bergman H (2009) Akineto-rigid vs. tremor syndromes in Parkinsonism. Curr Opin Neurol 22:387-93.
Zeng J, Wang G, Chen S-D (2007) ATP-sensitive potassium channels: novel potential roles in Parkinson's disease. Neurosci Bull 23:370-6.
Zhang F, Wang LP, Boyden ES, Deisseroth K (2006) Channelrhodopsin-2 and optical control of excitable cells. Nat Methods 3:785-92.
Zhang J, Russo GS, Mewes K, Rye DB, Vitek JL (2006) Lesions in monkey globus pallidus externus exacerbate parkinsonian symptoms. Exp Neurol 199:446-53.
Zhu Z, Bartol M, Shen K, Johnson SW (2002a) Excitatory effects of dopamine on subthalamic nucleus neurons: in vitro study of rats pretreated with 6-hydroxydopamine and levodopa. Brain Res 945:31-40.
Zhu ZT, Shen KZ, Johnson SW (2002b) Pharmacological identification of inward current

evoked by dopamine in rat subthalamic neurons in vitro. Neuropharmacology 42:772-81.

Zuch CL, Nordstroem VK, Briedrick LA, Hoernig GR, Granholm AC, Bickford PC (2000) Time course of degenerative alterations in nigral dopaminergic neurons following a 6-hydroxydopamine lesion. J Comp Neurol 427:440-54.